UNIVERSITY OF CALIFORNIA,
IRVINE

Exploring Microglial Homeostasis and Repopulation Dynamics using Colony-Stimulating Factor 1 Receptor Inhibition

DISSERTATION

submitted in partial satisfaction of the requirements
for the degree of

DOCTOR OF PHILOSOPHY

in Biological Sciences

by

Allison Rachel Najafi

Dissertation Committee:
Associate Professor Kim Green, Chair
Assistant Professor Mathew Blurton-Jones
Professor Andrea Tenner

2017

DEDICATION

To my favorite people (you know who you are).

Creation comes out of imperfection. It seems to come out of a striving and a frustration. This is where, I think, language came from…it came from our desire to transcend our isolation and have some connection with one another…so much of our experience is intangible. So much of what we perceive cannot be expressed…And yet, when we communicate with one another and we feel we have connected and think we're understood I think we have a feeling of almost spiritual communion. That may be transient, but it's what we live for.

"Waking Life"

TABLE OF CONTENTS

	Page
LIST OF FIGURES	iv
LIST OF ABBREVIATIONS	v
ACKNOWLEDGMENTS	vii
CURRICULUM VITAE	ix
ABSTRACT OF THE DISSERTATION	xiii
INTRODUCTION	1
CHAPTER 1: Microglial homeostasis in the adult brain	20
CHAPTER 2: A limited capacity for microglial repopulation in the adult brain	48
CHAPTER 3: Identification of a novel route of microglial repopulation along the rostral migratory stream and projecting axons	70
CONCLUDING REMARKS	96
REFERENCES	100

LIST OF FIGURES

		Page
Figure 1	Graphical abstract demonstrating myeloid cell ontogeny	3
Figure 2	CSF1R inhibition eliminates microglia from the adult brain	19
Figure 1.1	Rapid repopulation of the microglia-depleted brain with new cells that differentiation into microglia	26
Figure 1.2	Microglial repopulation occurs evenly throughout the brain	28
Figure 1.3	Treatment with the CSF1R inhibitor PLX3397 eliminates microglia in Rosa26-YFP	29
Figure 1.4	Repopulation does not occur from peripheral cells	31
Figure 1.5	Microglial repopulation occurs between 48 and 72 hours after CSF1R inhibitor withdrawal	34
Figure 1.6	IB4 reactivity and Pu.1 expression in repopulating microglia	36
Figure 1.7	Microarray analysis of the repopulating brain reveals extensive proliferation and a microglia-specific expression profile	37
Figure 1.8	Rapid repopulation in brains that are >95% depleted of microglia	39
Figure 1.9	Microglial repopulation is preceded by proliferation of a non-microglial cell type throughout the CNS	40
Figure 1.10	Fate mapping reveals a nestin-expressing microglia progenitor cell that becomes the repopulating microglia	42
Figure 1.11	Inhibition of CSF1R alone is sufficient to both eliminate and repopulate microglia	44
Figure 2.1	Cyclic treatment of WT mice with PLX3397 (290 mg/kg)	54
Figure 2.2	Rate of microglial repopulation depends on extent of depletion	55
Figure 2.3	Cyclic treatment of WT mice with higher dose of PLX3397 (600 mg/kg)	57
Figure 2.4	Differentially expressed genes between treatment cycles with 600 mg/kg PLX3397, obtained via RNA-seq analysis	58

Figure 2.5	Microglial morphology and astrocyte staining of groups from cyclic treatment with 600 mg/kg PLX3397	60
Figure 2.6	Pathway analysis and further comparison of differentially expressed genes, obtained via RNA-seq	63
Figure 2.7	Cyclic treatment of WT mice with 600 mg/kg PLX3397, and 28d withdrawal periods	64
Figure 2.8	Properties of returning cells with long recovery cycles of 600 mg/kg PLX3397	65
Figure 3.1	Assessment of early repopulation following 7-day treatment with 600 mg/kg PLX3397	76
Figure 3.2	Altered repopulation dynamics following 100% microglial elimination with 14d PLX3397 (600 mg/kg)	79
Figure 3.3	Immune cell gene expression changes persist at 28d recovery	81
Figure 3.4	Repopulating cells do not originate from the choroid plexus	84
Figure 3.5	Differentially repopulated cells first appear along RMS and projecting axons	85
Figure 3.6	Absence of $CCR2^{+}$ cells with differential RMS-associated repopulation	87
Figure 3.7	Differential repopulation occurs in the absence of CCR2 signaling	88
Figure 3.8	RMS microglia labeled by CSF1R lineage tracing are depleted with 14d PLX3397 (600 mg/kg) treatment	90
Figure 3.9	Returning microglia are initially proliferative	91
Figure 3.10	Repopulating cells are dependent on CSF1R signaling	92

LIST OF ABBREVIATIONS

Aβ	beta-amyloid
ACO	Anterior commissure
AD	Alzheimer's disease; sAD(sporadic) or fAD(familial)
ATP	Adenosine triphosphate
BBB	Blood brain barrier
BM	Bone marrow
BP	Basal progenitor
CCR2	C-C chemokine receptor type 2
CD11b	Cluster of differentiation 11b; *aka* ITGAM, *aka* CR3
CNS	Central nervous system
CR3	Complement receptor 3, *aka* ITGAM, *aka* CD11b
CSF	Cerebrospinal fluid
CSF1	Colony-stimulating factor 1
CSF1R	Colony-stimulating factor 1 receptor
DAMP	Damage-associated molecular pattern
EAE	Experimental autoimmune encephalomyelitis
EMP	Erythro-myeloid precursor
GFAP	Glial fibrillary acidic protein
IBA1	Ionophore calcium-binding adapter molecule 1
IFNγ	Interferon gamma
IL	Interleukin
ITGAM	Integrin alpha M; a*ka* CD11b, *aka* CR3
KO	Knock out
LPS	Lipopolysaccharide
LV	Lateral ventricle
MHC-II	Major histocompatibility complex class II
NO	Nitric oxide
OB	Olfactory bulb
OPC	Oligodendrocyte precursor cell
PAMP	Pathogen associated molecular patterns
PRR	Pattern recognition receptor
RMS	Rostral migratory stream\
SEZ	Subependymal zone
SVZ	Subventricular zone
TLR	Toll-like receptor
TNF-α	Tumor necrosis factor-alpha
TREM2	Triggering receptor expressed on myeloid cells 2
WT	Wild-type
YS	Yolk sac

ACKNOWLEDGMENTS

I cannot thank my mentor, Dr. Kim Green, enough for his guidance. He is truly talented, incredibly creative, and intuitive when it comes to experimental design, with an amazing and innate sense of innovation and vision. Working for Kim has never felt like “work” - it is easy to be motivated whilst working for someone whom I respect so highly. Most importantly, Kim has fostered a lab dynamic with an exceptional level of comradery and respect for one another. The laughter generated during my graduate studies was the fuel for much of this thesis, and I recognize how incredibly lucky I am to have found my closest friends within the Green Lab.

I would like to thank my committee members, Professors Andrea Tenner and Mathew Blurton-Jones, for providing helpful suggestions and critique.

I thank Drs. Jakowec and Petzinger for adopting me into their lab family, where I have never felt such warmth at Christmas parties and backyard BBQ’s, and where I learned to love the brain. I also thank Dr. Chun, for providing me with the foundation to think like a scientist, and for being someone to look up to so completely.

Special thanks go to Elizabeth Spangenberg, Dr. Rachel Rice, Dr. Monica Elmore, Rafael Lee, Dr. Lindsay Hohsfield, and Joshua Crapser, for your assistance and keeping me in stiches.

Finally, I thank my husband for his unwavering, unselfish support for so, so long, and my dear friends Kenneth Cimino and Simber Darabian, who inspire me and have become my family.

This work was supported in parts by NINDS 1R01NS083801 to KNG and NIH Training Grant AG00096. I thank Elsevier and Oxford University Press for permission to include copyrighted figures and text as part of my dissertation.

CURRICULUM VITAE

Allison Rachel Najafi

2010	Student Investigator, La Selva Biological Station, Puerto Viejo de Sarapiqui, Costa Rica Dr. Terry McGlynn
2011	Student Investigator, USC Translational Neuroscience Research Group, Keck School of Medicine, University of Southern California, Los Angeles, CA Drs. Michael Jakowec and Giselle Petzinger
2012	B.S. in Cellular and Molecular Biology, California State University, Dominguez Hills, Carson, CA
2015	M.S. in Biological Sciences, University of California, Irvine Dr. Kim N. Green
2017	Ph.D. in Biological Sciences, University of California, Irvine Dr. Kim N. Green

FIELD OF STUDY

Exploring Microglial Homeostasis and Repopulation Dynamics using Colony-Stimulating Factor 1 Receptor Inhibition

HONORS AND AWARDS

2012	FASEB scholarship for travel to Endocrine Society conference, California State University, Dominguez Hills
2013	HHMI-UCI Teaching Fellow Award, University of California, Irvine
2014	McGaugh Award for Excellence in Research, University of California, Irvine
2014-2016	NIH Training Grant recipient in the Neurobiology of Aging, University of California, Irvine
2015-2017	Achievement Rewards for College Students (ARCS) Foundation Scholar Award, University of California, Irvine
2016	First Place predoctoral “Elevator Pitch” competition, Convergent Science Training Grants Retreat, University of California, Irvine
2016	Second Place predoctoral poster award, ReMIND Emerging Scientists Syposium, University of California, Irvine

PUBLICATIONS

Original Reports *(Asterisk denotes co-first authorship)*

"Tesosterone effects on aggressive motivation, impulsivity and tyrosine hydroxylase." Wood R, Armstrong A, Fridkin V, Shah V, **Najafi AR**, Jakowec M. Physiology and Behavior. 2012 Dec ;110-111:6-12.

"Colony-stimulating factor 1 receptor signaling is necessary for microglia viability, unmasking a microglia progenitor cell in the adult brain." Elmore MRP*, **Najafi AR*,** Koike MA, Dagher NN, Spangenberg EE, Rice RA, Kitazawa M, Matusow B, Nguyen H, West BL, Green KN. Neuron. 2014 Apr 82(2):380-97.

"Colony-stimulating factor 1 receptor inhibition prevents plaque microglial plaque association and improves cognition in 3xTg-AD mice." Dagher NN***, Najafi AR*,** Neely K, Elmore MRP, White T, West BL, Green KN. Journal of Neuroinflammation. 2015 12:139.

"Eliminating microglia in Alzheimer's mice prevents neuronal loss without modulating amyloid-β pathology." Spangenberg EE, Lee RJ, **Najafi AR**, Rice RA, Elmore MRP, Blurton-Jones M, West BL, Green KN. Brain. 2016 139(4):1265-1281.

"Elimination of microglia improves cognitive function following cranial irradiation." Acharya MM, Green KN, Allen BD, **Najafi AR**, Syage A, Minasyan H, Le MT, Kawashita T, Giedzinski E, Parihar VK, West BL, Baulch JE, Limoli CL. 2016 Scientific Reports. 6:31545.

"Resolution of neuronal injury-induced chronic inflammation via CSF1R dependent microglia elimination and repopulation leads to recovery." Rice RA, Pham J, Lee RJ, **Najafi AR**, West BL, Green KN. Glia. 2017.

Reports in Progress

"A limited capacity for microglial repopulation in the adult brain." **Najafi AR**, Jiang S, Ng W, Mortazavi A, West BL, Green KN.

"Identification of a novel route of microglial repopulation along the rostral migratory stream and projecting axons." **Najafi AR**, Hohsfield LA, Ghorbanian Y, Inlay M, West BL, Green KN.

Abstracts and Posters **Indicates an oral presentation*

Najafi AR, West BL, Green KN (2016) Microglial homeostasis dynamics in response to CSF1R inhibition and withdrawal. Keystone Symposium: Microglia in the Brain. Keystone, Colorado, USA.

***Najafi AR** (2016) Extinguishing microglial inflammation. Convergent Science Training Grants Retreat. University of California, Irvine. Irvine, California, USA.

***Najafi AR** (2014) CSF1 receptor signaling is necessary for microglia viability, which unmasks a cell that rapidly repopulates the microglia-depleted adult brain. McGaugh Award for Excellence in Research. University of California, Irvine. Irvine, California, USA.

Najafi AR, Spangenberg E, Rice RA, Koike MA, West BL, Green KN (2014) Uncovering of a microglial progenitor cell in the adult and aged CNS. Federation of American Societies for Experimental Biology (FASEB) regional meeting. Big Sky, Montana, USA.

Najafi AR, Spangenberg E, Rice RA, Koike MA, West BL, Green KN (2014) Uncovering of a microglial progenitor cell in the adult and aged CNS. American Federation for Aging Research Conference, Santa Barbara, California, USA.

***Najafi AR** (2014) Discovery of a microglial progenitor in the adult CNS. Research and Education in Memory Impairments and Neurological Disorders (ReMIND) 5th Annual Emerging Scientists Symposium at the University of California, Irvine. Irvine, California, USA.

Najafi AR, Shah V, Toy WA, Wood R, Petzinger GM, Jakowec M (2012) Experience-Dependent Neuroplasticity in Dopamine-Linked Models of Parkinson's Disease and Aggression. Life Sciences Research Poster Presenter, 14th Annual Undergraduate Symposium, University of Southern California. Los Angeles, California, USA.

Toy WA, Vuckovic MG, **Najafi AR**, Shah V, Petzinger GM, Meshul CK, Moore C, Fisher BE, Walsh JP, Akopian GK (2012) Intensive treadmill exercise restores dendritic spines in the dopamine depleted mouse striatum. Annual USC Translational Neuroscience Retreat, Lake Arrowhead, California, USA.

TEACHING

2007-2008	YMCA Program Leader, Whittier Elementary
2012	General Chemistry, CSU Dominguez Hills
2012	Transition to Teaching Tutor, CSU Dominguez HIlls
2013	Bio 93: From DNA to Organisms
2014	N110: Neurobiology
2014	N113: Neurobiology Lab

ABSTRACT OF THE DISSERTATION

Exploring Microglial Homeostasis and Repopulation Dynamics Using Colony-Stimulating Factor 1 Receptor Inhibition

By

Allison Rachel Najafi

Doctor of Philosophy in Biological Sciences

University of California, Irvine, 2017

Associate Professor Kim Green, Chair

Microglia are the primary immune effector cells in the CNS, responsible for the majority of inflammatory responses in the brain. Microglial homeostatic signals and replicative properties are largely unknown - however, early studies indicate that microglial turnover is low and proliferation is rare (Lawson et al., 1992), which could result in the acquisition of age-related deficiencies and senescence. As microglia age they become dysregulated, exhibiting an altered inflammatory profile, reduced phagocytic efficiency, and impaired migratory abilities (Godbout and Johnson, 2004; Frank et al., 2006; Damani et al., 2011; Njie et al., 2012). Given the dysregulation of aged microglia, activation of these cells could incite a chronic self-perpetuating cycle of inflammation and toxicity, contributing to neuronal death. We have recently discovered that microglia are fully dependent upon colony stimulating factor-1 receptor (CSF1R) signaling for their survival in the adult brain, and through the administration of small molecule inhibitors of the CSF1R, we have previously demonstrated we can eliminate >99% of all microglia brainwide (Elmore et al. 2014). Furthermore, my data show that the microglia-depleted

brain has a profound ability to repopulate with new cells once CSF1R inhibitors are withdrawn, indicating that microglial elimination is fully reversible.

The goal of my dissertation is to determine the source and properties of repopulated microglia in order to establish whether these cells can be used for potential therapeutic purposes – either to resolve chronic neuroinflammatory processes or, more ambitiously, to reverse microglial senescence in the aged brain. Indeed, I have discovered that microglial repopulation arises both from nestin^{+} progenitor cells and surviving microglia in the adult brain. To assess the regenerative capacity of these progenitor cells, I treated mice with multiple cycles of CSF1R inhibition followed by withdrawal of inhibitors - each cycle consists of 7 days of inhibition followed by a 7- or 28-day withdrawal period. These studies determined that there is a limited capacity for microglial repopulation. However, this capacity can be expanded by increasing recovery time between cycles.

In addition, by increasing the exposure to CSF1R inhibitors, I have found that I can eliminate 100% of microglia from the adult brain, and that this results in a drastically altered repopulation pattern. Not only is the number of returning Iba1^{+} cells greatly diminished following complete microglial ablation, but cells initially only appear in white matter tracts along the rostral migratory stream (RMS) and projecting axons, and at early timepoints do not express the microglia-specific marker P2ry12. Eventually, these Iba1^{+} cells spread throughout the brain parenchyma, although cortical microglia numbers, even with extended time, do not reach those of control and continue to exhibit an altered RNA profile relative to control. These results not only highlight the presence of distinct microglial subtypes within the CNS and suggest multiple routes of

repopulation, but also reveal that we have an unprecedented level of control over CNS myeloid cells.

INTRODUCTION

A. Hematopoietic origins and development

Microglial ontogeny

Microglia are the primary immune cells of the CNS, acting as surveyors and responders in the event of damage or injury. Although they were first discovered by del Rio-Hortega in the 1930's, little was known about the origins of microglia until recently. It is now widely accepted that microglia are myeloid cells that derive from the yolk sac (YS) during development, but for decades the physical and temporal origin of these cells was unclear. A popular hypothesis was that adult microglia are derived from bone marrow (BM) hematopoietic cells. The concept of a "mononuclear phagocyte system" was proposed in the 1970s, grouping together BM promonocytes, blood monocytes, and tissue macrophages, with the belief that these cells have a common origin (van Furth et al., 1972). The hypothesis of a common lineage was supported with the finding that a clonogenic progenitor in the BM can give rise to monocytes, dendritic cells, and macrophages (Fogg et al., 2006). However, whether BM cells actively contribute to adult populations of tissue macrophages under normal conditions was unknown. Fate mapping studies with Cre recombinase reporter lines have been able to track YS progeny and more carefully characterize myeloid cell differentiation during development, and the maintenance of myeloid populations during adulthood. Results from these studies have shown that the vertebrate YS is the first site of hematopoiesis (El-Nefiawy et al., 2002; Ginhoux et al., 2010; Schulz et al., 2012). Hematopoietic progenitors in the YS begin expressing Runx1, a transcription factor known to be necessary for the differentiation of hematopoietic stem cells (HSCs), at E7.5 of mouse embryonic

development (Ginhoux et al., 2010) . The process of generating these progenitors in the YS is termed “primitive hematopoiesis,” and primarily contributes to microglia and some tissue macrophage populations (Langerhans and Kupffer cells). This first wave of hematopoiesis is sufficient in maintaining these adult populations without contribution from hematopoietic cells generated later in development (Ginhoux et al., 2010; Yona et al., 2013) .

Additional fate-mapping studies have further clarified the temporal development of primitive hematopoietic cells, as well as characterized the progenitors giving rise to different cell types. Erythro-myeloid progenitors (EMPs) are derived from YS blood islands or hemogenic endothelia, and as such, all progeny from these cells can be labeled by tamoxifen-inducible Tie2-Cre mice (Perdiguero et al., 2015). Studies using these mice have shown that EMPs labeled at E7.5 contribute to adult tissue-resident macrophages, including microglia, Langerhans cells, and Kupffer cells (Perdiguero et al., 2015), suggesting a common progenitor for microglia and peripheral macrophages. Further work has shown that although EMPs do appear to contribute to both microglia and peripheral macrophages, there are two waves of temporally distinct EMPs between E7.5 and E8.5. The first wave of EMPs occurs at E7.5 and contributes to YS macrophages, which directly give rise to microglia, without a monocytic intermediate (Hoeffel et al., 2015), while the second wave of EMPs generated at E8.5 migrate into the fetal liver to generate multiple myeloid lineages (i.e. skin, kidney, lung tissue macrophages) through a monocytic intermediate (Fig. 1). Therefore, there is a precise temporal distinction between derivation of microglia and peripheral macrophages from EMPs, further defined by whether cells go through a monocytic intermediate.

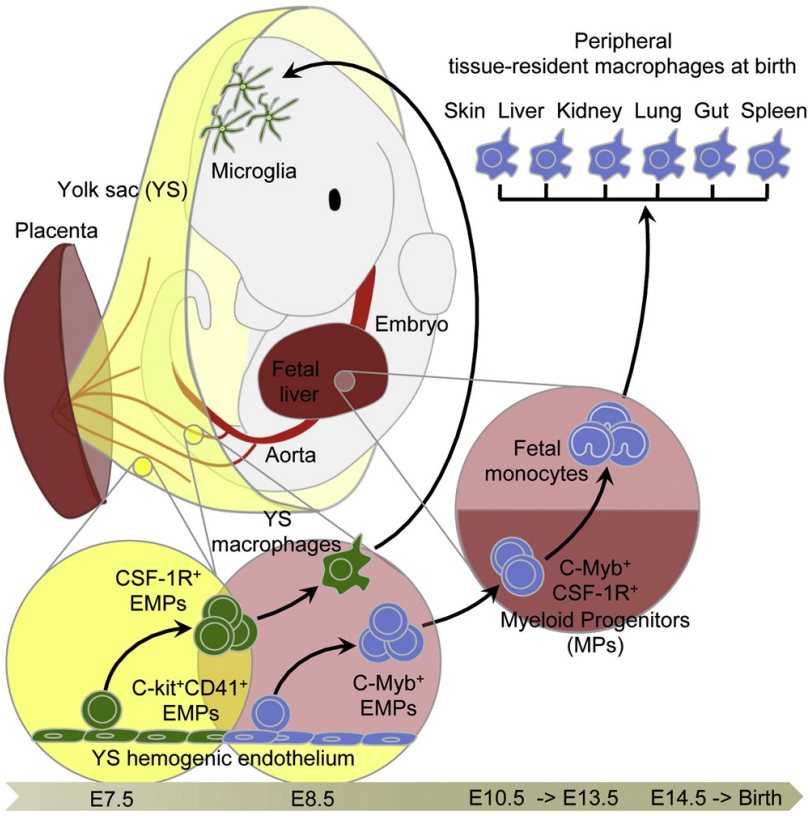

Figure 1. Graphical abstract demonstrating myeloid cell ontogeny. Fate mapping using Tie2-Cre mice has elucidated myeloid cell ontogeny. EMPs generated at E7.5 produce YS macrophages which directly colonize the brain to become microglia; EMPs generated at E8.5 migrate into the fetal liver, where they then produce fetal monocytes and subsequently peripheral tissue macrophages through a fetal monocyte intermediate (Hoeffel et al., 2015).

Interestingly, the brain is the first organ to be colonized with myeloid cells (Sorokin et al. 1992). At E8.5, YS-derived Runx1^{+} progenitors begin to colonize the brain through blood vessels (Ginhoux et al. 2010), but also in regions devoid of vascularization, possibly via ventricles and/or the meninges (Cuadros et al. 1993). These early myeloid cells in the CNS express canonical microglial markers such as CD45, CD11b, F4/80, and CX3CR1, starting at E9.5 (Ginhoux et al. 2010). Following this, the blood-brain barrier (BBB) forms around E13.5, which occurs concurrently with fetal monocyte release into the bloodstream. It has been postulated that the presence of early microglia in the CNS establishes a niche that helps prevent fetal liver-derived cells from infiltrating the brain (Ginhoux et al., 2013). Once the progenitors have colonized the brain, rapid proliferation occurs, resulting in the generation of ~95% of the total microglial population within two weeks of birth (Alliot et al., 1999). The resulting population of microglia is

primarily self-sustained for the remainder of the animal's lifetime (Lawson et al., 1992), and microglia maintain an autonomous population that is not replenished by peripheral monocytes or macrophages under normal conditions (Ajami et al., 2007).

As the origin of microglia and other macrophages has already been detailed here, when referring to the macrophages of the brain, it is important to note that the brain is also populated with non-parenchymal resident CNS macrophages, which exist in the brain in the perivascular space, meninges, and choroid plexus. For several years, it was believed that these cells are replenished by BM-derived cells throughout the lifespan of the animal (Hickey et al., 1992), but recent work has revealed that only choroid plexus macrophage are appreciably reconstituted by BM-derived cells under normal conditions in adulthood (Goldmann et al., 2016), showing that relative to microglia, meningeal, and perivascular macrophages, choroid plexus macrophages differ in the source of population maintenance. However, meningeal and perivascular macrophages also differ from microglia in morphology, expression profiles, and signal responses (Goldmann et al., 2016). Perivascular macrophages express increased levels of CD45, and, unlike microglia, express CD206 and CD36. Meningeal macrophages appear to maintain amoeboid morphologies, displace their cell bodies frequently during homeostastic conditions, and rely on Irf8, but not Myb (a classic transcription factor for myeloid cells) signaling for development (Goldmann et al., 2016). It is important to note that the YS also serves as a site of primitive hematopoiesis for some peripheral macrophages and that these macrophages begin circulating in the blood and colonize the embryo between E9.5-E10.5 (Schulz et al. 2012), after microglia begin colonizing the brain (Ginhoux et al. 2013).

Signals for microglia development/differentiation

In addition to a unique ontogeny, microglia follow different signaling pathways relative to HSC-derived macrophages for differentiation and development. HSCs, monocytes, and granulocytes are dependent on the expression of the transcription factor c-Myb for their differentiation during development (Soza-Ried et al., 2010; Schulz et al., 2012; Schulz et al. 2012). However, microglia and some peripheral tissue macrophages develop normally in the absence of c-Myb expression (Schulz et al., 2012). In contrast, Pu.1 is a transcription factor that is necessary for the differentiation of macrophages (DeKoter et al., 1998), but nonessential for HSC development (Dakic et al. 2005). These results further suggest that microglia and some tissue macrophages follow a developmental pathway that is distinct from HSC progeny.

As previously mentioned, Runx1 is a transcription factor necessary for the differentiation of microglia from progenitors, but additionally, signaling mediated by this transcription factor is essential for microglial proliferation (Samokhvalov et al., 2007). Studies indicate that the expression of Runx1 maintains microglia in an immature state – i.e. when microglia first appear in the developing brain, they display an amoeboid morphology, but upon downregulation of Runx1 expression, microglia become ramified, indicative of mature inactivated microglia (Zusso et al. 2012).

The CSF1R is expressed on myeloid-lineage cells and signaling through this receptor is known to be involved in the differentiation, proliferation, and migration of these cells in the periphery (Patel and Player, 2009). Intriguingly, mice lacking CSF1R are born without microglia, suggesting that this receptor is essential for their development (Erblich et al. 2011; Ginhoux et al. 2010). The CSF1R has two natural ligands – CSF1

and IL-34. Mice lacking either of its ligands also display reduced numbers of microglia in the brain (Wegiel et al. 1998), but it is not surprising that the loss of the CSF1 receptor has a more severe effect than the loss of the CSF1 ligand alone, likely due to compensatory signaling by IL-34 (Wang et al., 2012). However, IL-34 and CSF1 do not display similar expression patterns in the developing brain – IL-34 is very highly expressed in the postnatal brain, and is likely preferentially expressed in specific regions of the developing brain, as revealed by regional decreases of microglial numbers in IL-34 mutants (Wei et al. 2010).

B. Microglia vs. peripheral macrophage phenotypes

Although microglia are considered the resident macrophages of the brain, there are important distinctions that set them apart from their peripheral macrophage counterparts, besides their ontogenesis. Since monocytes have been shown to enter the brain and adopt a microglia-like morphology and phenotype under certain conditions (i.e. conditions in which the BBB integrity is compromised), the relative contribution of each particular cell type to disease states still remains unclear. Unfortunately, it has historically been nearly impossible to differentiate microglia from infiltrated monocytes, as there is almost complete overlap in phenotypic expression between microglia and the monocytes that have engrafted to differentiate into macrophages. Opportunely, several recent studies have identified unique microglial signatures through RNA profiling (Beutner et al., 2013; Chiu et al., 2013; Hickman et al., 2013; Butovsky et al., 2014; Bennett et al., 2016). Microglial specific genes include *Tmem119*, *Fcrls*, *Olfm13*, and *P2ry12*. Importantly, infiltrated monocytes that take up residence in the CNS and adopt

a microglia-like phenotype never adopt this expression profile (Butovsky et al. 2014). The identification of this profile allows more specific studies of the functional differences between microglia and infiltrated monocytes/macrophages.

Infiltration of peripheral monocytes

Whether microglia are replenished by infiltrating monocytes, and to what extent, is still a heavily contentious topic. Many models of BM transplantation, in which donor cells were shown to engraft in the host brain, have been criticized for their use of irradiation, which alone compromises BBB integrity and allows for peripheral cell leakage into the CNS. This confound has been addressed by the generation of chimeric mice through surgical parabiosis (Ajami et al., 2007). In these animals, ~50% blood chimerism was achieved, meaning blood generated by each animal circulated throughout both animals. In the absence of irradiation, and with or without a neural lesion, there was no significant infiltration of chimeric partner-derived cells into the brain parenchyma (Ajami et al., 2007).

Recent investigations would suggest that monocytes infiltrate into and effectively engraft in the brain parenchyma only under certain circumstances. For example, direct injection of donor BM cells into the host's circulation resulted in successful engraftment of donor cells into brain parenchyma (Hess et al. 2004; Echmann et al. 2001). In non-disease models, the injection of BM cells is necessary for engraftment, as chimeric mice achieved by parabiosis does not result in engraftment. These seemingly conflicting results illustrate the ability of BM progenitor cells to directly migrate to and engraft in the CNS parenchyma. The data suggest that these cells are not normally present in

circulation, and it is only by the artificial introduction of them into circulating blood that they are able to infiltrate the CNS effectively. Additionally, using a parabiosis model to assess donor-derived monocyte infiltration in a mouse model of multiple sclerosis (experimental autoimmune encephalomyelitis (EAE), it has been shown that CCR2 signaling recruited monocytes to the spinal cord during severe disease onset (Ajami et al., 2011). These studies found a correlation between disease severity and the relative number of infiltrated monocytes. Interestingly, monocytes first appeared near the meninges of the spinal cord, suggesting that infiltration is not necessarily due to BBB breakdown. In addition, monocytes engrafted into the CNS parenchyma, but all infiltrated donor-derived cells were absent 3 months later (Ajami et al., 2011). These data show that even in severe disease models (EAE specifically being a disease in which infiltration is characteristic and a correlate of disease severity), when infiltrating cells do enter the CNS parenchyma, they are short-lived and have not been shown to maintain the long-term microglial resident population (Ajami et al., 2011).

The specific dynamics of microglia population maintenance are largely unknown, but studies indicate that they have particularly low turnover in the uninjured brain (Lawson, Perry, and Gordon 1992). Interestingly, it has recently been revealed that many adult macrophage populations in the periphery are independently maintained without replenishment from hematopoietic stem cells (Sieweke and Allen 2013). In the periphery, populations of resident macrophage appear to be maintained by the indefinite dividing of macrophages. Thus, in the case of various peripheral tissues, macrophage turnover, similar to microglial turnover, appears not to be dependent on progenitors or replenishment from circulating monocytes (Sieweke and Allen 2013).

C. Normal microglial function and decline with aging and disease

Normal microglial immune function

Microglia “at rest” are highly dynamic cells, constantly extending and retracting processes to survey the local environment (Nimmerjahn et al., 2005). These immune cells sense insults in the local environment through a variety of different receptors, including pattern recognition receptors, purinergic receptors, and scavenger receptors expressed on their cell surface (Boucsein et al. 2003; Toyomitsu et al. 2012; Stolzing and Grune 2004; Cartier et al. 2005). Once a stimulus is detected, microglial responses to injury or insult are almost instantaneous – within minutes or seconds, microglia can orient themselves in response to chemotactic signaling (Davalos et al. 2005). Despite such efficient and varied responses, microglia are considered poor antigen-presenters. In their resting state, these cells do not express MHC I or II. However, upon activation, microglia can present MHC antigens, although not as effectively as dendritic cells (DCs) or their peripheral macrophage counterparts (Hayes et al., 1987; Hickey et al., 1992; Gehrmann et al., 1995).

Macrophage and microglial activation states have typically been described as either classical (M1, pro-inflammatory) or alternative (M2, anti-inflammatory), although this is likely to be an oversimplification and activation is probably more accurately represented by a spectrum of activation states. Upon presentation of a pathogen or injury, microglia initially secrete pro-inflammatory molecules (TNFα, IL-1β, ROS, etc.) to combat the invasive species and defend tissue (Colton and Wilcock 2010). Although this classical inflammatory state is necessary for ultimate resolution of the insult, the secretion of many pro-inflammatory molecules can be neurotoxic, especially when prolonged (Kraft

and Harry, 2011). This response, during acute injury, is subsequently followed by a repair and wound-healing phase, characterized by the secretion of anti-inflammatory molecules, such as IL-10 and TGFβ (Colton and Wilcock 2010).

Microglia express many different receptors and are able to respond not only to invading pathogens, but also to signals of tissue damage (Nimmerjahn et al., 2005), and as such, respond differentially depending on the insult. Pathogen- and damage/danger-associated molecular patterns (PAMPs/DAMPs) act as microglial activation signals through PRRs, such as toll-like receptors (TLRs) expressed on microglia. These TLRs help to initiate, execute, and regulate the immune response (Hanisch et al., 2008) . The expression of specific complement receptors by microglia are important for motility (C5a – (Nolte et al. 1996)), clearance of apoptotic neurons (Fraser et al., 2010) and the release of IL-6, TNFα, and NO (Schafer et al. 2000). ATP, released by dead or dying cells, can also act as a "danger" signal through microglial purinergic receptors, initiating secretion of cytokines and inflammatory proteins (Kettenmann et al. 2011). Conversely, it has been demonstrated that when responding to apoptotic cells, microglia may release anti-inflammatory signals (Savill et al. 2002; Gregory and Pound 2011; De Simone, Ajmone-Cat, and Minghetti 2004). In many cases, microglia respond to multiple competing signals, and the presence of multiple microglial activation states is often characteristic of chronic inflammatory disease (Colton and Wilcock 2010). Ultimately, because of the poor regenerative ability of the CNS, it is important that microglia quickly and thoroughly resolve issues that may arise, preventing further damage to the local environment.

Regional differences in microglial gene expression and proposed function

At first glance, microglia appear to be a homogeneous population with similar properties and functions throughout the brain, but upon closer inspection, intrinsic regional differences are revealed. Immunostaining of microglia with F4/80 revealed increased microglial densities in hippocampus and olfactory telencephalon compared to cortex and cerebellum, and an overall increase in density in gray matter areas compared to white (Lawson et al., 1990). This study estimated the percentage of microglial cells of total neural cells to vary between 5% in the cortex and corpus callosum, to 12% in the substantia nigra (Lawson et al., 1990). However, this method of quantification relies on equal immunoreactivity of all microglia to F4/80, and more recent studies utilizing CX3CR1-eGFP mice show a marked difference in immunoreactivity to canonical microglial markers (e.g. Iba1, P2ry12) between parenchymal and periventricular microglia along the RMS (Ribeiro Xavier et al., 2015). In fact, less than half of microglia lining the RMS stained positively for Iba1. This suggests that initial estimates of regional microglial densities may need to be reexamined, but also highlights differences in marker expression between regions.

Beyond apparent regional differences in microglia number, evidence suggests key variances in microglial phenotype between region. Morphologically, white matter microglia exhibit bipolar arborization, while gray matter microglia display radial processes (Lawson et al., 1990). These differences between white and gray matter extend beyond morphology, as microglia in white matter areas display greater basal expression levels of CD86 and MHC II than in the cortex (Styren et al., 1990; Sasaki and Nakazato, 1992; Gehrmann et al., 1993; Carson et al., 2007), suggesting a shift in

activation profile. Interestingly, during development, white matter areas, including the internal capsule and cerebral peduncle are the first to be colonized by microglia (Ueno et al., 2013). Additionally, differences in response to stimuli have been noted, with substantia nigral neurons appearing particularly susceptible to lipopolysaccharide, both *in vivo* and *in vitro*, mediated at least in part by increased density of, and total cytokine release by, microglia in this region compared to hippocampus and cortex (Kim et al., 2000).

A recurring finding in the study of regional differences in microglia is that white matter areas, including those surrounding subventricular zones (SVZs) and the RMS, host a unique phenotype of microglia as compared to the rest of the brain. In rats, isolated microglia from distinct regions of the brain show baseline differences in the expression of inflammatory molecules between the olfactory bulb (OB), substantia nigra, striatum, hippocampus, and amygdala – specifically, increased levels of CD68, IL-1β, and P2X7R in the OB (Doorn et al., 2015). SVZ/RMS microglia exhibit altered morphology, similar to activated microglia, with enlarged cell bodies and thick processes. One of the canonical markers of microglia is the purinergic receptor P2ry12, which allows microglia to sense neuronal damage through the release of ATP, and provokes extension of processes and subsequent microglial activation (Davalos et al., 2005; Haynes et al., 2006). However, although labeled by the CX3CR1-eGFP reporter line, many microglia along the RMS express diminished levels of canonical markers (Iba1, IB4, P2ry12) (Ribeiro Xavier et al., 2015). Upon further examination, microglia in this region were found to be unresponsive to ATP (possibly due to reduced expression of purinergic receptors), and did not appreciably phagocytose neuroblasts, with the exception of microglia in the OB

(Ribeiro Xavier et al., 2015). Cells along the SVZ/RMS are proposed to have a specific function in promoting neuroblast cell survival, and may assist in the migration of new neurons to the OB (Ribeiro Xavier et al., 2015). Moreover, microglia isolated from the SVZ have 20x the proliferative potential in vitro than any other region analyzed in the brain (Marshall et al., 2008). Altogether, these data demonstrate that some of the most distinct differences in microglial function by region lie in white vs. gray matter areas, and suggest that microglia may have region-specific functions.

Microglial communication with other CNS cell types

Microglia have a close relationship with other cell types - a major function of microglia is to protect neurons and maintain CNS homeostasis, which occurs through neuron-microglia cross-talk. In addition, neurons are thought to play an active role in maintaining microglia in a quiescent state. One of the mechanisms by which this is proposed to occur is through the CX3CR1-CX3CL1 signaling axis. Microglia express the receptor for the CX3CL1, a chemokine ligand expressed by neurons. Application of CX3CL1 *in vitro* to a co-culture of microglia and neurons reduced neuronal death via diminished inflammation (Zujovic et al., 2000; Mizuno et al., 2003), and CX3CR1 deficiency *in vivo* resulted in increased microglial activity (Cardona et al., 2006). Additionally, the immunoglobulin CD200 is constitutively expressed by neurons, the receptor for which is expressed by microglia (Wright et al., 2001), and has been shown to suppress immune function (Hoek et al., 2000). Although neurons appear to have a role in maintaining homeostasis, they are also capable of signaling to microglia to mount an immune response. Release of glutamate and matrix metalloproteinase-3 (MMP3) by

apoptotic neurons triggers an inflammatory response by microglia, resulting in secretion of pro-inflammatory molecules, such as TNFα and IL-1β (Cho et al., 2009).

Signaling between microglia and neuroblasts or basal progenitors (BPs) within the SVZ is reported to be reciprocal and nuanced. During development, clusters of microglia form around the SVZ just prior to the onset of neurogenesis (Monier et al., 2007), and it is believed that BPs recruit microglia to the SVZ via signaling through CXCL12 (released by BPs) and CXCR4/CXCR7 receptors (expressed by microglia) (Arno et al., 2014). Studies have shown that by depleting these BPs or reducing CXCL12 signaling, microglial homing to the SVZ is impaired (Arno et al., 2014). Additionally, development of BPs is also dependent on microglia, as evidenced by a decreased number of BPs in the constitutive CSF1R$^{-/-}$ mice. Microglia continue to influence the neurogenic niche into adulthood. Previous evidence has shown that microglia-conditioned media increases neuroblast production in SVZ tissue (Chen et al., 2006; Gemma and Bachstetter, 2013), an effect thought to be mediated by secreted IGF-1 and BDNF (Ziv and Schwartz, 2008). Activated microglia also have the capacity to either support or inhibit neurogenesis, depending on the stimuli and molecules secreted. Microglia cultured with either IFNγ or IL-4 effectively induced neurogenesis; microglia treated with LPS were also successful in increasing neurogenesis, but only upon neutralization of TNF-α (Butovsky et al., 2006).

Microglia have close relationships with brain macroglia (oligodendrocytes and astrocytes) as well. Both oligodendrocytes and their precursor cells respond to dynamic changes in microglial cytokine expression. Conditioned media from both Arg1- (considered anti-inflammatory) and iNOS-expressing (considered pro-inflammatory)

microglia increased proliferation of oligodendrocyte precursor cells (OPCs). However, Arg1-expressing microglia were shown to drive OPC differentiation into mature oligodendrocytes and prevent apoptosis of OPCs, which appears to be mediated by the TGFβ superfamily member Activin-A (Miron et al., 2013). It's hypothesized that the initial pro-inflammatory activation of microglia is needed during demyelinating injury in order to clear myelin debris (remyelination cannot occur without this clearance), but that remyelination is dependent on the switch from pro- to anti-inflammatory microglial phenotype (Miron and Franklin, 2014). Moreover, mature oligodendrocytes are susceptible to microglia-secreted proinflammatory cytokines as well, and have been shown to produce poor-quality myelin as a result of this inflammatory signaling (Pang et al., 2003; Peferoen et al., 2014).

Astrocytes are also very sensitive to changes in microglial activation. The microglial field has moved away from the labels "M1" and "M2" to denote a binary pro- and anti-inflammatory system, but astrocytes have been shown to have a relatively predictable reactivity profile that can be categorized as "A1" (harmful to neurons) and "A2" (neurotrophic). Both of these states are dependent on cytokines secreted by microglia. Upon release of IL-1α, C1q, and TNFα (a cocktail of classic pro-inflammatory cytokines), astrocytes take on an A1 phenotype, meaning they lose neurotrophic functions and contribute to neuronal death (Liddelow et al., 2017). This phenotype of astrocyte is commonly found in neurodegenerative tissue. Conversely, A2 astrocytes, generated in response to ischemia and a surrogate to the anti-inflammatory microglial state, exhibit a neuroprotective phenotype and promote tissue repair (Liddelow et al., 2017). These findings implicate astrocytes as an intermediary in tissue damage or

repair following injury, and suggest that microglia indirectly exert these effects through astrocytes.

Microglial dysregulation with aging and disease

Given the long lifespan of microglia in the CNS without replenishment from peripheral sources, it is not surprising that microglia have been shown to accumulate age-related deficiencies, such as telomere shortening and oxidative damage (Flanary and Streit 2004; Streit et al. 2008). Moreover, as senescence ensues, investigations have demonstrated that these cells become dysregulated in their inflammatory responses, including phagocytic efficiency and migratory abilities (Luo et al., 2010; Flanary et al. 2007). Previous studies have shown that microglia are the most changed of the glial cells with age (Streit and Xue 2010), which is likely due to the fact that they are very long lived. *In vitro* studies have shown that aged microglia actively internalize up to ~50% less material than young microglia (Njie et al. 2012; Floden and Combs 2006), indicative of reduced phagocytic efficiency. Aged microglia also exhibit functional and morphological changes at resting state and in response to injury or LPS (Godbout et al. 2005). In response to focal injury, aged microglia show a delayed acute reaction followed by a sustained response once the cells have locally aggregated, indicating that microglia are less effective initially and slower to return to a homeostatic phenotype (Damani et al. 2011). Aged microglia not only express lower levels of anti-inflammatory cytokines (such as IL-10), but they also express higher basal levels of activation markers (i.e. MHC II antigens) and neurotoxic pro-inflammatory cytokines (i.e. IL-6, TNFα) (Perry et al., 1993; Sierra et al., 2007) (Frank et al. 2006; Letiembre et al. 2007;

Ye and Johnson 1999). As mentioned previously, it is suggested that under normal conditions, signaling from neurons via CX3CL1 and CD200 helps to maintain microglia in a quiescent state, but levels of both of these molecules are diminished with age (Wynne et al. 2010; Frank et al. 2006), indicating a loss of homeostatic regulation with age.

Conditions that are associated with increased inflammatory cytokine expression and chronic inflammation are also associated with increased risk for Alzheimer's disease and other neurodegenerative disorders, suggesting a link between inflammation and neurodegeneration. Acutely activated microglia are beneficial for resolving injury and illness, but a chronically inflamed brain, due to the prolonged activation of microglia, can produce toxic levels of cytokines and other pro-inflammatory neurotoxic factors (Heppner et al., 2015; Theriault et al., 2015; van Rossum and Hanisch 2004). Acutely activated microglia have been shown to become dysregulated if they remain activated chronically, exhibiting exaggerated pro-inflammatory cytokine expression (von Bernhardi et al., 2010).

Alzheimer's disease is characterized by the presence of extracellular beta-amyloid (Aβ) plaques and intracellular neurofibrillary tau tangles. This accumulation in the brain suggests that 1) Aβ may be produced and secreted at a rate that cannot be controlled by microglia, 2) microglial phagocytosis is impaired, allowing for the accumulation of Aβ aggregates and subsequent plaques, or 3) a combination of both scenarios. β-amyloid has also been shown to directly induce microglial cytokine secretion (Dhawan et al., 2012).

In the Alzheimer's brain, activated microglia are found to be associated with Aβ plaques, indicating a potentially chronically activated state for as long as the plaques are present. In addition, there also appears to be a brainwide elevation of pro-inflammatory cytokines secreted by microglia, also reflective of a chronic inflammatory response in Alzheimer's disease (von Bernhardi et al., 2010; Wilcock et al., 2014). Given the dysregulation of aged microglia and their impaired phagocytic efficiency, an activated population of microglia throughout the brain could incite a cycle of inflammation, toxicity, and neuronal death.

D. CSF1 receptor signaling is necessary for microglia viability

It has recently been reported that administration of CSF1R inhibitors causes microglial cell death (Elmore et al. 2014). Treatment with 290 mg/kg in chow of PLX3397, a potent CSF1R inhibitor, was shown to reduce $IBA1^+$ cell numbers by more than 99% brainwide within 3 weeks (Fig 2). Remaining microglia during treatment exhibit larger cell bodies and increased process thickness typically associated with a more phagocytic phenotype (Neumann et al., 2009), and more efficient clearance of microglial debris. In this study, reduction of $IBA1^+$ cells was not merely due to a downregulation of the IBA1 microglial marker. Moreover, despite having lost their entire microglial compartment, CSF1R inhibitor- treated mice appear healthy and show no cognitive deficits in any task assessed (Elmore et al. 2014).

These data inform us that we can eliminate the entire microglial population in the adult brain with no detrimental effects. This is a unique tool which provides us with the exploratory ability to answer fundamental questions about microglial function,

homeostasis, and involvement in disease. My thesis will primarily pursue questions related to microglial homeostasis in the adult brain.

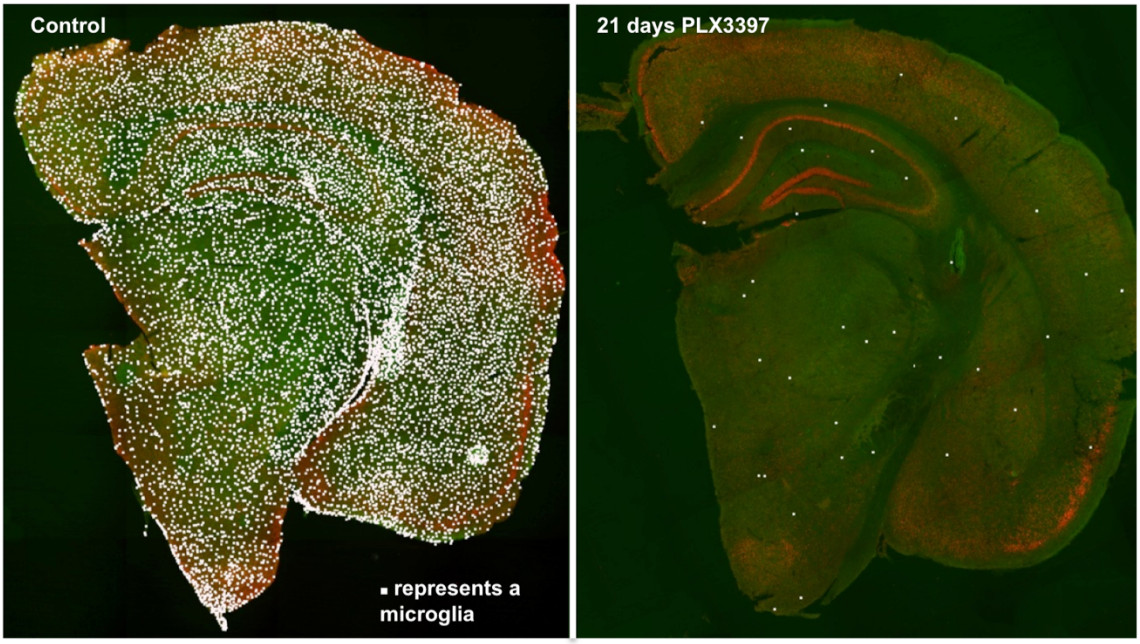

Figure 2. CSF1R Inhibition Eliminates Microglia from the Adult Brain 2 month-old wild-type mice (C57BL/6/129 mix; n = 4–5 per group) were treated with 290 mg/kg PLX3397 or control diet for 21 days. Half-brain from a control-treated mouse is shown on the left, and a PLX3397-treated mouse is shown on the right. Immunostaining for IBA1 was performed, and each microglia is represented by a white dot, superimposed via Imaris software. Microglial numbers are robustly decreased, with only a handful of remaining microglia after 21 days of treatment. (Elmore et al., 2014)

CHAPTER ONE

MICROGLIAL HOMEOSTASIS IN THE ADULT BRAIN

INTRODUCTION

Microglia colonize the CNS during development, originating from uncommitted c-Kit$^+$ EMPs found in the yolk sac (Hoeffel et al., 2015). These c-Kit$^+$ cells develop into CD45$^+$/c-Kit$^-$/ CX3CR1$^+$ YS macrophages that migrate to the CNS and differentiate into microglia. The development of these cells is dependent upon Pu.1 and Irf8 expression (Kierdorf et al., 2013), as well as the CSF1R (Erblich et al., 2011; Ginhoux et al.,2010). After migration of these progenitors to the CNS, the BBB forms, effectively separating the microglia from the periphery. Infiltration of peripheral monocytes or macrophages into the CNS does not occur under normal conditions (Mildner et al., 2007; Ginhoux et al., 2010), and thus microglia form an autonomous population.

The CSF1R is expressed by macrophages, microglia, and osteoclasts (Patel and Player, 2009), and it has two natural ligands: CSF1 and IL-34 (Lin et al., 2008). CSF1 regulates the proliferation, differentiation, and survival of macrophages (Patel and Player, 2009), with mice lacking either CSF1 or the CSF1R showing reduced densities of macrophages in several tissues (Li et al., 2006). Furthermore, CSF1R knockout mice are devoid of microglia (Erblich et al., 2011; Ginhoux et al., 2010) and die before adulthood. In the brain, it has been demonstrated that microglia are the only cell type that expresses the CSF1R under normal conditions (Erblich et al., 2011; Nandi et al., 2012).

Administration with CSF1R inhibitors (290 mg/kg PLX3397 in chow) is sufficient to cause microglial cell death, eliminating >90% of cells within 7-14 days of treatment. While we have determined that microglia remained eliminated for the duration of treatment, whether it be weeks or months, in this study, I wished to explore what would happen once the CSF1R inhibitor treatment was ended. We were provided with an unprecedented opportunity to explore if, and how, the brain responds to the absence of microglia and its associated signaling. Given the prior literature that microglia are long-lived cells with a low turnover rate in the normal brain (Lawson et al., 1992), and that under normal conditions microglia are not replenished by infiltration of peripheral cells (Ajami et al., 2007), I hypothesized that once microglia were eliminated with PLX3397, the adult brain would remain devoid of microglia. I also hypothesized that the handful of remaining microglia (~5% of microglia survive CSF1R inhibition treatment) during treatment would slowly proliferate, resulting in small clusters of microglia 28 days after removing the CSF1R inhibitors.

MATERIALS AND METHODS

Compounds

PLX3397 was provided by Plexxikon, Inc. and formulated in standard chow by Research Diets Inc. at 290 mg/kg.

Animal Treatments

All rodent experiments were performed in accordance with animal protocols approved by the Institutional Animal Care and Use Committee at the University of California,

Irvine. 2-18 month-old male and female mice were provided with PLX3397 in chow for 7-28 days. At the conclusion of experiments, mice were sacrificed via CO2 inhalation and perfused transcardially with 1X phosphate-buffered saline (PBS). Brains were extracted and dissected down the midline, with one half flash-frozen on dry ice for subsequent RNA and protein analyses, and the other half drop-fixed in 4% paraformaldehyde (PFA) in 1X PBS. Fixed brains were cryopreserved in a 30% sucrose solution, frozen, and sectioned at 40 mm on a Leica SM2000 R sliding microtome for subsequent immunohistochemical analyses. For BrdU labeling experiments, BrdU (Invitrogen) was administered IP at 10ml/kg BW and mice sacrificed 5 or 24 hours later. CCR2-RFP mice were obtained from Jackson Laboratory and aged to 1-month old. Mice were treated with either PLX3397 or vehicle for 7 days to deplete microglia, and then PLX3397 withdrawn, to stimulate repopulation (n=4/group). Five days later mice were sacrificed and their brains examined for RFP expression in repopulating cells.

Immunoblotting

Brain homogenates and immunoblotting were prepared as previously described (Green et al., 2011). Antibodies and dilutions used in this study include: nestin (1:1000; Millipore), CCR2 (1:1000; Abcam), CSF1R (1:1000; Cell Signaling), and GAPDH (1:10,000; Sigma-Aldrich). Quantitative densitometric analyses were performed on digitized images of immunoblots with Image J (NIH).

Confocal microscopy

Fluorescent immunolabeling followed a standard indirect technique (primary antibody followed by fluorescent secondary antibody), as previously described (Neely et al., 2011). Cell counts were obtained by scanning regions at 10X at comparable sections in each animal, followed by automatic analyses using Bitplane Imaris 7.4. Acid pretreatments were used for BrdU detection. Primary antibodies used include: anti-IBA1 (1:1000; Wako), anti-IB4 lectin (1:200; Invitrogen), anti-GFAP (1:1,000; Abcam), anti-BrdU (1:1000; Abcam), anti-CD45 (1:100; Abcam), anti-nestin (1:1000; Millipore), anti-CD34 (1:1000; Abcam), anti-Ki67 (1:1000; Abcam), anti-c-Kit (1:1000; Abcam), anti-Pu.1 (1:1000; Cell Signaling), anti-CCR2 (1:1000; Abcam), anti-CSF1R (1:1000; Cell Signaling). Stained tissue was mounted on slides and coverslipped with Dapi Fluoromount-G (SouthernBiotech).

mRNA Extraction and Microarray

Total mRNA was extracted from frozen half brains using an RNeasy Mini Kit (Qiagen). RNA was purified, and quality was verified using the Agilent BioAnalyzer (Agilent Technologies). Microarrays were processed at the University of California Irvine DNA and Protein MicroArray Facilitiy (UCI Core), using Affymetrix Mouse gene 2.0 microarrays, using a robotic system and following manufacturer's recommendations. Microarrays were assessed for quality by using Affymetrix Expression Console software, following sample and chip quality guidelines from Affymetrix. Probe Logarithmic Intensity Error (PLIER) values were calculated from raw CEL files using Expression Console v1.1 software (Affymetrix) to give expression values. Significance

was calculated using Cyber T (Kayala and Baldi, 2012) and ranked via probabilities of differential expression (PPDE) values.

Statistics

Statistical analysis of data employed the unpaired student T-test to compare between treated and control groups. When multiple comparisons were assessed, one-way ANOVA with post-hoc Newman-Keuls Multiple Comparison Test analysis was performed (Graphpad Prism 5). For all analyses, statistical significance was accepted at $p<0.05$; trends at $p<0.10$.

RESULTS

Microglia repopulate the adult brain after recovery from CSF1R inhibitor treatment

In order to explore the homeostasis of microglia in the adult brain, 18 month-old wild-type mice were treated with PLX3397 for 28 days to eliminate microglia. After 28 days of treatment, all mice were switched to control chow, and sacrificed at one of the following time points: 0, 3, 7, 14, and 21 days later to assess the state of the microglial compartment and determine if any proliferative events had occurred (n=4 per group; Fig. 1.1A). Remarkably, within 3 days of removing the inhibitors, $IBA1^+$ cells appeared throughout the brain, albeit with very different morphologies to resident microglia in control brains (Fig. 1.1B, D). The somas of these new cells appeared much larger, with shortened and thickened processes. By 7 days' recovery, the total number of microglia exceeds beyond that of control mice, with an intermediate morphology between that of

the cells seen at 3 days and microglia in a control-treated brain (Fig. 1.1B-H). By 14 days' recovery, microglial numbers stabilize to untreated levels, and the new cells assume a normal ramified morphology. Thus, the microglia-depleted brain is rapidly repopulated through increases in cell numbers, resulting in an intermediate population of amoeboid cells. The cells seen at the 3-day recovery time point are unique, in that they are grossly larger than resident control-treated microglia (Fig. 1.1I), and they arrange themselves throughout the CNS evenly, rather than in discrete locations (Fig. 1.2). Curiously, we also found that these cells express a number of unique markers not seen in microglia in control brains, nor in surviving microglia in PLX3397-treated brains (Fig. 1.1J). They are very strongly positive for the lectin IB4, as well as CD45. Many of these cells are $Ki67^+$, indicative of active proliferation, and $CD34^+$ (a marker of HSCs). Approximately 10% of $IBA1^+$ cells at 3 days of recovery stain positively for c-kit, another HSC marker. The majority of these cells are also $nestin^+$, a surprising finding given that microglia are derived from a myeloid lineage and nestin is a neuroectodermal marker. However, at day 7, $IBA1^+$ cells are negative for CD45, IB4, CD34, c-kit, nestin, and Ki67, they assume a more typical microglia morphology, and have repopulated the entire CNS. By 14 days of recovery, $IBA1^+$ cells appear morphologically indistinguishable from microglia in untreated brains, and cell numbers are comparable to controls (Fig. 1.1H). Furthermore, mRNA profiling of CSF1R inhibitor-treated brains shows loss of microglia markers with treatment, consistent with microglia elimination, followed by recovery consistent with repopulation (Fig. 1.7A-C). Thus, these results

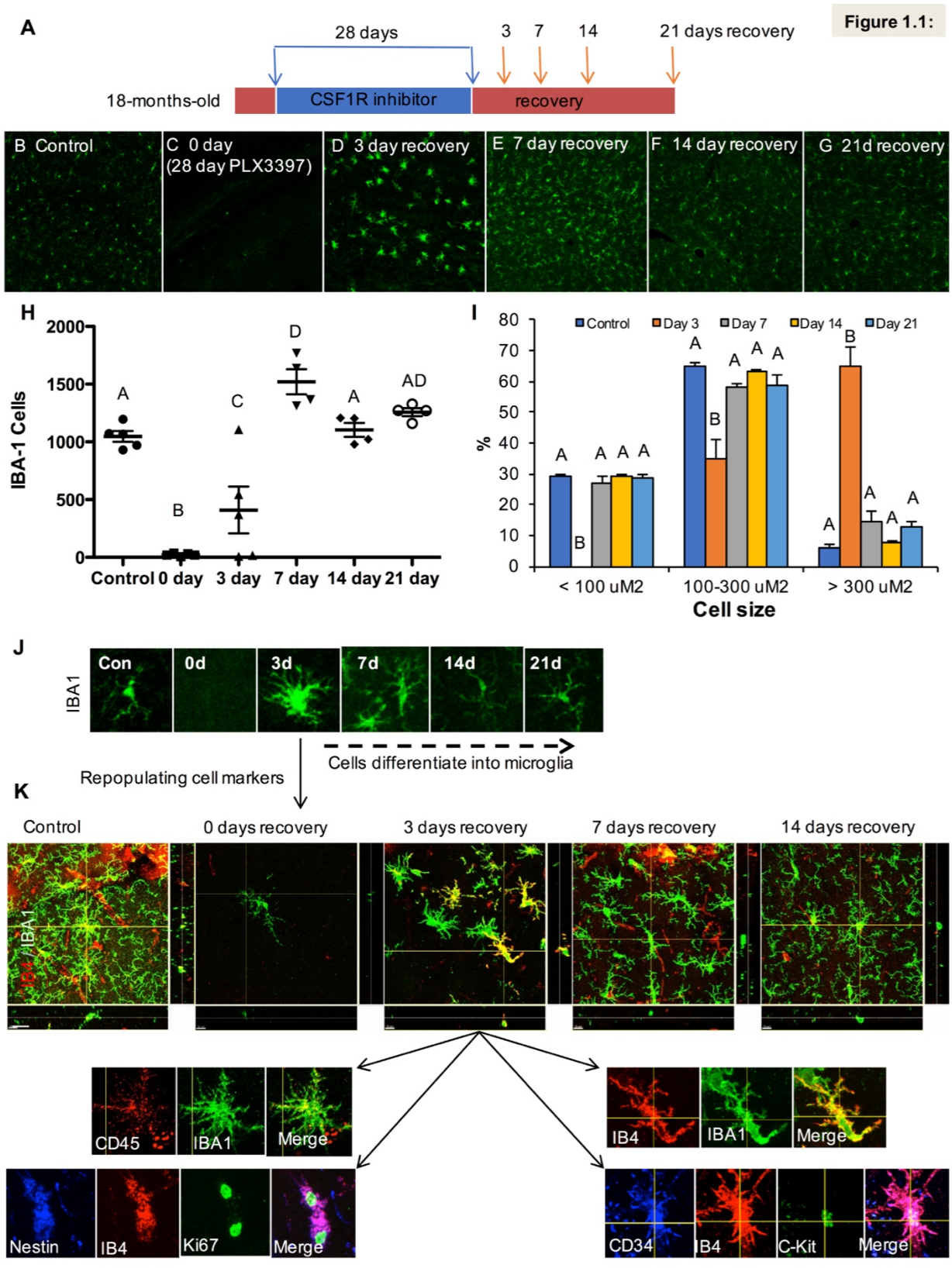
A
28 days
3
7
14
21 days recovery
18-months-old
CSF1R inhibitor
recovery
B Control
C 0 day
(28 day PLX3397)
D 3 day recovery
E 7 day recovery
F 14 day recovery
G 21d recovery
H
IBA-1 Cells
2000
1500
1000
500
0
A
B
C
D
A
AD
Control 0 day
3 day
7 day
14 day
21 day
I
Control
Day 3
Day 7
Day 14
Day 21
%
80
70
60
50
40
30
20
10
0
< 100 uM2
100-300 uM2
> 300 uM2
Cell size
J
IBA1
Con
0d
3d
7d
14d
21d
Repopulating cell markers
Cells differentiate into microglia
K
Control
0 days recovery
3 days recovery
7 days recovery
14 days recovery
IBA1 / IBA1
CD45
IBA1
Merge
IB4
IBA1
Merge
Nestin
IB4
Ki67
Merge
CD34
IB4
C-Kit
Merge

Figure 1.1:

Figure 1.1. Rapid repopulation of the microglia-depleted brain with new cells that differentiate into microglia. ***A,*** 18-month-old wild-type mice were treated with PLX3397 for 28 days to deplete microglia. Inhibitors were withdrawn, and groups of mice sacrificed 0, 3, 7, 14, and 21 days later (n = 4–5 per group). ***B–G,*** IBA1 immunostaining revealed microglia throughout the untreated (control) brains (***B***) and elimination of microglia in mice treated with PLX3397 (***C***). New $IBA1^+$ cells appeared throughout the CNS at the 3-day recovery time point with different morphologies to control resident microglia (***D***). Cell numbers increased by the 7-day recovery time point, and the morphology of the cells begin to appear more ramified (***E***). By 14 days of recovery (***F***) and 21 days of recovery (***G***), the $IBA1^+$ cells appear ramified and have fully repopulated the CNS. ***H,*** Quantification of the number of $IBA1^+$ cells in the hippocampal field. ***I,*** Analysis of cell body size. $IBA1^+$ cells at the 3-day recovery time point are larger than resident microglia. The size of these cells normalizes over the following recovery time points. ***J,*** Cells at the 3-day recovery time point express a number of unique markers, including CD45, nestin, Ki67, CD34, and c-Kit. They also show high immunoreactivity to the IB4 lectin. Cells in control brains and at the 7-, 14-, and 21-day recovery time points are negative for all these markers. Same capital letter(s) above conditions (***H*** and ***I***) indicates no significant difference ($p > 0.05$) via one-way ANOVA with post hoc Newman-Keuls multiple comparison test. Error bars indicate SEM. Scale bar represents 20 mm. (Elmore et al. 2014)

indicate that the adult brain has a highly plastic and dynamic microglial population and is capable of fully repopulating itself following microglial elimination, even in the aged brain.

CSF1R inhibition eliminates microglia

Given the rapid repopulation of the brain with new cells following CSF1R inhibitor-mediated microglial elimination and subsequent drug withdrawal, we wished to ascertain whether microglia were truly eliminated with CSF1R inhibition, rather than downregulating their microglial signature (i.e. cell surface expression). If CSF1R inhibition were causing a loss of microglial cell identity, explaining their disappearance when probed with myeloid markers, then the subsequent withdrawal of the drug could allow them to regain their microglial identity, explaining the rapid repopulation that we observe. To address this possibility, we crossed CSF1R-iCRE mice with Rosa26YFP reporter mice to generate offspring that express YFP in all CSF1R expressing cells under control of the Rosa26 locus (Fig. 1.3A). As such, these mice express YFP in all microglial progeny, as well as any potential cells that have differentiated from microglia. Accordingly, immunolabelling for microglia with IBA1 and YFP indicates that the expression of YFP is restricted to the microglial compartment (Fig. 1.3B), and that both

Figure 1.2:

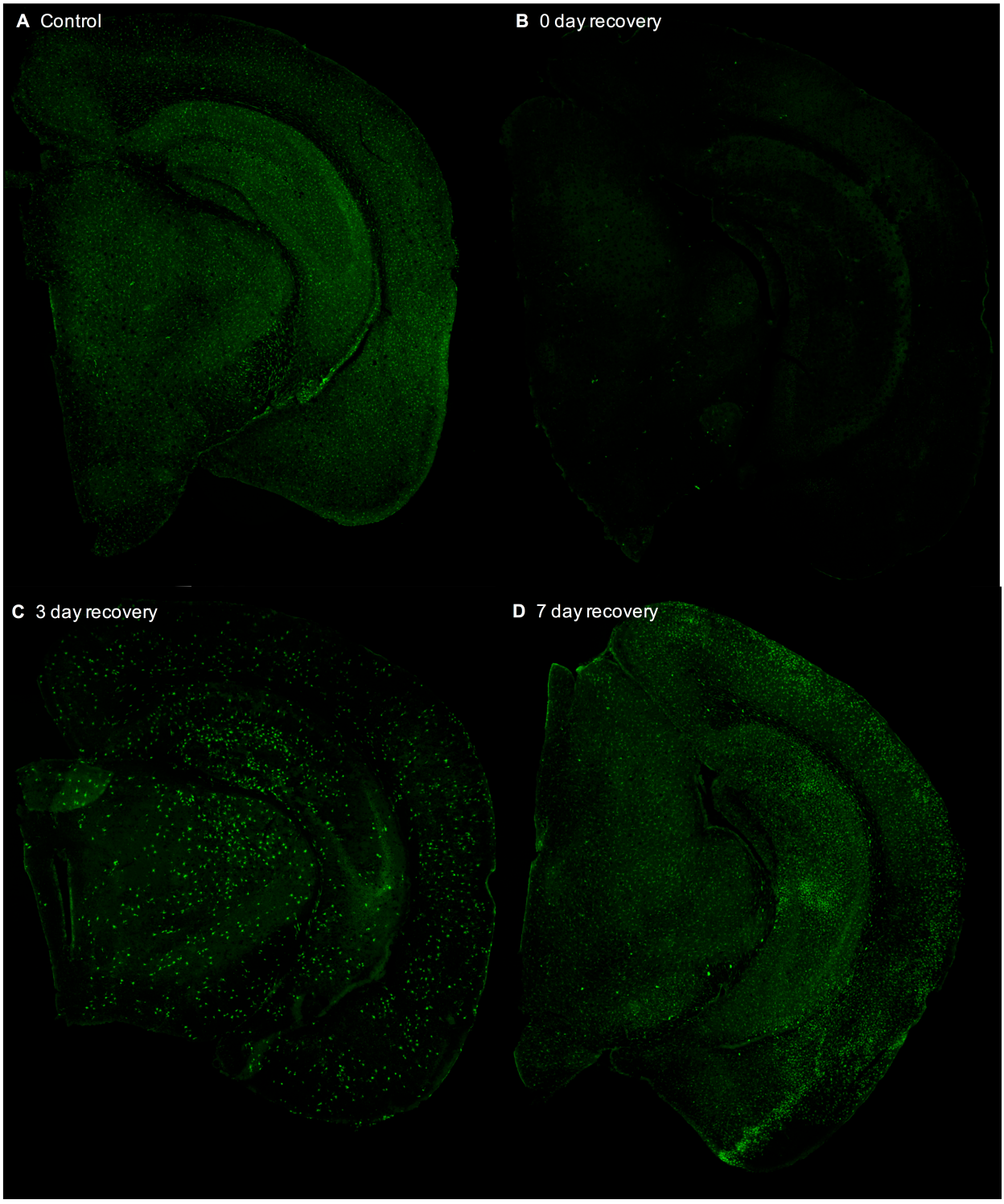

Figure 1.2. Microglial repopulation occurs evenly throughout the brain. Representative brain stiches from Figure 4 stained with anti-IBA1 – control (***A)*** 28 days treated with PLX3397 (n=4/group) ***(B)***, 3 days recovery ***(C)***, and 7 days recovery ***(D)***. Repopulating microglia shown in ***(C)*** appear throughout the CNS rather than in discrete locations. (Elmore et al. 2014)

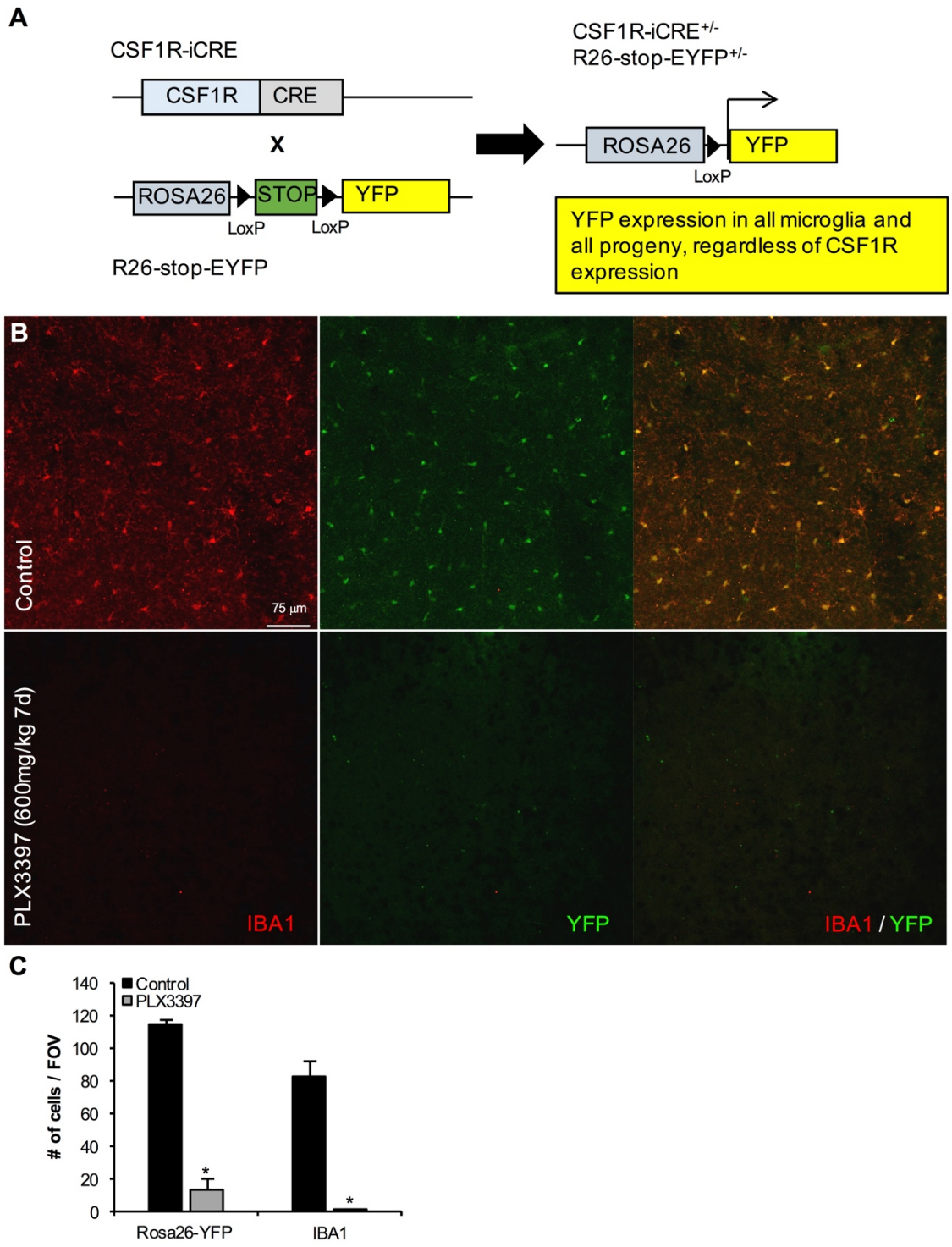

Figure 1.3

Figure 1.3. Treatment with the CSF1R inhibitor PLX3397 eliminates microglia in Rosa26-YFP mice. 2-month old mice were treated with PLX3397 (600 mg/kg) for 7 days to eliminate microglia (n=4/group). ***A,*** Schematic of the breeding strategy to yield offspring with YFP-expressing microglia. ***B,*** Immunolabeling for microglia (IBA1 in red) and expression of YFP in $CSF1R^{+}$/derived cells (YFP in green). ***C,*** Quantification of the number of YFP+ and IBA1+ cells is reduced in the cortex by 88% ($P<0.0001$) and 99% ($P<0.0001$), respectively, with PLX3397 treatment. Statistical significance is denoted by *$P<0.05$. Error bars indicate SEM (N=4/group). (Spangenberg et al., 2016)

IBA1$^+$ and YFP$^+$ cells are eliminated with PLX3397 treatment. Quantification of YFP and IBA1 expression revealed an 88% and 99% reduction in cell number with PLX3397-treatment, respectively (Fig. 1.3C). This conclusively demonstrates that treatment with the CSF1R inhibitor PLX3397 eliminates microglia in the adult mouse brain, rather than simply causing a transient loss of microglial signature.

Microglial repopulation does not occur from peripheral cells

Given the observation that new cells rapidly appear within the microglia-depleted brain which then appear to differentiate into microglia, we next set out to explore where these newly repopulated cells came from. Since the 3-day recovery cells express CD34, an HSC marker, this indicated that these new cells may originate from peripheral HSC sources. We therefore set out to discern if infiltration of peripheral cells were contributing to repopulation. To that end, two experiments were performed. Firstly, we set out to establish if repopulation would still occur while peripheral CSF1 receptors are inhibited with a compound that does not cross the BBB, PLX6668. If microglial repopulation is due to peripheral infiltration, repopulation would not be able to occur while the peripheral CSF1 receptors were inhibited. Two-month old wild-type mice were treated with 290 mg/kg chow PLX3397 for 14 days to deplete microglia. At this point, PLX3397 was replaced with either 75- or 200 mg/kg PLX6668 chow (n=3 per group; Fig. 1.4A). Three days later, mice were sacrificed and half-brains taken for mRNA analyses, and repopulation assessed. Repopulation (as assessed by mRNA levels of *Aif1, Csf1R, Trem2,* and the microglial-specific markers *Siglech, Tmem119)* occurred in the control- and both PLX6668-treated groups, but not in the continued PLX3397-treated group (Fig 1.4B). Therefore, while the peripheral CSF1 receptors were blocked

with PLX6668, the brain was still able to repopulate itself with new microglia. From these findings, we conclude that repopulation does not occur from peripheral cells, and therefore must occur from within the CNS. Nevertheless, we set out to confirm via an alternate approach if infiltration of monocytes could represent a source of repopulating

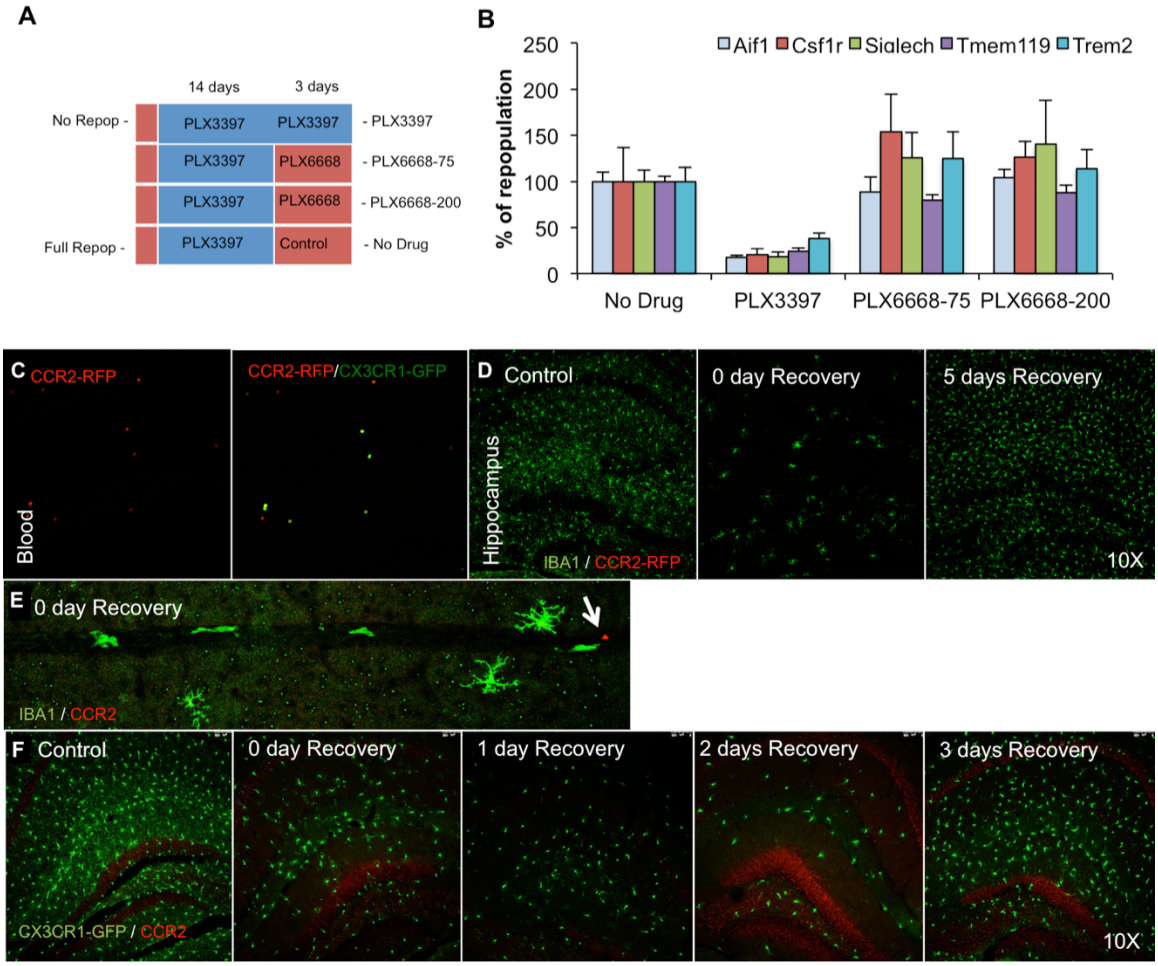

Figure 1.4. Repopulation does not occur from peripheral cells. ***A,*** 2 month-old wild-type mice were treated for 14 days with 290 mg/kg chow PLX3397 to deplete microglia (n=4/group). This was then replaced with CSF1R inhibitors that do not cross the blood brain barrier (PLX6668). ***B,*** mRNA levels for *Aif1, Csf1R*, *Siglech*, *Tmem119, and Trem2*, normalized to control chow (i.e., normal repopulation), show repopulation occurs in all PLX6668-treated groups. ***C,*** Blood from a CCR2-RFP$^{+/-}$/CX3CR1-GFP$^{+/-}$ mouse shows RFP expression in the monocytes, as expected. ***D-F,*** 1 month-old CCR2-RFP$^{+/-}$ mice were treated with PLX3397 or vehicle for 7 days (n-4 per group). A third group was placed on PLX3397 for 7 days and then the drug withdrawn for 5 days to stimulate repopulation (n=4). Brain sections were stained for IBA1 and imaged, with the hippocampal region shown. No RFP expression was seen in any of the repopulating cells or anywhere else in the parenchyma of the brain. ***E,*** A single RFP cell was found within a blood vessel of the cortex of one of the animals, highlighted by the arrow. ***F,*** Brain sections from CX3CR1-GFP$^{+/-}$ mice that had undergone repopulation for 1, 2, and 3 days after drug withdrawal were stained for CCR2. No CCR2 expression was seen in any repopulating cells at any time point, though it was observed in neuronal bodies. Error bars indicate SEM. (Elmore et al., 2014)

cells. We treated CCR2-RFP$^{+/-}$ mice with PLX3397 for 7 days, then withdrew the drug for 5 days to stimulate repopulation (n=4 per group). We confirmed that monocytes specifically expressed RFP in these mice, as described by Saederup *et al*., by analyzing the blood of these animals (sample shown is obtained from a CCR2-RFP$^{+/-}$ x CX3CR1-GFP$^{+/-}$ mouse; Fig. 1.4C). However, upon examination of the CNS, we were unable to find substantial numbers of RFP-expressing cells in control, microglia-depleted, or repopulated animals (Fig. 1.4D) despite robust microglial repopulation, confirming that monocytes do not contribute to repopulation. We were able to find a handful of RFP^{+} cells in the 12 brains examined, but these always appeared to be within blood vessels (Fig. 1.4E). I also performed immunostains for CCR2 in repopulating brains at 0, 1, 2, and 3 days recovery, in the event that monocytes were able to enter the CNS and then rapidly differentiate into microglia by the 5-day time point in the experiment described previously (Fig. 1.4F). While neurons stained positively for CCR2 (which has been previously reported (Banisadr et al. 2005; van der Meer et al. 2000)), none of the repopulating IBA1^{+} cells stained positively for CCR2. Additionally, I performed stains for T-cells (anti-CD3) and dendritic cells (anti-CD11c), but found no evidence for either cell type in the repopulating brains (data not shown). Importantly, a recent study has also recapitulated these results by showing microglial repopulation in organotypic slice culture, which lack a periphery (Valdearcos et al. 2014). Thus, these experiments clearly demonstrate that repopulation of the microglia-depleted adult CNS does not occur from peripheral sources, and must occur from within the CNS.

Early microglial repopulation events highlight robust nestin-expressing cells

Having ruled out contributions of peripheral cells to repopulation of the microglia-depleted brain, I next set out to explore the events that occurred during early repopulation, between drug withdrawal (0 day recovery) and the 3-day recovery time point, when we had observed cells first appearing. We treated 2 month-old CX3CR1-GFP$^{+/-}$ mice with PLX3397 for 7 days, and then withdrew the drug for 0, 1, 2, or 3 days (n=4 per group; Fig. 1.5A). Treatment with PLX3397 for 7 days resulted in elimination of 50-70% of microglia in these mice (Fig. 1.5B-C). Microglia remained absent until day 2 of recovery, but by day 3, the microglia population had quadrupled from that of day 2 (Fig. 1.5H). These data highlight a period of 48-72 hours during which critical events occur for microglial repopulation, which is consistent with the results from the 18 month-old mice (Fig. 1.1). PK measurements of PLX3397 concentration in brain tissue revealed that the drug was quickly cleared from the brain within 24 hours of withdrawal, with only trace amounts detected by 1-day recovery (Fig. 1.5I). Thus, microglia continue to be eliminated for at least 24 hours in the absence of drug. I also performed flow cytometry for GFP^{+} cells from the liver and spleen to examine the effects of CSF1R inhibition in the periphery (Fig. 1.5G). GFP^{+} cell numbers in the liver were not changed with either treatment or repopulation; reductions were seen in the spleen by day 2 of recovery, but numbers increased again the following day. In accordance with Figure 2J, microglia were strongly positive for IB4 at both the 2- and 3-day recovery time points (Fig. 1.6A), but curiously, in this younger cohort of animals, repopulating cells were negative for CD34 and c-Kit (data not shown). Additionally, I explored the expression of Pu.1, a microglial transcription factor important for differentiation of myeloid lineage cells from progenitors (Kueh et al. 2013), and found that Pu.1 staining is markedly increased

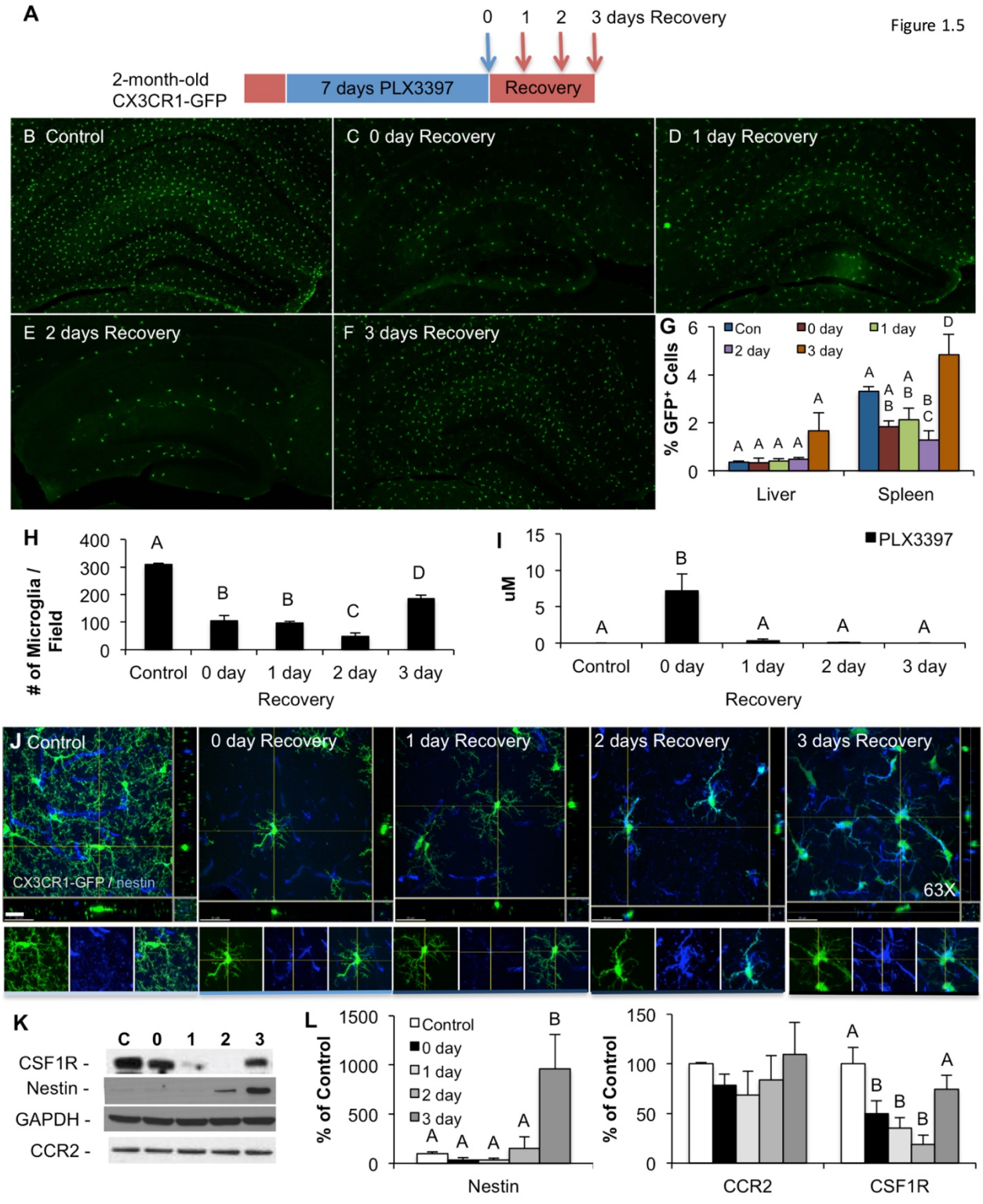
A
0 1 2 3 days Recovery
2-month-old
CX3CR1-GFP
7 days PLX3397
Recovery
B Control
C 0 day Recovery
D 1 day Recovery
E 2 days Recovery
F 3 days Recovery
G
% GFP+ Cells
Con
0 day
1 day
2 day
3 day
Liver
Spleen
H
# of Microglia / Field
Control
0 day
1 day
2 day
3 day
Recovery
I
uM
PLX3397
Control
0 day
1 day
2 day
3 day
Recovery
J Control
0 day Recovery
1 day Recovery
2 days Recovery
3 days Recovery
CX3CR1-GFP / nestin
63X
K
C 0 1 2 3
CSF1R -
Nestin -
GAPDH -
CCR2 -
L
% of Control
Control
0 day
1 day
2 day
3 day
Nestin
% of Control
CCR2
CSF1R

Figure 1.5

Figure 1.5. Microglial repopulation occurs between 48 and 72 hr after CSF1R inhibitor withdrawal. ***A,*** To investigate early repopulation events, 2-month-old CX3CR1-GFP$^{+/-}$ mice were treated with PLX3397 for 7 days. The inhibitor was then withdrawn, and groups of mice were sacrificed 1, 2, and 3 days later (n = 4/group). ***B-F,*** Representative sections shown from the hippocampus of each of these groups, in which microglia express GFP. ***G,*** Flow cytometry of GFP^{+} cells from the liver and spleen of these animals. Con, control. ***H,*** Quantification of whole-brain sections for microglial numbers shows a reduction of ~70% with 7 days of PLX3397 treatment. Microglial numbers continue to decline for 2 days after inhibitor withdrawal but rapidly recover between days 2 and 3. ***I,*** Brain levels of PLX3397 show rapid clearance of the drug from the CNS. ***J,*** GFP^{+} cells strongly express nestin at the 2- and 3-day recovery time points. 63X Z-stacks obtained by confocal microscopy and maximal projections are shown. Scale bar represents 20 μm. Separate channels and merge are shown for each of the time points in the panels below. ***K,*** Western blots of whole-brain homogenates show significant increases in nestin and CSF1R with repopulation, but no changes in CCR2. ***L,*** Quantification of ***K*** normalized to glyceraldehyde-3-phosphate dehydrogenase (GAPDH) as a loading control. Same capital letter(s) above conditions ***(G, H, I, and L)*** indicates no significance ($p > 0.05$) via one-way ANOVA with post hoc Newman-Keuls multiple comparison test. Error bars indicate SEM. (Elmore et al. 2014)

in microglia at the 2- and 3-day recovery time points (Fig. 1.6B). Similarly to the 18 month-old mice, repopulating microglia were also strongly positive for nestin at the 2- and 3-day recovery time points (Fig. 1.5J), while no expression was seen in the other groups. Indeed, Western blot of whole brain homogenates revealed ~1000% increase in steady state levels of nestin at day 3 of recovery (Fig. 1.5K and quantified in L). I next probed for steady state levels of CSF1R via Western blot, and found them to be reduced at recovery days 0, 1, and 2, but restored by recovery day 3. Additionally, levels of the monocyte marker CCR2 revealed no changes via immunoblot (Fig. 1.5K, L), corroborating that repopulation does not occur from peripheral monocytes.

Figure 1.6

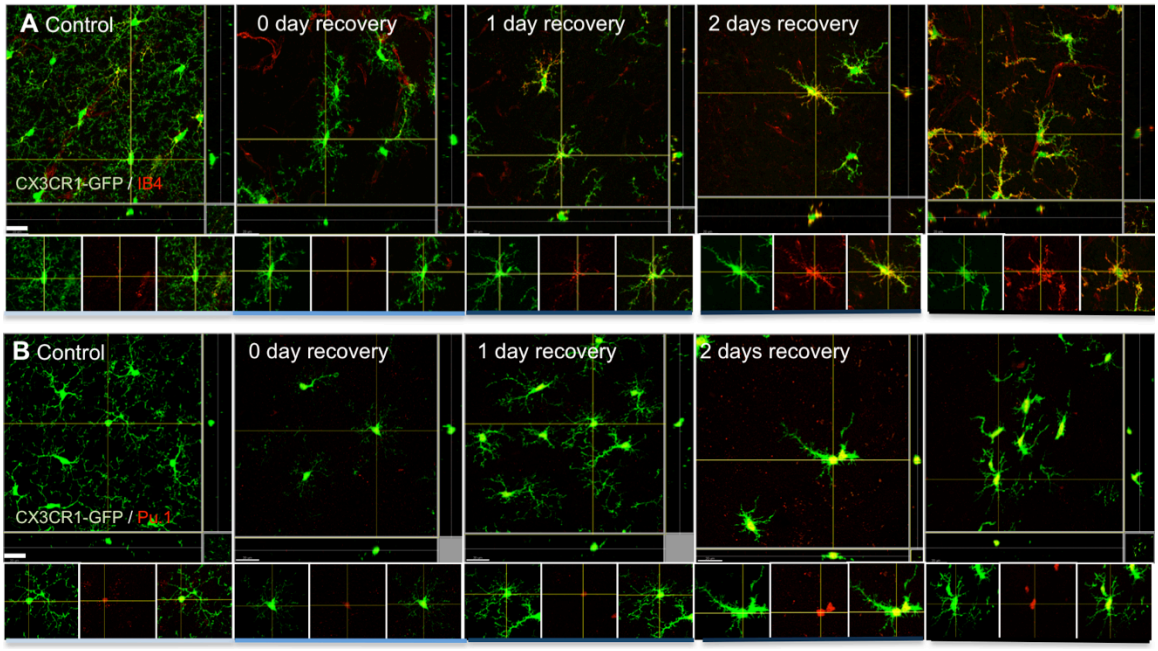

Figure 1.6: IB4 reactivity and Pu.1 expression in repopulating microglia. 2 month-old CX3CR1-GFP$^{+/-}$ mice were treated with PLX3397 for 7 days. The inhibitor was then withdrawn and groups of mice sacrificed 1, 2, and 3 days later (n=4 per group). A) GFP^{+} cells strongly bind the IB4 lectin at the 2-and 3-day recovery time points. B) GFP^{+} cells also strongly express the transcription factor Pu.1 at the 2- and 3-day recovery time points. 63X Z-stacks were obtained by confocal microscopy and maximal projections are shown. Separate channels and merge are shown for each of the time points in the panels above. Scale bar represents 20 μM. (Elmore et al. 2014)

Repopulation occurs from a resident microglial-progenitor cell in the CNS

To gain insight into the origin(s) and properties of repopulating cells, I conducted microarray analysis of mRNA extracted from whole-brain homogenates of control and recovery days 1 and 3. I selected recovery day 1 rather than day 0, as it is a time point at which microglia are eliminated, but the drug is no longer in the system (Fig. 1.5H, I). Significant changes in gene expression were determined by Cyber T analysis and ranked in order of significance, with the top 30 differentially expressed genes shown in Fig 1.7A-C. Reductions in known microglial-associated genes were the most commonly changed genes in the 1-day recovery group compared to controls, including the recently

identified microglial-specific genes *p2ry12*, *p2ry13*, *Siglech*, and *slc2a5* (Gautier et al., 2012; Chiu et al., 2013). Additionally, microglial-associated genes *Csf1R*, *ITGAM,* and *CX3CR1* were reduced. To build a gene expression profile of the repopulating brain and cells, we compared both day-1 recovery (microglia remain depleted) and control brains to day-3 recovery (repopulation has just begun to occur). In both comparisons, increases in gene expression associated with cell proliferation and cell cycle control were highly prevalent (Fig. 1.7B, C), including *mki67*, as well as *Ube2c*, *Ccna2*, *Prr11,* and *Top2a*. Thus, the expression profile of the repopulating brain supports the notion that repopulation is dependent upon proliferation.

Additionally, I compared levels of myeloid gene expression in recovery day 1 (microglia-depleted) against recovery day 3 (repopulating) (Fig. 1.7D). Myeloid genes were increased, as expected. However, I found several microglial-specific genes to be significantly increased, which are not expressed in peripherally derived macrophages, including *F11r*, *Gpr165, Gpr84*, *Olfml3*, *Serpine2*, and *Siglech* (Chiu et al. 2013; Gautier et al. 2012). The microglial-specific gene *Tmem119* was not detected via microarray; however, Real Time PCR of mRNA extracted from 3-day repopulating brains revealed increases for both microglial-specific genes *Tmem119* and *Siglech* (Fig. 1.8), as well as microglial-associated genes *Aif1*, *CSF1R*, *Cx3cr1,* and *Trem2*, providing validation of the microarray data. Additionally, I found no significant changes in macrophage-specific

Figure 1.7: Microarray analysis of the repopulating brain reveals extensive proliferation and a microglia-specific expression profile. mRNA was extracted from the whole brains of control, day 1 recovery, and day 3 recovery groups from Figure 5. Microarray was performed via Affymetrix Mouse Gene 2.0. Gene expression changes were ranked by significance, as determined by Cyber T analyses, and the top 30 changes are shown for (A) control brains versus day 1 recovery (microglia depleted and drug cleared from CNS), (B) day 1 recovery versus day 3 recovery (repopulated brain), and (C) control brains versus day 3 recovery. Fold change and probabilities of differential expression (PPDE) are shown. Gene symbols highlighted in tan are known to be associated with microglia, those in dark green are microglia-specific over macrophages, and those in blue are associated with cell cycle progression and proliferation. No macrophage-specific genes were changed. D) Comparison of significant expression values for myeloid genes between day 1 recovery and day 3 recovery ($p<0.05$). Error bars indicate SEM. (Elmore et al. 2014)

Microglia-Depleted CNS → Microglia-Repopulating CNS

A) Top 30 significant expression changes: Control Versus Day 1

Gene	fold	PPDE(p)	Gene Description
P2ry12	-2.205	1.000	purinergic receptor P2Y, G-protein coupled 12
Ctss	-2.127	1.000	cathepsin S
Trem2	-1.917	1.000	triggering receptor expressed on myeloid cells 2
Csf1r	-1.752	1.000	colony stimulating factor 1 receptor
Laptm5	-1.721	1.000	lysosomal-associated protein transmembrane 5
Selplg	-1.891	1.000	selectin, platelet (p-selectin) ligand
Cd33	-1.949	1.000	CD33 antigen
Tyrobp	-1.575	1.000	TYRO protein tyrosine kinase binding protein
Gpr84	2.196	1.000	G protein-coupled receptor 84
Itgam	-1.986	1.000	integrin alpha M
Hexb	-1.486	1.000	hexosaminidase B
Gfap	1.598	1.000	glial fibrillary acidic protein
Ly86	-1.449	1.000	lymphocyte antigen 86
Ide	1.384	0.999	insulin degrading enzyme
Gm10790	-2.042	0.999	predicted gene 10790
Siglech	-1.932	0.999	sialic acid binding Ig-like lectin H
Mpeg1	-2.419	0.999	macrophage expressed gene 1
Unc93b1	-1.655	0.999	unc-93 homolog B1 (C. elegans)
Pld4	-1.777	0.999	phospholipase D family, member 4
Rnase4	-1.727	0.999	ribonuclease, RNase A family 4
Cd53	-1.604	0.999	CD53 antigen
P2ry13	-1.555	0.998	purinergic receptor P2Y, G-protein coupled 13
C1qb	-1.457	0.998	complement component 1, q subcomponent, beta
Cx3cr1	-1.490	0.998	chemokine (C-X3-C) receptor 1
Fcrls	-1.483	0.998	Fc receptor-like S, scavenger receptor
C1qc	-1.533	0.997	complement component 1, q subcomponent, C chain
Fcgr3	-1.496	0.996	Fc receptor, IgG, low affinity III
Arpc1b	1.355	0.996	actin related protein 2/3 complex, subunit 1B
Hpgds	-1.543	0.996	hematopoietic prostaglandin D synthase
Acta2	1.398	0.995	actin, alpha 2, smooth muscle, aorta
Abca9	-1.595	0.995	ATP-binding cassette, sub-family A (ABC1), member 9
Ccl12	6.004	0.994	chemokine (C-C motif) ligand 12
Tspan2	1.304	0.993	tetraspanin 2
Stab1	-1.499	0.992	stabilin 1
Slc2a5	-1.604	0.990	solute carrier family 2, member 5

B) Day 1 Versus Day 3

Gene	fold	PPDE(p)	Gene Description
Ube2c	7.211	1.000	ubiquitin-conjugating enzyme E2C
Mki67	3.845	1.000	antigen identified by monoclonal antibody Ki 67
Ccna2	3.243	1.000	cyclin A2
Clec7a	3.481	1.000	C-type lectin domain family 7, member a
Prr11	2.589	1.000	proline rich 11
Ctsc	2.705	1.000	cathepsin C
Top2a	2.341	1.000	topoisomerase (DNA) II alpha
Ly86	3.098	1.000	lymphocyte antigen 86
Hist1h2be	1.532	1.000	histone cluster 1, H2be
Ccnb2	2.136	1.000	cyclin B2
Cd36	4.061	1.000	CD36 antigen
Hist1h2ak	2.268	1.000	histone cluster 1, H2ak
Rnase4	2.218	1.000	ribonuclease, RNase A family 4
Cdk1	2.830	1.000	cyclin-dependent kinase 1
Ifi30	4.302	0.999	interferon gamma inducible protein 30
Hist1h2bn	1.864	0.999	histone cluster 1, H2bn
Il1a	2.727	0.999	interleukin 1 alpha
Lcp1	2.194	0.999	lymphocyte cytosolic protein 1
Apobec3	1.780	0.999	apolipoprotein B mRNA editing enzyme
Cks2	1.680	0.999	CDC28 protein kinase regulatory subunit 2
Hist1h2an	1.610	0.999	histone cluster 1, H2an
Gfap	1.437	0.998	glial fibrillary acidic protein
Itgam	2.105	0.998	integrin alpha M
C4b	1.489	0.998	complement component 4B (Chido blood group)
Nt5dc2	1.456	0.998	5'-nucleotidase domain containing 2
Nusap1	2.110	0.998	nucleolar and spindle associated protein 1
Arhgdib	1.793	0.998	Rho, GDP dissociation inhibitor (GDI) beta
Hist2h2aa1	1.544	0.998	histone cluster 2, H2aa1
Hist1h2ao	1.386	0.998	histone cluster 1, H2ao
Rac2	2.204	0.997	RAS-related C3 botulinum substrate 2
Ctsz	1.418	0.997	cathepsin Z
Slc43a3	1.676	0.997	solute carrier family 43, member 3
Msn	1.550	0.997	moesin
Bub1	2.19	0.996	budding uninhibited by benzimidazoles 1 homolog
Gusb	1.539	0.996	glucuronidase, beta

C) Control Versus Day 3

Gene	fold	PPDE(p)	Gene Description
Ube2c	8.261	1.000	ubiquitin-conjugating enzyme E2C
Mki67	4.599	1.000	antigen identified by monoclonal antibody Ki 67
Gfap	2.296	1.000	glial fibrillary acidic protein
Gpr84	3.845	1.000	G protein-coupled receptor 84
Ccna2	3.626	1.000	cyclin A2
C4b	2.070	1.000	complement component 4B (Chido blood group)
Clec7a	4.104	1.000	C-type lectin domain family 7, member a
Ctsc	2.978	1.000	cathepsin C
Top2a	3.180	1.000	topoisomerase (DNA) II alpha
Prr11	2.900	1.000	proline rich 11
Ccl12	12.719	1.000	chemokine (C-C motif) ligand 12
Cdk1	3.401	1.000	cyclin-dependent kinase 1
Arpc1b	1.855	1.000	actin related protein 2/3 complex, subunit 1B
Smc4	1.987	1.000	structural maintenance of chromosomes 4
Ccnb2	2.359	1.000	cyclin B2
Nt5dc2	1.614	1.000	5'-nucleotidase domain containing 2
Nusap1	2.918	1.000	nucleolar and spindle associated protein 1
Hist1h2be	1.573	1.000	histone cluster 1, H2be
Opalin	1.540	1.000	oligodendrocytic myelin paranodal and inner loop protein
Il1a	3.165	1.000	interleukin 1 alpha
Cks2	1.908	1.000	CDC28 protein kinase regulatory subunit 2
Bub1	2.757	1.000	budding uninhibited by benzimidazoles 1 homolog
Fam111a	2.847	1.000	family with sequence similarity 111, member A
Lcp1	2.387	1.000	lymphocyte cytosolic protein 1
Kif11	2.045	1.000	kinesin family member 11
Ifi30	4.331	1.000	interferon gamma inducible protein 30
Tagln2	1.748	1.000	transgelin 2
Hist1h2bl	1.467	1.000	histone cluster 1, H2bl
Slc14a1	1.472	1.000	solute carrier family 14 (urea transporter), member 1
Hist1h3a	2.745	1.000	histone cluster 1, H3a
Cd36	3.643	1.000	CD36 antigen
Cd180	3.534	1.000	CD180 antigen
Pla2g4a	1.931	1.000	phospholipase A2, group IVA
Hist1h2an	1.658	1.000	histone cluster 1, H2an
Hist1h2ao	1.410	1.000	histone cluster 1, H2ao

Known Microglial-Specific Gene | Known Microglial-Associated Gene | Known Macrophage-Specific Gene | Known Cell Cycle-Associated Gene

D Significantly upregulated myeloid genes Day 1 Versus Day 3

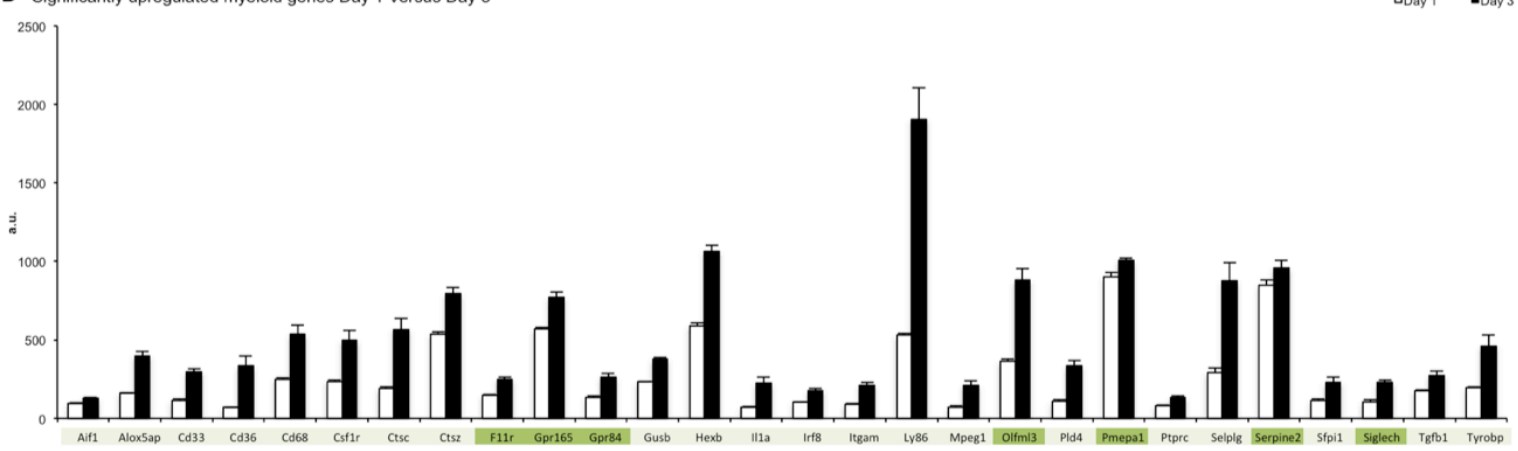

genes in the microarray dataset including *Fn1*, *Slp1*, *Saa3*, *Prg4*, *Cfp*, *Cd5L*, *GM11428*, *Crip1 Pf4*, and *Alox15* (Gautier et al. 2012) (data not shown). The monocyte-specific marker *CCR2* was not changed. Thus, these data further support the notion that repopulating cells have an expression profile of microglia and not of peripheral myeloid cells, and that repopulation is a result of proliferation rather than infiltration.

Figure 1.8

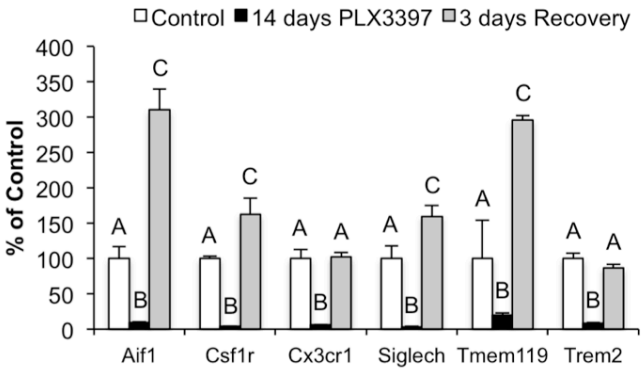

Figure 1.8: Rapid repopulation in brains that are >95% depleted of microglia. 2 month-old wild-type mice were treated with PLX3397 or vehicle for 14 days to deplete microglia. A third group had PLX3397 removed and was allowed to repopulate for 3 days. RT-PCR from mRNA extracted from intact half forebrains shows robust depletion of the microglia/myeloid markers AIF1, CSF1R, CX3CR1, SIGLECH, TMEM119, and TREM2, which are all significantly increased with repopulation.

Having determined that repopulation occurs from cell proliferation, I next stained the early-repopulating CX3CR1-GFP$^{+/-}$ brain tissue with anti-Ki67 as a marker of cell proliferation. At the 2-day recovery time point, I found the brain to contain many microglia-negative (GFP^{-}/Ki67^{+}) cells throughout; these cells were not seen in control, 0-, or 1-day recovery brains (Fig. 1.9A, B with quantification in C-E). By 3 days of recovery, most Ki67^{+} cells were also GFP^{+}, suggesting that these dividing, Ki67^{+} cells are potential microglial progenitors. A fraction of surviving microglia also expressed Ki67 at the 2-day timepoint, suggesting that surviving microglia were also contributing to repopulation.

Proliferating cells can also be labeled and tracked with the thymidine analog BrdU, thus allowing us to track the fate of the Ki67^{+}/proliferating cells to determine if they do indeed become microglia. I tagged proliferating cells with BrdU (single injection IP) at the 2-day

recovery time point (Fig. 1.10A-H). In the first cohort, mice were sacrificed 5 hours after injection and their brains were analyzed to confirm that the proliferating cells incorporated BrdU. Indeed, 5 hours post-injection, many non-microglial cells were shown to have incorporated BrdU (Fig. 1.10B, C; $IBA1^-$), while only 30% of all $BrdU^+$ cells expressed microglial markers (Fig 1.10B, C with quantification in G, H). In control animals, BrdU is not incorporated into appreciable numbers of cells (Fig. 1.10A and quantified in G, H) or in those depleted of microglia and maintained on the inhibitor (data not shown). Thus, BrdU-incorporated non-microglial cells correspond to the potential microglia progenitor cells. Having determined that the proliferating potential progenitor cells incorporate BrdU, in a second cohort of animals, I sacrificed the mice 24

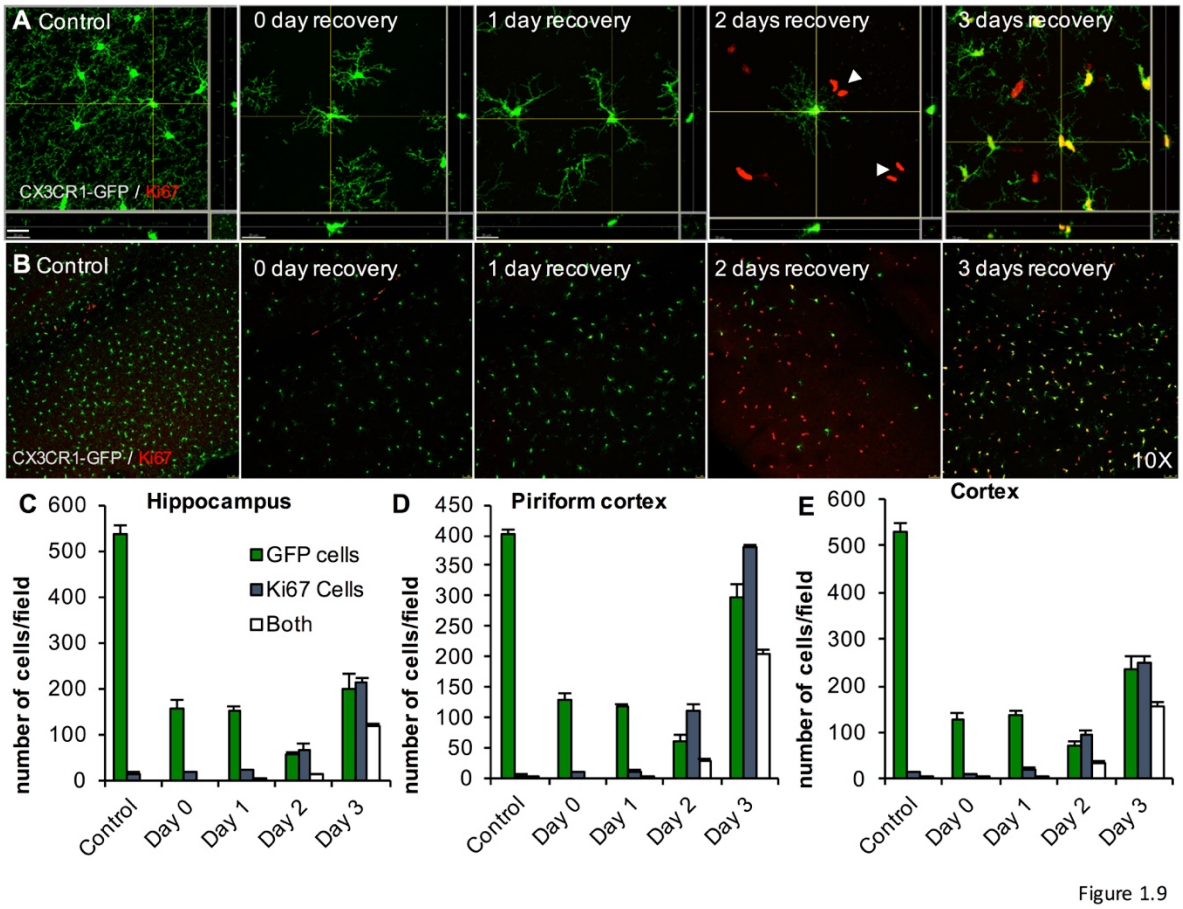

Figure 1.9

Figure 1.9. Microglial Repopulation Is Preceded by Proliferation of a Nonmicroglial Cell Type throughout the CNS (A) Using the same experimental groups as shown in Figure 5, repopulating brains were stained for the cell proliferation marker Ki67. Few $Ki67^+$ cells were seen in control, 0-, or 1-day recovery groups. A fraction of the GFP^+ cells expresses Ki67 at the 2-day recovery time point, and a majority of the GFP^+ cells express Ki67 at the 3-day recovery time point. $Ki67^+/GFP^-$ cells appeared throughout the CNS at 2 days of recovery, usually with two nuclei adjacent to one another (highlighted by arrows). Far fewer $Ki67^+/GFP^-$ cells were seen at the 3-day recovery time point. The 63X Z-stacks obtained by confocal microscopy and maximal projections are shown. Scale bar represents 20 μm. (B–E) Images of $Ki67^+$ and GFP^+ cells from the cortex are shown to illustrate the number of proliferating, but GFP^-, cells that appear at the 2-day recovery time point, as quantified in (C) for the hippocampal region, (D) for the piriform cortex, and (E) for the cortex. Error bars indicate SEM. (Elmore et al. 2014)

hours after BrdU administration, in order to track their fate over the next day. 24 hours later, virtually all BrdU-incorporated cells were microglia (as determined by IBA1 staining; Fig. 1.10E, F and quantified in G, H), with very few $BrdU^+/IBA1^-$ cells observed (Fig. 1.10H). These results demonstrate that the non-microglial proliferating/BrdU-incorporating cells become microglia within 24 hours, and provides further evidence that these cells as microglial progenitors.

Given the finding that potential microglial progenitor cells are stimulated to proliferate and differentiate into microglia, I reasoned that these progenitors would also express some of the markers that the initial repopulating microglia express, such as nestin. Indeed, co-staining for Ki67 and nestin in 2-day repopulating brains revealed that these newly appeared proliferating cells express nestin, with fine $nestin^+$ processes radiating out from the cell body (Fig. 1.10K-N, with magnified images in L and N), lending further credence to the idea that these proliferating nestin-expressing cells become the repopulated microglia. As controls, I show that these cells do not express either GFAP (Fig. 1.10I) or MAP2 (Fig. 1.10J). Finally, I confirmed that the BrdU-incorporated non-microglial cells found 5 hours after BrdU administration (Fig. 1.10B) also expressed nestin (Fig. 1.10O, P).

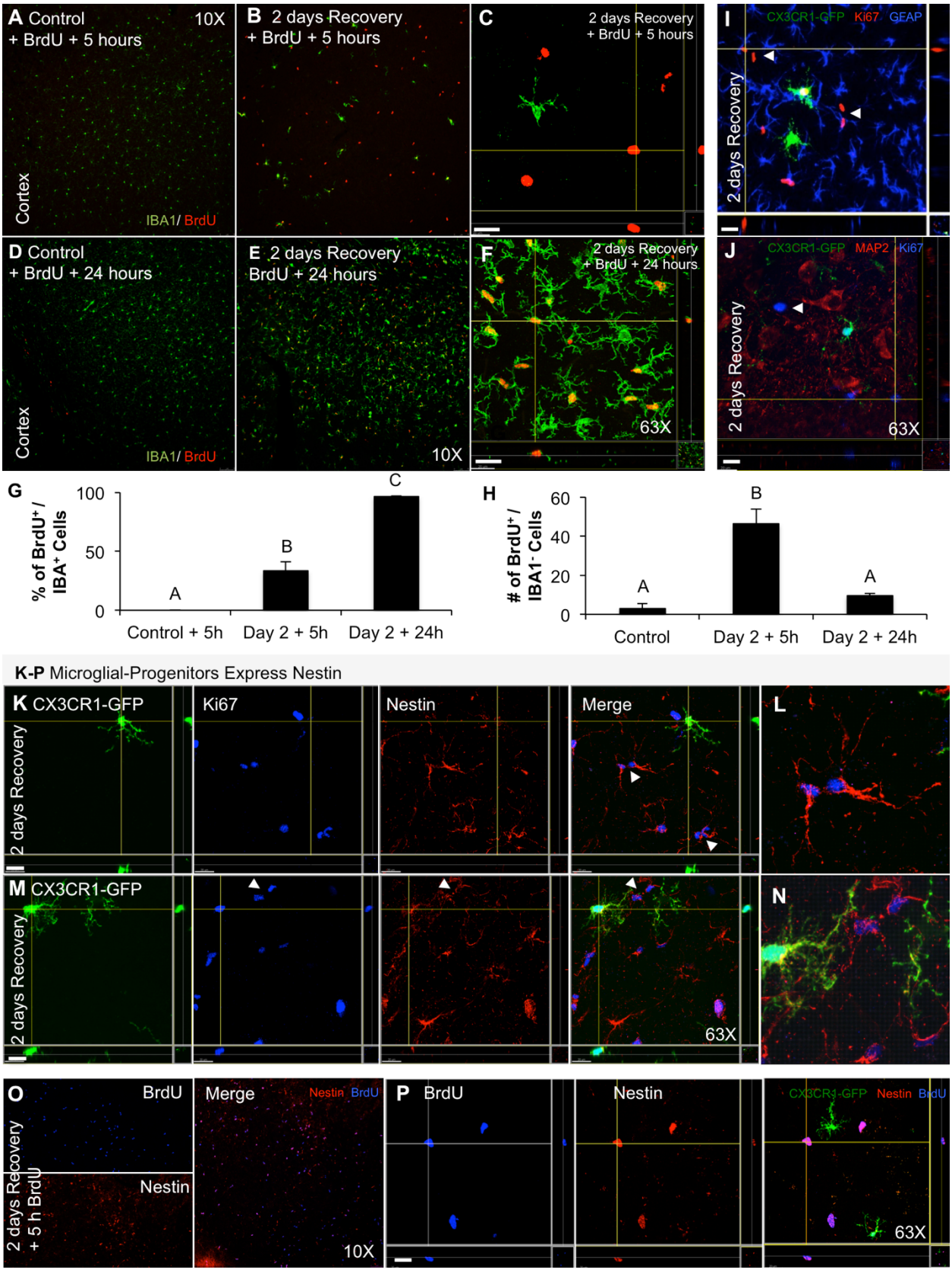
A Control
+ BrdU + 5 hours
10X
Cortex
IBA1/ BrdU
B 2 days Recovery
+ BrdU + 5 hours
C
2 days Recovery
+ BrdU + 5 hours
I
CX3CR1-GFP Ki67 GEAP
2 days Recovery
D Control
+ BrdU + 24 hours
Cortex
IBA1/ BrdU
E 2 days Recovery
BrdU + 24 hours
10X
F
2 days Recovery
+ BrdU + 24 hours
63X
J
CX3CR1-GFP MAP2 Ki67
2 days Recovery
63X
G
% of BrdU+ / IBA+ Cells
100
50
0
A
B
C
Control + 5h
Day 2 + 5h
Day 2 + 24h
H
# of BrdU+ / IBA1- Cells
60
40
20
0
A
B
A
Control
Day 2 + 5h
Day 2 + 24h
K-P Microglial-Progenitors Express Nestin
K CX3CR1-GFP
Ki67
Nestin
Merge
L
2 days Recovery
M CX3CR1-GFP
2 days Recovery
63X
N
O
BrdU
Nestin
2 days Recovery
+ 5 h BrdU
Merge
Nestin BrdU
10X
P
BrdU
Nestin
CX3CR1-GFP Nestin BrdU
63X

Figure 1.10

Figure 1.10. Fate Mapping Reveals a Nestin-Expressing Microglia Progenitor Cell that Becomes the Repopulating Microglia. ***A-F,*** To determine whether the nonmicroglial $Ki67^+$ proliferating cells were becoming microglia, 2-month-old wild-type mice were treated with PLX3397 or vehicle to deplete microglia. The inhibitor was withdrawn and BrdU was administered 2 days later to label proliferating cells (n = 3–4 per group). Mice were sacrificed 5 or 24 hr later (n = 4 per group). Representative images of the cortical region are shown for controls ***(A)*** and the 2-day recovery group ***(B)*** for IBA1 and anti-BrdU at 5 hr after BrdU administration. The 63X maximal projection Z-stacks are shown for the 2-day recovery group + 5 hr BrdU ***(C)***, revealing that the majority of BrdU-incorporated cells are not microglia. ***D-F,*** Representative images of the cortical region are shown for controls ***(D)*** and the 2-day recovery group ***(E)*** for IBA1 and anti-BrdU at 24 hr after BrdU administration. The 63X maximal projection z-stacks (Elmore et al. 2014) are shown for the 2-day recovery group at 24 hr after BrdU administration (F), revealing that the majority of BrdU-incorporated cells are now microglia. ***G,*** Quantification of ***(A-F)*** shows that only 30% of BrdU-incorporated cells are microglia after 5 hr but that 96% become microglia after 24 hr. ***H,*** Quantification of the total amount of $BrdU^+$/nonmicroglial cells per field of view shows that most of these cells have differentiated into microglia within 24 hr. ***I-N,*** $CX3CR1\text{-}GFP^{+/-}$ mice were treated for 7 days with PLX3397, and 2 days after inhibitor withdrawal, $Ki67^+/GFP^-/nestin^+$ cells are induced throughout the CNS (highlighted with white arrowheads in K and M; two different fields of view are shown, with a 63X zoom image of the nestin-expressing cells shown in ***L*** and ***N***). In addition, costains with Ki67 show that the repopulating cells do not express GFAP ***(I)*** or MAP2 ***(J)***. ***O, P,*** BrdU-incorporated cells in the 2-day recovery brains (sections obtained from B), also express nestin (microglia only shown in the 63X merge). Same capital letter above conditions ***(G and H)*** indicates no significant difference ($p>0.05$) via one-way ANOVA with post hoc Newman-Keuls multiple comparison test. Error bars indicate SEM. Scale bars represent 20 μm.

CSF1R inhibition is sufficient for both microglial elimination and repopulation

The compound used in all experiments detailed in this document so far is PLX3397 - a CSF1R inhibitor that targets both CSF1 and a related receptor, c-kit. Since c-kit is a stem cell-related gene, it was important to ensure that effects of microglial elimination and repopulation were due to inhibition of the CSF1 receptor, and not due to off-target effects of also inhibiting c-kit. To this end, I treated 2 month-old wild-type mice with a similar CSF1R inhibitor, PLX5622, which only inhibits the CSF1 receptor, and has no effects on c-kit. Treating with this compound for 7 days eliminated ~90% of microglia (Fig. 1.11A-B), and repopulation of microglia followed removal of the inhibitor, in a similar fashion to that achieved by CSF1R inhibition via PLX3397 (Fig. 1.11A-B).

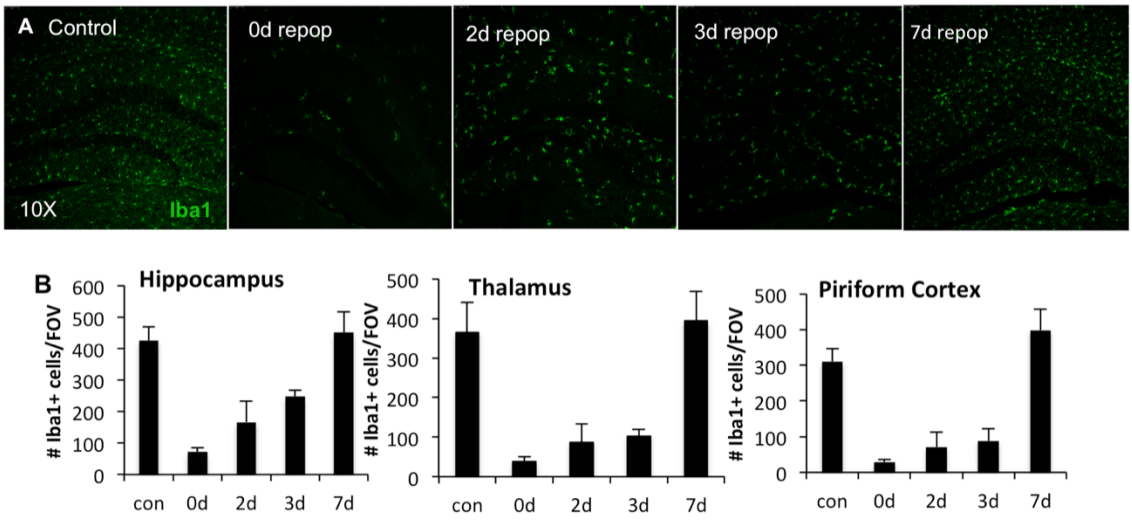

Figure 1.11: Inhibition of CSF1R alone is sufficient to both eliminate and repopulate microglia. 2 month-old WT mice were treated with 1200 mg/kg PLX5622, a CSF1R inhibitor that does not target c-kit (n=4/group). ***A,*** Anti-Iba1 staining revealed microglial elimination after 7 days of treatment, followed by a return of Iba1^{+} cells after removal of the compound. ***B,*** Quantification of the number of Iba1+ cells/FOV in hippocampus, thalamus, and piriform cortex revealed similar patterns for microglial elimination and repopulation as treatment with PLX3397.

DISCUSSION

Dependence of Microglia on CSF1R Signaling in the Adult Brain

Studies have highlighted the importance of the CSF1R to the development of microglia, with mice lacking the CSF1R being born devoid of microglia (Erblich et al., 2011; Ginhoux et al., 2010). Unfortunately, these mice have developmental defects and usually die by adulthood, by which time some microglia are observed (Erblich et al., 2011). Mice lacking either of the two CSF1R ligands, CSF1 (Wegiel et al., 1998) or IL-34 (Wang et al., 2012), also have reduced densities of microglia throughout the CNS. Thus, the CSF1R is heavily implicated in the development of microglia. However, it is unknown what role the CSF1R plays in microglia homeostasis and viability in the adult brain. Our results show that microglia in the adult brain are fully dependent upon

CSF1R signaling for their survival and that we can eliminate virtually all microglia from the CNS for extended periods through the administration of CSF1R inhibitors. Thus, CSF1R signaling appears to act as a requisite growth factor receptor for microglia, and its blockade drives microglia to their death. Growth factor withdrawal is known to induce apoptosis in many other cell types, including HSCs (Cornelis et al., 2005) and macrophages (Chin et al., 1999). Consequently, we can take advantage of this dependency to manipulate microglial levels in the adult brain through administration of CSF1R inhibitors, allowing studies into microglia function that have not been possible before. Moreover, the CSF1R provides an ultimate drug target for neuroinflammation, in that we can now eliminate microglia rather than just suppress aspects of their activity.

Rapid Repopulation of the Microglia-Depleted Brain

Having shown that we could eliminate >99% of all microglia from the adult brain, we asked the question of whether new cells could replace the lost microglia and repopulate the CNS. Microglia colonize the CNS during development, before E9 (Ginhoux et al., 2010). Once the CNS has formed, these microglia are long lived and have the capacity to divide and self-renew in an autonomous cell population, but the dynamics and regulation of resident microglia numbers are not fully understood. In the periphery, macrophage populations are thought to be replenished by circulating monocytes derived from multipotent HSCs found in the BM, although this view has been challenged (Hashimoto et al., 2013; Sieweke and Allen, 2013). In contrast, the brain is separated from circulation by the BBB, and experiments have shown that there is little infiltration of peripheral HSCs/monocytes/macrophages into the CNS to help maintain or replenish

microglia under normal, nonirradiated conditions (Mildner et al., 2007; Ajami et al., 2011; Greter and Merad, 2013). Thus, we set out to explore whether repopulation could occur in the adult brain, as well as the consequences of with- drawing CSF1R antagonists once microglia were depleted. We initially predicted that the brain would remain absent of microglia for some time, given our current knowledge about the origins and proliferative properties of microglia; but remarkably, we found that the CNS can fully repopulate with new microglia within just 7 days. Furthermore, the returning number of microglia is identical to that in untreated mice, showing astonishing and precise regulation of the microglial population within a very short period of time. Repopulating microglia derive from proliferation, as shown with Ki67 expression and incorporation of BrdU, rather than infiltration of peripheral cells into the CNS. Initially, repopulating microglia show very different morphologies and expression patterns to resident microglia, such as immunoreactivity for nestin, but they rapidly differentiate into ramified microglia over a 7- to 14-day period.

Crucially, we find that the repopulating brain induces the proliferation of nestin-expressing cells throughout the CNS that appear to become the repopulating microglia. This finding helps to explain why these initial microglia strongly express nestin and how microglia numbers can be restored in a very short time, given that there are so few surviving microglia. It should be noted that the surviving microglia themselves also proliferate, as evidenced by the expression of Ki67 and observations of cytokinesis (i.e., Figure 1.7A, 3-day recovery), revealing that repopulation may occur partly from nestin-expressing proliferating progenitors and partly from proliferation of surviving cells. Of note, microglia are of a myeloid lineage rather than the neuroectodermal lineage that

nestin expression would suggest, leading us to question why the repopulating microglia express nestin. In explaining this, it is possible to generate microglia from embryonic stem cells (ESCs) (Beutner et al., 2010); ESCs are differentiated to a neuronal, nestin^{+} lineage and then the neuronal growth factors are removed, resulting in microglia. Hence, ESCs need to pass through a nestin^{+} stage on their way to becoming microglia, in line with the cells that we describe in this study, providing clear evidence that repopulating microglia strongly express nestin. In addition, several previous studies have shown subsets of microglia to be able to express nestin under certain conditions, such as in culture (Yokoyama et al., 2004), after traumatic brain injury (Sahin Kaya et al., 1999), or after optic nerve injury (Wohl et al., 2011) where proliferating, BrdU-incorporating microglia initially also express nestin. A study has also highlighted that the CSF1R negatively regulates the expansion of nestin^{+} progenitors in the developing brain, an intriguing parallel with our own findings in the adult brain and the relationship between CSF1R signaling and nestin-expressing progenitors and microglia (Nandi et al., 2012). Similar repopulation kinetics have been reported in an alternative model of microglial depletion (Bruttger et al., 2015) utilizing an acute administration of diphtheria toxin, which also confirmed that repopulation occurred from within the CNS, with no peripheral contributions. These studies show that the adult brain has a remarkable capacity to repopulate the entire microglial tissue, and gives insights into the regulation of microglial homeostasis and inflammatory responses.

CHAPTER TWO

A LIMITED CAPACITY FOR MICROGLIAL REPOPULATION IN THE ADULT BRAIN

INTRODUCTION

Microglia are the primary innate immune cells of the CNS, capable of sensing and responding to insults in the local environment (Nimmerjahn et al., 2005). During development, they also have a crucial role in synaptic sculpting (Paolicelli et al., 2011; Schafer et al., 2012), as well as regulation of neurogenesis (Antony et al., 2011), and this function is maintained in the adult brain, where they continue to regulate neuronal structures and connections (Tremblay et al., 2010; Rice et al., 2015). Unique among myeloid cell types, microglia directly originate from yolk sac macrophage precursors, and colonize the CNS early in development (Hoeffel et al., 2015; Alliot et al., 1999; Ginhoux et al., 2010). Due to the presence of the BBB, microglia are separated from myeloid cell populations in the periphery, and are long-lived and self-sustaining in their isolation (Lawson et al., 1992).

We previously discovered that microglia are dependent upon signaling through the colony-stimulating factor 1 receptor (CSF1R) for their survival (Elmore et al., 2014). Administration of BBB-permeant CSF1R inhibitors leads to the rapid elimination of up to 99% of microglia in a dose-dependent fashion (Dagher et al., 2015). While other myeloid populations also express the CSF1R, microglia appear to be uniquely dependent on its signaling for survival. Accordingly, other myeloid populations are not depleted (Elmore et al., 2014), again showing divergence between microglia and other myeloid cell types. Microglia can be depleted for the duration of CSF1R inhibitor

administration, but withdrawal of inhibitors from the microglia-depleted brain stimulates rapid repopulation (Elmore et al., 2014). Repopulation occurs both from proliferation of the few surviving microglia and from a pool of CNS-resident proliferating cells (which we deem “progenitors”) that appear to differentiate into new microglia over the course of several days, but the relative contributions are unknown. Overall, within ~14 days of inhibitor withdrawal, the CNS is fully repopulated with similar microglia densities, spacing, and morphologies to controls (Elmore et al., 2015). Similar repopulation kinetics have been reported in an alternative model of microglial depletion (Bruttger et al., 2015) utilizing an acute administration of diphtheria toxin, which also confirmed that repopulation occurred from within the CNS, with no peripheral contributions. These studies show that the adult brain has a remarkable capacity to repopulate the entire microglial tissue, and gives insights into the regulation of microglial homeostasis and inflammatory responses.

Here, I have explored the kinetics and capacity of the adult brain for microglial repopulation and find that the rate of repopulation is proportional to the extent of microglia depletion. Furthermore, I find that there is a finite capacity for repopulation, with multiple repopulation cycles leading to brain conditioning that can no longer support repopulation.

MATERIALS AND METHODS

Compounds

PLX3397 was provided by Plexxikon, Inc. and formulated in standard chow by Research Diets Inc. at 290- and 600mg/kg.

Animal Treatments

All rodent experiments were performed in accordance with animal protocols approved by the Institutional Animal Care and Use Committee at the University of California, Irvine. 2-9 month-old age-matched male mice were provided with control chow or PLX3397 chow for 7 days at a time, for 1, 2, or 3 cycles of treatment. Following each treatment cycle, PLX3397 was withdrawn and all mice maintained on control chow for 7 or 28 days. At the conclusion of experiments, mice were sacrificed via CO_2 inhalation and perfused transcardially with 1X phosphate-buffered saline (PBS). Brains were extracted and dissected down the midline, with one half flash-frozen on dry ice for subsequent RNA and protein analyses, and the other half drop-fixed in 4% paraformaldehyde (PFA) in 1X PBS. Fixed brains were cryopreserved in a 30% sucrose solution, frozen, and sectioned at 40 μm on a Leica SM2000 R sliding microtome for subsequent immunohistochemical analyses.

Confocal microscopy

Fluorescent immunolabeling followed a standard indirect technique (primary antibody followed by fluorescent secondary antibody), as previously described (Elmore et al., 2014). Primary antibodies used include Iba1 (1:1000; Wako), GFAP (1:10,000; Abcam), S100b (1:1000, Abcam), TGFβ1 (1:100; Abcam), Cd11b (1:100; Bio-Rad), P2ry12 (1:500; Sigma) and Tmem119 (1:3; courtesy of Dr. Ben Barres). Colocalization scores and numbers of myeloid cells and astrocytes were determined using the colocalization and spots modules in Bitplane Imaris 7.5 software.

RNA Extraction and RNA-Seq Processing

RNA was extracted and purified from frozen half brains using an RNA Plus Universal Mini Kit (Cat. #73404, Qiagen, Hilden, Germany) per the manufacturer's instructions. Total RNA was monitored for quality control using the Agilent Bioanalyzer Nano RNA chip and Nanodrop absorbance ratios for 260/280nm and 260/230nm. Library construction was performed according to the Illumina TruSeq RNA v2 protocol. The input quantity for total RNA within the recommended range and mRNA was enriched using oligo dT magnetic beads. The enriched mRNA was chemically fragmented. First strand synthesis used random primers and reverse transcriptase to make cDNA. After second strand synthesis the ds cDNA was cleaned using AMPure XP beads and the cDNA was end repaired and then the 3' ends were adenylated. Illumina barcoded adapters were ligated on the ends and the adapter ligated fragments were enriched by nine cycles of PCR. The resulting libraries were validated by qPCR and sized by Agilent Bioanalyzer DNA high sensitivity chip. The concentrations for the libraries were normalized and then multiplexed together. The multiplexed libraries were sequenced using paired end 100 cycles chemistry for the HiSeq 2500. The version of HiSeq control software was HCS 2.2.58 with real time analysis software, RTA 1.18.64.

RNA-seq, Gene Ontology, and Pathway analysis

Single-end RNA-seq reads were first aligned using Bowtie v. 0.12.8 (Langmead et al., 2009) to the reference mouse transcriptome GENCODE,vM4. Gene expression level was quantified using RSEM v.1.2.12 (Li and Dewey, 2011) with expression values

normalized into Fragments Per Kilobase of transcript per Million mapped reads (FPKM). Samples with >20,000,000 uniquely mapped reads and >75% uniquely mapping efficiency were considered for downstream analyses. Differential expression analysis was performed using edgeR (Robinson et al., 2010) on protein-coding genes and lncRNAs. Differentially expressed genes were selected by using p-value <0.005 and false discovery rate (FDR)<0.05. Gene ontology analysis was performed with DAVID (Huang da et al., 2009b, a) Fisher's exact test p-value lower than 0.05. KEGG pathways analysis was performed with PaintOmics v. 2.0 (Garcia-Alcalde et al., 2011).

Statistics

All analyses, with the exception of RNA-seq were performed using one-way ANOVAs with post-hoc Tukey's Multiple Comparison tests for all multiple comparisons (Graphpad Prism 6). For non-RNA-seq analyses, statistical significance was accepted at $p<0.05$; trends at $p<0.10$.

RESULTS

Capacity for normal microglial repopulation with cycles of partial depletion:

Our previous data found that 7 days' treatment with the CSF1R/c-kit inhibitor PLX3397 at 290 mg/kg in chow led to ~50-70% microglia depletion brainwide (Elmore et al., 2014). Withdrawal of the inhibitor then stimulated repopulation both from unidentified proliferating cells and surviving cells (Elmore et al., 2014). As repopulation derives from a progenitor source within the brain, we reasoned that there may be a finite pool of these progenitors, and thus a finite capacity for repopulation. To assess the capacity of

the brain for microglial repopulation, I subjected 2-month old male mice (n=4/group) to multiple cycles of depletion and repopulation (Figure 2.1A). I found that 7 days' treatment with PLX3397 (290 mg/kg in chow) led to ~50% elimination of microglia, which was only partly recovered with 7 days of repopulation. A similar pattern was found with a second round of elimination/repopulation (Figure 2.1 B, C), showing that the brain can recover from at least 2 rounds of partial elimination and repopulation.

The rate of microglial repopulation is proportional to the extent of microglial depletion:

As 7 days' treatment with 290 mg/kg PLX3397 reduced microglial numbers by 50% and only resulted in partial repopulation (Figure 2.2A, C), I increased the potency of the CSF1R inhibitor to determine if a higher concentration could more thoroughly ablate microglia in this time frame. We reformulated chow at a concentration of 600 mg/kg PLX3397, and found that 7 days' treatment with this higher concentration led to 98.8% depletion of microglia (Figure 2.2B, D). Furthermore, upon inhibitor withdrawal, powerful repopulation was observed, with brain microglia levels reaching 150% of controls within 7 days (Figure 2.2B, D). This overshoot is consistent with results from mice treated for 4 weeks with 290 mg/kg PLX3397, leading to 95% depletion of microglia (Chapter 1; Elmore et al., 2014). By comparing this rate of repopulation with that observed with 50% microglial depletion, repopulation is much stronger and more rapid with higher levels of microglia depletion.

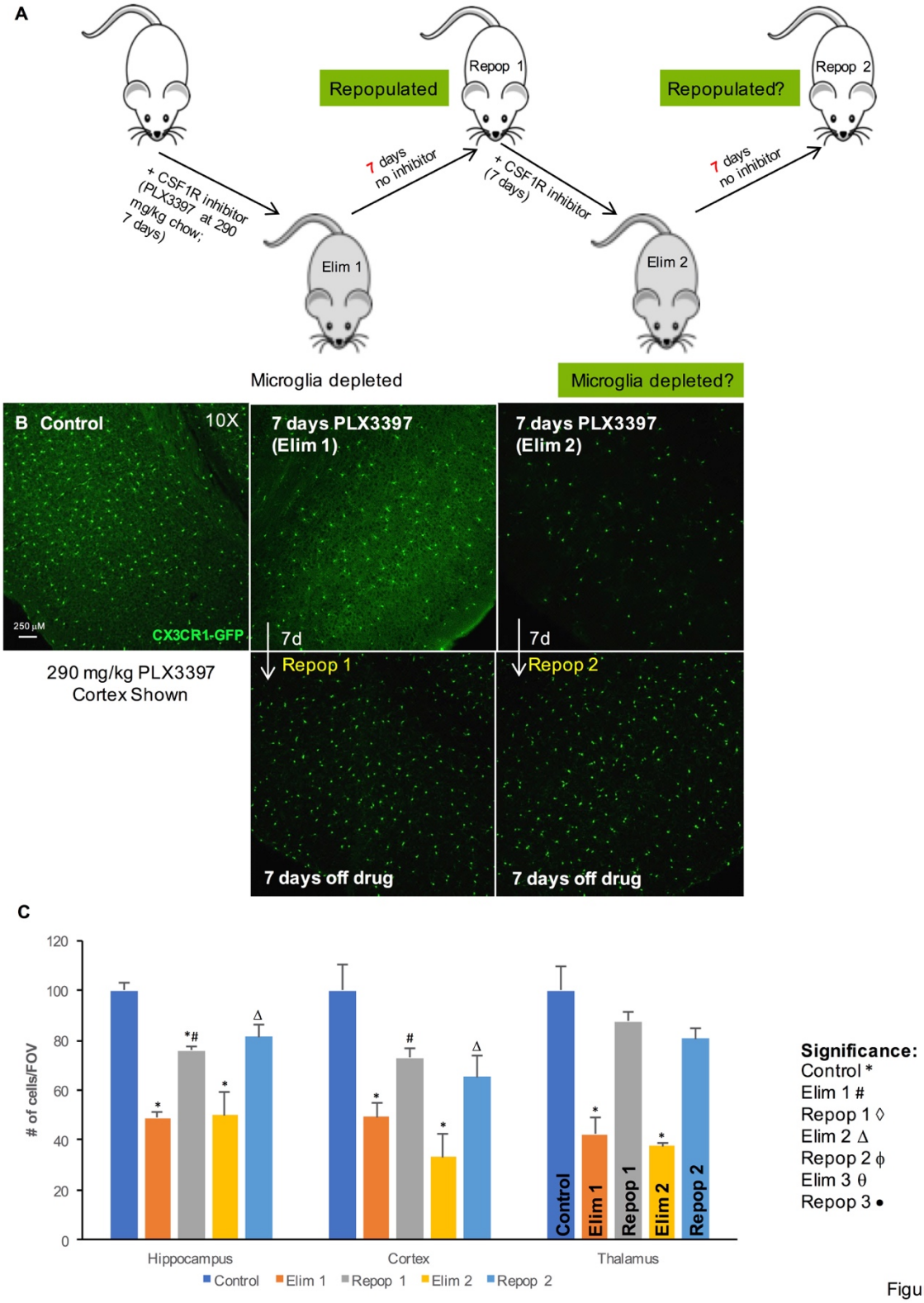

Figure 2.1

Figure 2.1. Cyclic treatment of WT mice with PLX3397 (290mg/kg). ***A,*** Schematic depicting experimental paradigm of dose and duration of treatment and withdrawal cycles (n=4/group). ***B,*** 10X representative images of CX3CR1-GFP^{+} cells in cortical regions. ***C,*** Quantification of number of GFP^{+} cells per FOV. Error bars represent SEM, (n=4). $p<0.05$; significance symbols represent comparison groups: Control *, Elim 1 #, Repop 1 ◊, Elim 2 Δ, Repop 2 ϕ.

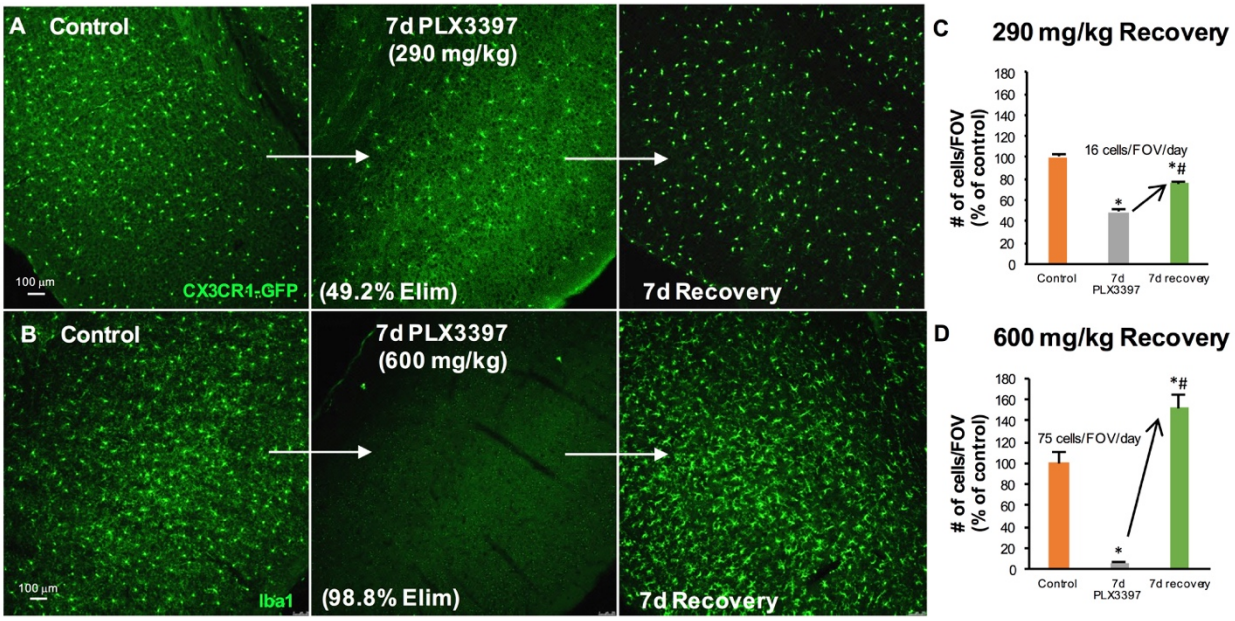

Figure 2.2

Figure 2.2 Rate of microglial repopulation depends on extent of depletion. ***A,*** 10X representative images of cortical regions; mice treated with PLX3397 (290 mg/kg) for 7 days (n=4/group). ***B,*** 10X representative images of cortical regions; mice treated with higher dose of PLX3397 (600 mg/kg) for 7 days. ***C,*** Quantification of GFP^+ cells/FOV with 290 mg/kg PLX3397, normalized to percent of Control, reveals an increase of an average of 16 cells/FOV/day between treatment and recovery groups; recovery group does not reach control levels. ***D,*** Quantification of $Iba1^+$ cells/FOV with 600 mg/kg PLX3397, normalized to percent of Control, reveals an increase of an average of 75 cells/FOV/day between treatment and recovery groups; recovery group surpasses control levels. Error bars represent SEM, (n=4). $p<0.05$; significance

A finite capacity for microglial repopulation with cycles of thorough depletion:

Having now identified a formulation of PLX3397 that potently eliminates ~99% of microglia within 7 days, we set out to further explore the capacity of the brain for repopulation using this formulation. To that end, we subjected 2-month old male mice to 3 cycles of elimination and repopulation (7 days on drug, 7 days off drug per cycle; n=4/group; Figure 2.3A). Microglia were robustly eliminated for all 3 cycles, but repopulation was only observed in the first cycle (Figure 2.3B, C), with very few cells repopulating in cycles 2 and 3. Thus, the adult brain has a finite capacity for microglial repopulation, and appears to only have sufficient pools available for one round of repopulation, at least with rapid cycles of elimination/repopulation.

Transcriptome analyses of microglia depleted and repopulated brains:

I extracted whole brain RNA from Control, Elim (7 days 600 mg/kg PLX3397), Repop 1 (successful repopulation), and Repop 2 and 3 (unsuccessful repopulation), and performed RNA-seq. FPKM values were obtained, and differential expression of significantly altered genes ($p < 0.005$ and FDR < 0.05) calculated (Figure 2.4). Analyses of Control vs. Elim brains revealed reductions in 254 genes, and 15 upregulated genes (Figure 2.4A, B). Using cell type specific expression databases (Zhang et al., 2014), I found that the clear majority of the downregulated genes are expressed strongly, or solely, in microglia, allowing us to assemble a core set of microglia expressed genes (Figure 2.4C, D), validating several studies on brain extracted microglia (Butovsky et al., 2014; Bennett et al., 2016). I divided other differentially expressed genes into those expressed by astrocytes, neurons, oligodendrocyte precursors (OPC), new oligodendrocytes, myelinating oligodendrocytes, or endothelial cells, and displayed expression of Repop groups in a heatmap (Figure 2.4E). Within the list of 15 upregulated genes between Control and Elim are the astrocyte-expressed genes GFAP, mt2, and serpina3n. Immunostaining for GFAP confirmed marked increases in GFAP expression with all cycles of elimination and repopulation, while S100b, an alternative astrocyte marker, was increased only with each elimination cycle (Figure 2.5B-C).

Figure 2.3 Cyclic treatment of WT mice with higher dose of PLX3397 (600 mg/kg). ***A,*** Experimental paradigm: schematic depicting dose and duration of treatment and withdrawal cycles (n=4/group). ***B,*** Representative whole brain stitches of $Iba1^+$ cells in each group. ***C,*** Quantification of number of Iba1+ cells/FOV for hippocampus, cortex, and thalamus. Error bars represent SEM, (n=4). $p<0.05$; significance symbols represent comparison groups: Control *, Elim 1 #, Repop 1 ◊, Elim 2 Δ, Repop 2 ϕ, Elim 3 θ, Repop 3 •.

Interestingly, I found

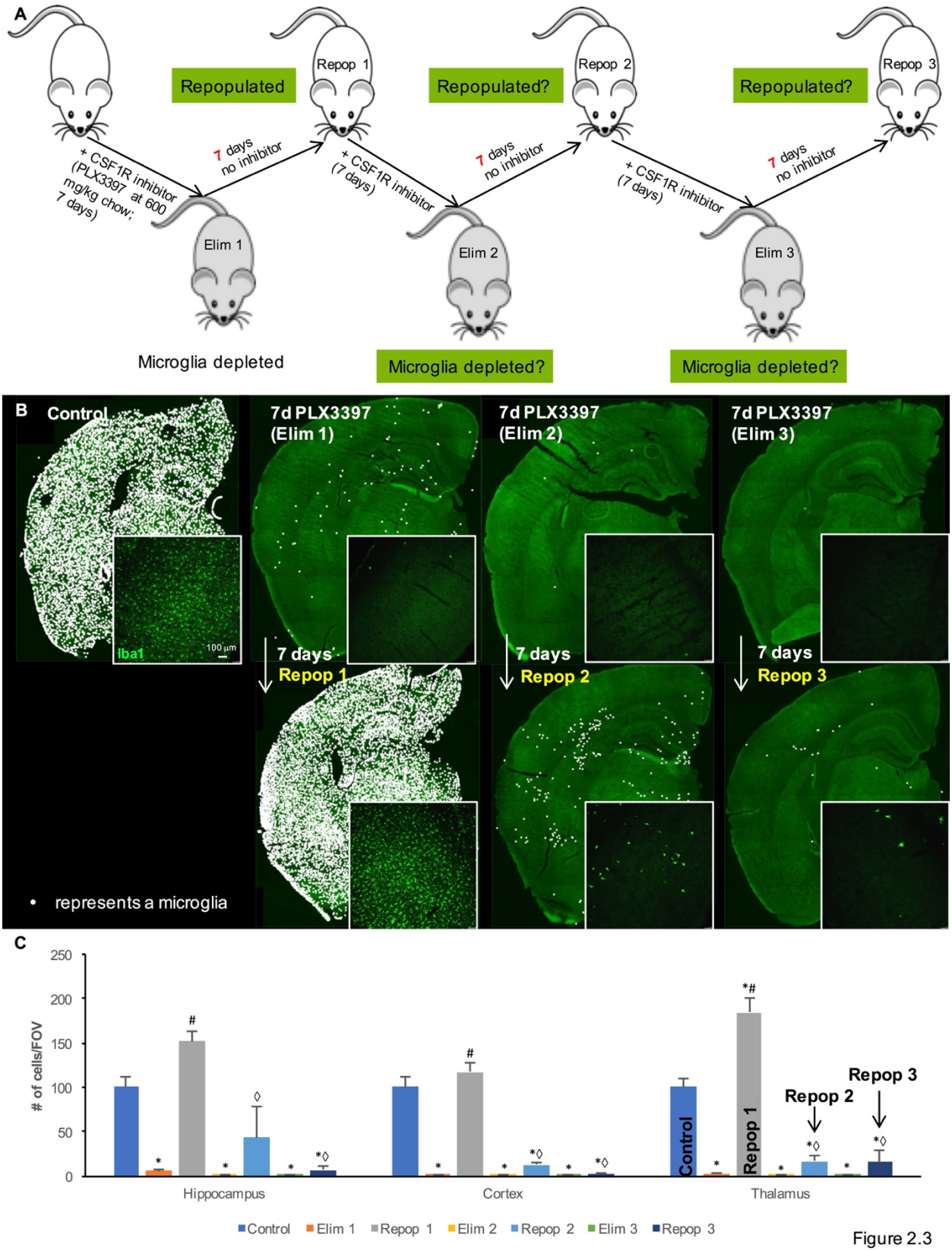
A
Repopulated
Repopulated?
Repopulated?
Repop 1
Repop 2
Repop 3
+ CSF1R inhibitor (PLX3397 at 600 mg/kg chow; 7 days)
7 days no inhibitor
+ CSF1R inhibitor (7 days)
7 days no inhibitor
+ CSF1R inhibitor (7 days)
7 days no inhibitor
Elim 1
Elim 2
Elim 3
Microglia depleted
Microglia depleted?
Microglia depleted?
B
Control
7d PLX3397 (Elim 1)
7d PLX3397 (Elim 2)
7d PLX3397 (Elim 3)
Iba1
100 µm
7 days Repop 1
7 days Repop 2
7 days Repop 3
• represents a microglia
C
# of cells/FOV
250
200
150
100
50
0
Hippocampus
Cortex
Thalamus
Control
Repop 1
Repop 2
Repop 3
Control
Elim 1
Repop 1
Elim 2
Repop 2
Elim 3
Repop 3

Figure 2.3

Figure 2.4 Differentially expressed genes between treatment cycles with 600 mg/kg PLX3397, obtained via RNA-seq analysis. ***A,*** Number of significant differentially expressed genes between each group analyzed. ***B-E,*** Differentially expressed genes between Con and Elim. ***B,*** Heatmap of significant differentially expressed genes. ***C,*** Differentially expressed genes stratified by those commonly expressed by CNS cell types reveals 164 downregulated microglial genes. ***D,*** List of 164 downregulated microglial genes termed "core" microglial genes. ***E,*** Heatmaps of differentially expressed genes stratified by CNS cell type reveals increase in common astrocyte-expressed genes, and decrease in common oligodendrocyte-expressed genes. ***F-H,*** Differentially expressed genes between Con and Repop 1. ***F,*** Heatmap of significant differentially expressed genes. ***G,*** Differentially expressed genes stratified by those commonly expressed by CNS cell types reveals 139 upregulated microglial genes. ***H,*** IPA reveals upregulation of many downstream genes from IFNγ.

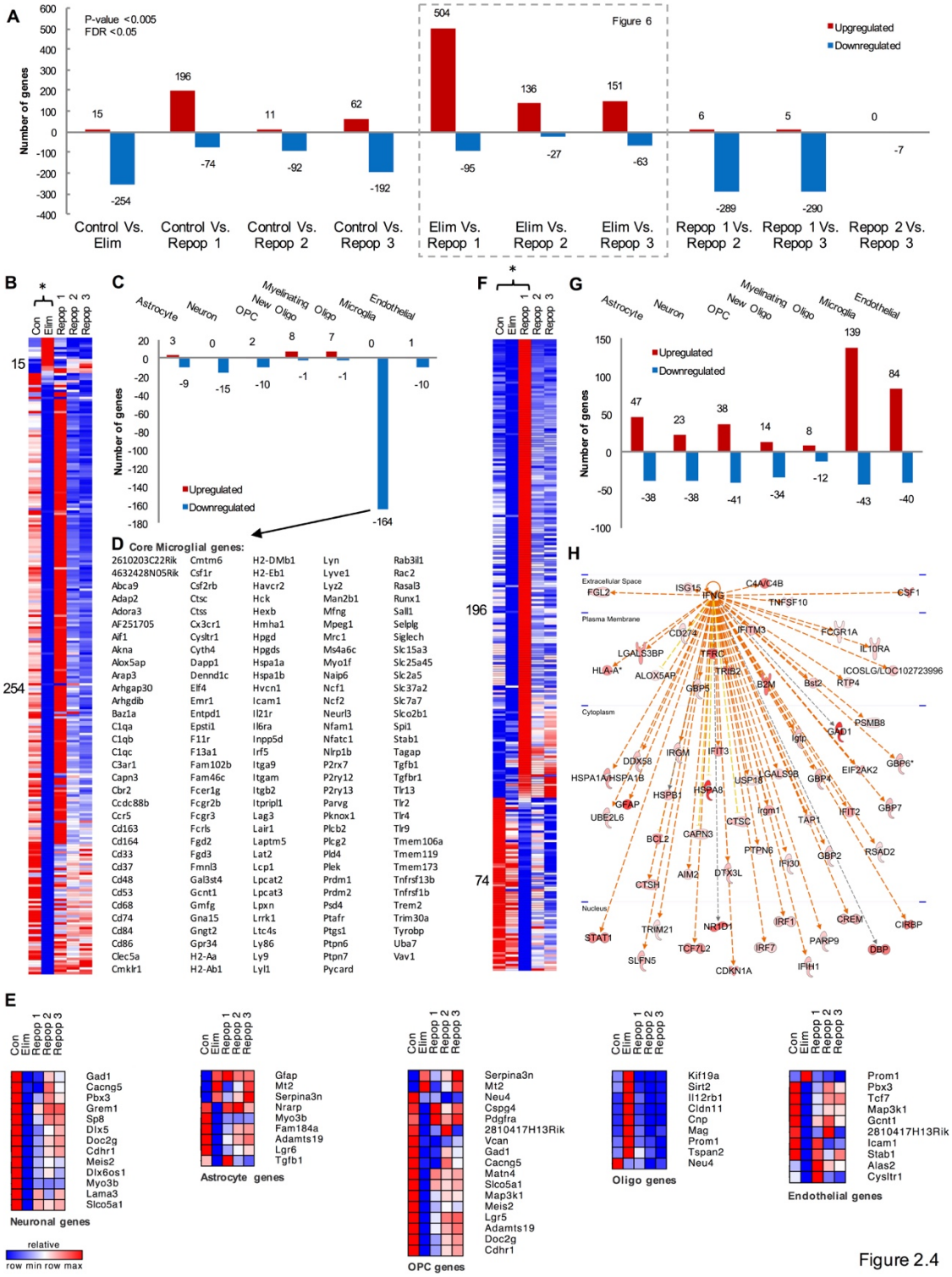

Figure 2.4

that cortical astrocytes progressively increase their expression of TGFβ1 with each cycle.

Most other upregulated genes between Control and Elim are those commonly expressed by oligodendrocytes (Figure 2.4E). The remaining downregulated genes are commonly expressed by neurons, astrocytes, OPC's, and endothelial cells (Figure 2.4E). We cannot discount that these genes could also be expressed in microglia, and hence their downregulation may be a direct result of microglial elimination, rather than an effect on a specific cell type.

We next compared differentially expressed genes between Control and Repop 1 brains (the successful repopulation; Figure 2.4F). 196 genes were significantly upregulated, and the clear majority of these are commonly microglia-expressed (Figure 2.4G), in accordance with the overshoot in microglia numbers with 7-days repopulation (Figure 2.2B, D). However, pathway analyses of all differentially expressed genes revealed an IFNγ-activated gene signature (Figure 2.4H), suggesting that repopulating microglia are initially in an activated state at this point. In agreement, I previously showed that repopulating cells at day 7 express CD45 (Chapter 1; Elmore et al., 2014), a marker of activation, and have amoeboid morphologies (Figure 2.5A), which ramify by 14 days (Elmore et al., 2015). Further pathway analysis of upregulated genes revealed extensive activation of immune responses, including cytokine and chemokine signaling pathways, while downregulated

Figure 2.5 Microglial morphology and astrocyte staining of groups from cyclic treatment with 600 mg/kg PLX3397. ***A,*** 63X representative z-stack images of Iba1+ cells reveal grossly different morphologies between each repopulation cycle. ***B-D,*** Astrocyte staining and quantification. ***B,*** 10X representative images of S100+/GFAP+ cells during each cycle. ***C,*** Quantification of GFAP+ and S100+ cells reveals an increase in number of GFAP+ cells with the first repopulation cycle, which remains elevated, and an increase in number of S100+ cells with the second elimination. ***D,*** 63X representative images of Iba1/GFAP/TGF$_{\beta}$1 immunoreactivity reveals a shift in the expression of TGFβ-1 to within astrocytes.

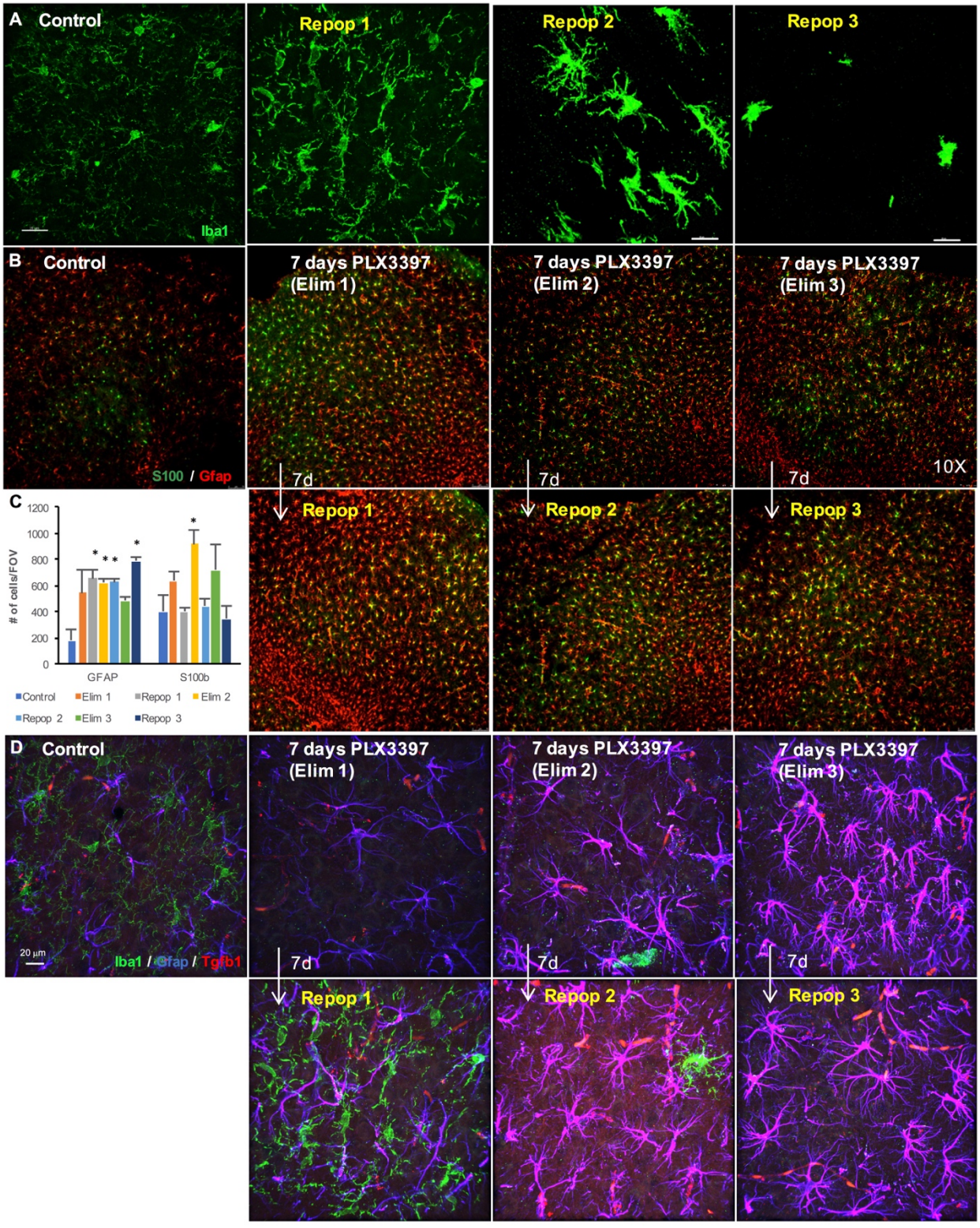

Figure 2.5

genes were associated with antigen processing and presentation, as well as MAPK signaling (Figure 2.6A).

Given the failure to repopulate in cycles 2 and 3, most gene expression changes from Control brains were downregulated microglia-expressed genes, due to the cells' absence. We therefore compared differentially expressed genes between Eliminated mice and Repop groups 1, 2, and 3 (Figure 2.6B-I). Common upregulated genes to all comparisons were involved with cell adhesion molecules, HSC lineage, and chemokine signaling, while oligodendrocyte genes OLIG1 and OLIG2 were among the shared downregulated genes (Figure 2.6H). There were 336 unique upregulated and 45 downregulated genes between Elim vs. Repop 1, demonstrating that Repop 1 is dissimilar from the other two Repop groups, as expected. Interestingly, the Elim vs. Repop 3 comparison revealed unique upregulations in gene expression of endothelial cell-expressed TBX15, MEOX1, and FOXC1 (Figure 2.6G). Repop 2 and 3 are virtually identical to one another, with only 7 differentially expressed genes between them (Figure 2.6I).

Expanded capacity for microglial repopulation with increased recovery time:

Having shown that the adult brain has the capacity for just one complete round of microglial repopulation with the previous paradigm, I wanted to determine if that capacity could be increased by allowing more recovery time between cycles. To that end, groups of male mice (n=4/group) were treated with cycles of 7 days' treatment with PLX3397 (600 mg/kg), followed by 28 days of recovery (Figure 7A). This time, all three rounds of repopulation were successful, showing that the adult brain requires recovery

Figure 2.6

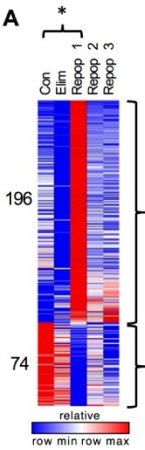

Up-regulated genes (196)

KEGG Term	PValue	Genes
mmu04622:RIG-I-like receptor signaling pathway	1.48E-04	**DDX58**, IFIH1, ISG15, **IRF7**, TRIM25, DHX58, CXCL10
mmu04650:Natural killer cell mediated cytotoxicity	5.98E-04	H2-K1, CD48, PIK3CG, ITGAL, PTPN6, TNFSF10, RAC2, PLCG2
mmu04060:**Cytokine-cytokine receptor interaction**	0.002382651	CCL12, TNFSF10, CSF2RB2, IL10RA, CXCL16, CSF1, TNFRSF13B, CSF3R, CSF2RB, CXCL10
mmu04662:B cell receptor signaling pathway	0.002599481	PIK3CG, PTPN6, RAC2, PLCG2, PIK3AP1, INPP5D
mmu04062:**Chemokine signaling pathway**	0.005906151	PIK3CG, CCL12, RAC2, HCK, CXCL16, STAT1, PLCB2, CXCL10
mmu04621:NOD-like receptor signaling pathway	0.006325643	NAIP6, CCL12, NAIP2, NAIP5, NLRP1B
mmu04630:**Jak-STAT signaling pathway**	0.009503344	PIK3CG, PTPN6, CSF2RB2, IL10RA, CSF3R, CSF2RB, **STAT1**
mmu04640:**Hematopoietic cell lineage**	0.017972969	TFRC, CD33, CSF1, CSF3R, FCGR1
mmu04620:**Toll-like receptor signaling pathway**	0.030688794	PIK3CG, **IRF7**, TLR2, **STAT1**, CXCL10
mmu04514:Cell adhesion molecules (CAMs)	0.037063036	H2-K1, ITGAL, SIGLEC1, PTPRC, ICOSL, CD274

Down-regulated genes (74)

KEGG Term	PValue	Genes
mmu04612:**Antigen processing and presentation**	0.005431568	HSPA1A, HSPA1B, HSPA5, CALR, HSPA8
mmu04010:MAPK signaling pathway	0.019672504	DUSP4, CACNG5, HSPB1, HSPA1A, HSPA1B, HSPA8

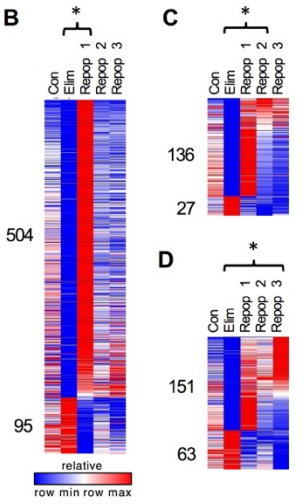

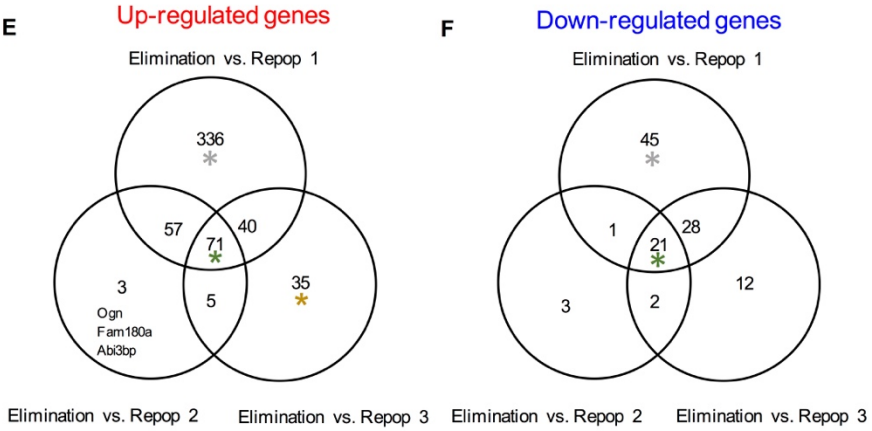

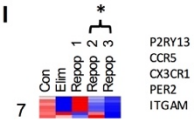

G Up-regulated genes

*

KEGG Term	Pvalue	Genes
mmu04612:Antigen processing and presentation	2.79E-05	H2-K1, TAP2, LGMN, TAP1, H2-EB1, H2-DMB1, IFI30, H2-T23, H2-Q6, B2M, TAPBP
mmu04621:NOD-like receptor signaling pathway	3.94E-04	NAIP6, NAIP2, NAIP5, CASP8, PYCARD, RIPK2, NLRP1B, CARD6
mmu04620:Toll-like receptor signaling pathway	0.001463683	CD86, **IRF7**, CASP8, TLR3, PIK3R5, **STAT1**, TLR7, CD14, CXCL10
mmu04630:Jak-STAT signaling pathway	0.001859732	IRF9, IL10RB, CSF2RB2, IL10RA, CSF2RB, IL2RG, PIK3R5, IL13RA1, **STAT1**, IFNGR1, IL6RA
mmu04514:Cell adhesion molecules (CAMs)	0.002050125	H2-K1, F11R, ICAM1, SIGLEC1, CD86, ITGA6, CD274, H2-EB1, H2-DMB1, H2-T23, H2-Q6
mmu04060:Cytokine-cytokine receptor interaction	0.002719752	CSF2RB2, TGFBR2, TGFB1, CXCL10, IL6RA, TNFRSF1B, TNFRSF11A, IL10RB, CXCL16, IL10RA, CSF2RB, IL2RG, IL13RA1, IFNGR1

*

KEGG Term	PValue	Genes
mmu04650:Natural killer cell mediated cytotoxicity	0.001011755	PTPN6, RAC2, FCER1G, ITGB2, VAV1, TYROBP
mmu04514:Cell adhesion molecules (CAMs)	0.002842017	PTPRC, H2-AA, H2-AB1, ITGB2, SELPLG, ITGAM
mmu04062:Chemokine signaling pathway	0.005809097	CCL12, DOCK2, RAC2, NCF1, CX3CR1, VAV1
mmu04662:B cell receptor signaling pathway	0.014425227	PTPN6, RAC2, PIK3AP1, VAV1
mmu04640:Hematopoietic cell lineage	0.016437982	CD33, H2-AA, ITGAM, CSF1R
mmu04612:Antigen processing and presentation	0.020323897	H2-AA, H2-AB1, CTSS, CD74

*

GO Term	PValue	Genes
GO:0009952~anterior/posterior pattern formation	0.025101075	ALDH1A2, **MEOX1**, **FOXC1**
GO:0048856~anatomical structure development	0.0500611	ALDH1A2, CAV1, **TBX15**, **MEOX1**, **FOXC1**, **SP7**, FLNC, GJB2
GO:0014033~neural crest cell differentiation	0.052077712	ALDH1A2, **FOXC1**
GO:0014032~neural crest cell development	0.052077712	ALDH1A2, **FOXC1**

H Down-regulated genes

*

GO Term	PValue	Genes
GO:0051726~regulation of cell cycle	0.002014726	CDKN1A, CALR, GADD45A, HSPA8, GPR3
GO:0006469~negative regulation of protein kinase activity	0.007350877	CDKN1A, GADD45A, SPRY4
GO:0051445~regulation of meiotic cell cycle	0.02750972	CALR, GPR3
GO:0044092~negative regulation of molecular function	0.04388074	CDKN1A, GADD45A, SPRY4

*

GO Term	PValue	Genes
GO:0030182~neuron differentiation	0.013080965	NFASC, CNP, **OLIG1**, **OLIG2**
GO:0007399~nervous system development	0.020108837	NFASC, CNP, **OLIG1**, CLDN11, **OLIG2**
GO:0048699~generation of neurons	0.023428938	NFASC, CNP, **OLIG1**, **OLIG2**
GO:0022008~neurogenesis	0.028645675	NFASC, CNP, **OLIG1**, **OLIG2**

Figure 2.6 Pathway analysis and further comparison of differentially expressed genes, obtained via RNA-seq. ***A,*** Pathway analysis of differentially expressed genes between Con and Repop 1 reveals 196 upregulated genes, many of which are associated with cytokine and chemokine signaling, Jak-STAT signaling, and general immune cell identity and functions; downregulated genes involved in antigen processing and MAPK signaling. ***B-D,*** Heatmaps of differentially expressed genes between Con vs. Repop 1, Con vs. Repop 2, and Con vs. Repop 3, respectively. ***E-F,*** Venn diagrams of common and unique differentially expressed genes between Elim vs. Repop 1, Elim vs. Repop 2, and Elim vs. Repop 3. ***E,*** Analysis of upregulated genes between the three comparisons, reveals 336 uniquely differentially expressed genes in Elim vs. Repop 1 comparison. ***F,*** Analysis of downregulated genes between the three comparisons. ***G-H,*** Pathway analysis of common and unique differentially expressed upregulated and downregulated genes between Elim vs. Repop 1, Elim vs. Repop 2, and Elim vs. Repop 3. Colored asterisks for analyses match those in venn diagrams from ***F.***

time between cycles for repopulation. Notably, the third recovery is less complete than the first two. Immunostaining revealed that cells in the third cycle still expressed functional CSF1R's (Figure 2.8A). Many macrophage and monocyte populations in the periphery also express the CSF1R, yet are not depleted with CSF1R inhibitors (Elmore et al., 2014; Valdearcos et al., 2014). Several microglia-specific markers have recently been identified, including P2RY12 (Butovsky et al., 2014), and TMEM119 (Bennett et al., 2016). Immunostaining revealed clear heterogeneity in P2RY12 expression in the 3rd repopulation study, with half the cells being ramified and expressing both Iba1 and P2RY12, and the other half being far less ramified and not staining for P2RY12 (Figure 2.8B, E-F). Similar results were seen with TMEM119 (Figure 2.8C, D, G). These two cell populations were found consistently throughout all brain regions surveyed. The observed effects (myeloid cells that are resistant to CSF1R inhibition and a lack of P2RY12/Tmem119 immunostaining) are consistent with a population of infiltrating cells from peripheral sources, with these multiple cycles of microglial depletion and repopulation.

Figure 2.7 Cyclic treatment of WT mice with 600 mg/kg PLX3397, and 28d withdrawal periods. ***A,*** Representative whole brain stitches of Iba1^{+} cells in each group. ***B,*** Quantification of number of Iba1+ cells/FOV in hippocampus, cortex, and thalamus reveals all three repopulation cycles match control numbers, although there are fewer cells in the third repopulation cycle than the first two cycles. ***C,*** 63X representative images of Iba1+ cells during each repopulation cycle, and the third elimination cycle.

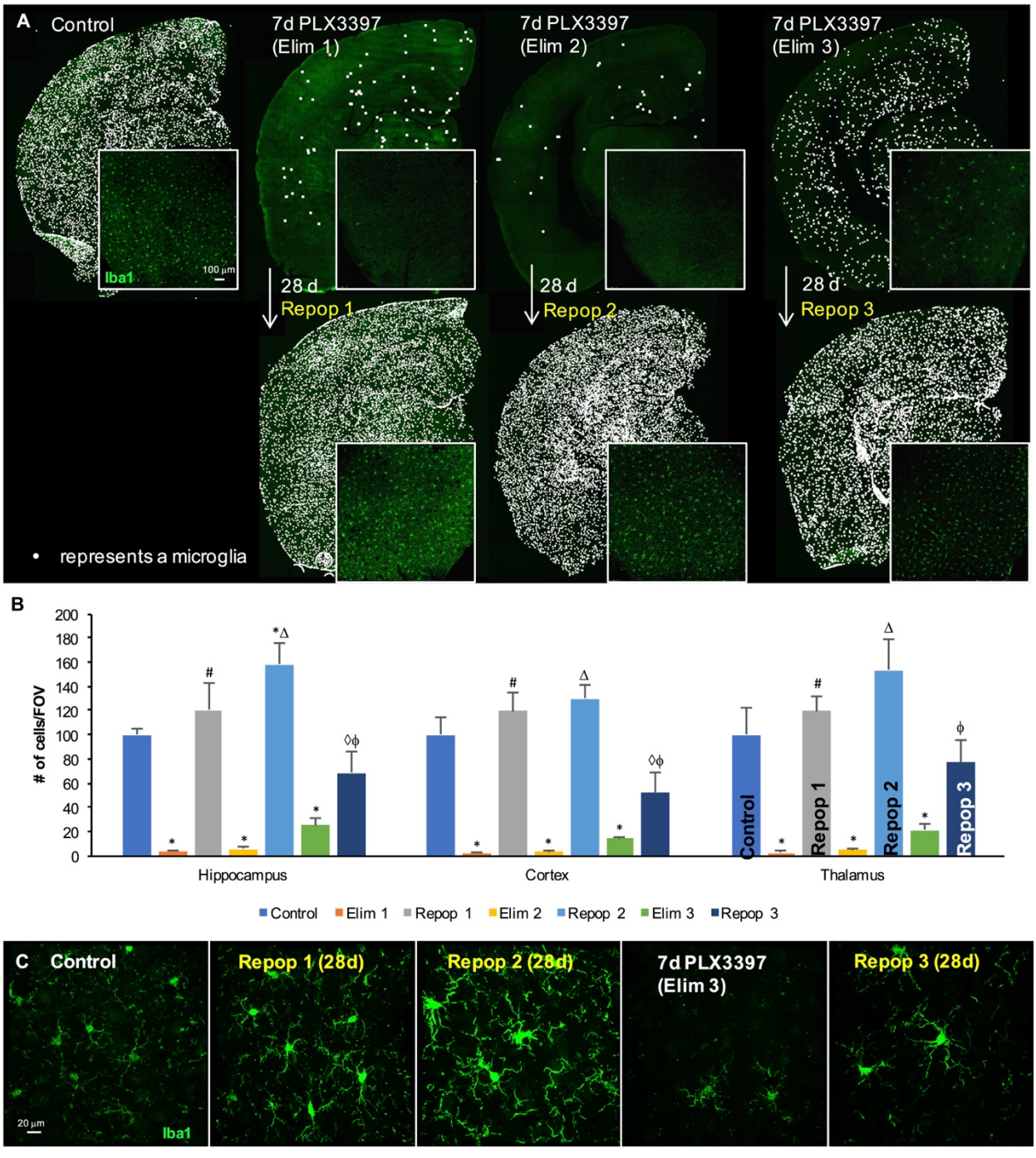
A
Control
7d PLX3397
(Elim 1)
7d PLX3397
(Elim 2)
7d PLX3397
(Elim 3)
Iba1
100 μm
28 d
Repop 1
28 d
Repop 2
28 d
Repop 3
• represents a microglia
B
# of cells/FOV
200
180
160
140
120
100
80
60
40
20
0
Hippocampus
Cortex
Thalamus
Control
Repop 1
Repop 2
Repop 3
Control
Elim 1
Repop 1
Elim 2
Repop 2
Elim 3
Repop 3
C
Control
Repop 1 (28d)
Repop 2 (28d)
7d PLX3397
(Elim 3)
Repop 3 (28d)
20 μm
Iba1

Figure 2.7

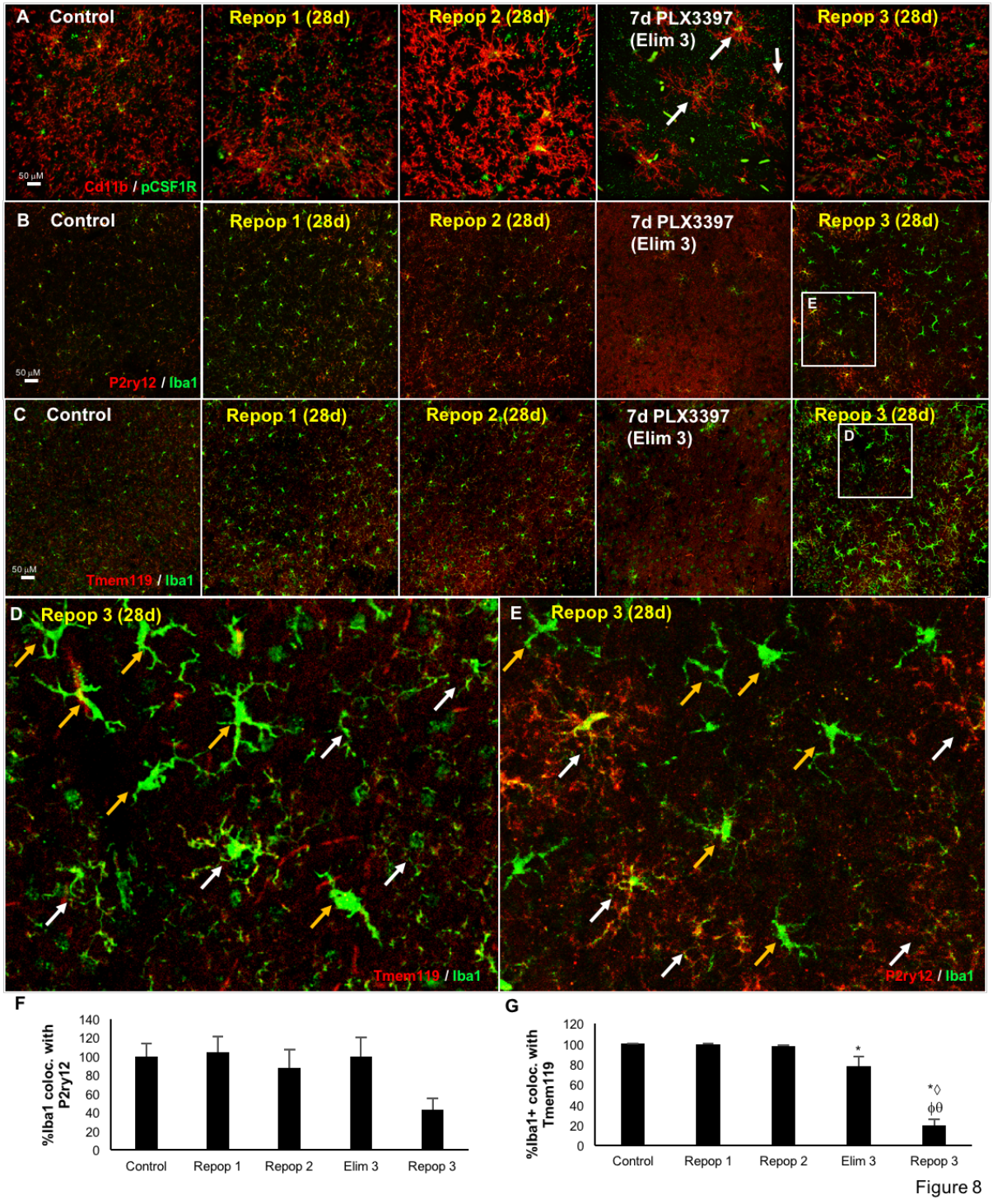

Figure 8

Figure 2.8 Properties of returning cells with long recovery cycles of 600 mg/kg PLX3397. ***A,*** 10X representative images of $Cd11b^{+}$ and $pCSF1R^{+}$ cells reveals surviving cells in the third elimination cycle still retain active CSF1 receptors. ***B, E,*** 10X representative images of cells staining positively for P2ry12 and/or Iba1 reveals subset of $Iba1^{+}$ cells that are not $P2ry12^{+}$. ***C,D,*** 10X representative images of cells staining postively for Tmem119 and/or Iba1 reveals subset of $Iba1^{+}$ cells that are not $Tmem119^{+}$. ***F- G,*** Quantification of percentage of Iba1+ area that colocalizes with P2ry12 and Tmem119 expression, respectively.

DISCUSSION

I previously demonstrated that microglial elimination via CSF1R inhibition and the subsequent removal of these antagonists stimulates proliferation and differentiation of unidentified precursor cells throughout the brain into microglia. However, the limits of repopulation via proliferation of these cells have not yet been determined. Here, I explored the dynamics of microglial repopulation following treatment with CSF1R inhibitors, and reveal that depending on the potency and duration of treatment with CSF1R inhibitors, there is a finite capacity for full brainwide microglial repopulation.

I sought to better understand the signals coordinating successful vs. failed repopulation cycles through whole-brain gene expression profiling, but not surprisingly, the great majority of genes that are differentially expressed between groups with and without microglia, are typically expressed by microglia. As expected, profiling of the microglia depleted brain reveal a core set of genes markedly downregulated with CSF1R inhibitor treatment that are known to be expressed solely or highly in microglia, and confirm several studies detailing gene expression in microglia extracted from brains (Beutner et al., 2013; Chiu et al., 2013; Hickman et al., 2013; Butovsky et al., 2014; Bennett et al., 2016). These genes include P2ry12, Tmem119, Fcrls, and Tgfbr1. Further gene expression profiling of repopulated brains showed that the returning microglia are clearly in an activated state, with a characteristic IFNγ-induced profile, and an upregulation of many pro-inflammatory cytokines and chemokines. As the depletion of microglia (via CSF1R inhibitors or other means) is artificial, we must be tapping into existing pathways and mechanisms to bring about rapid and powerful cell division and differentiation. We speculate that the brain may have evolved to rapidly produce large

quantities of microglia during times of infection, and thus the default phenotype for rapidly repopulating microglia would be a state in which to fight and contain potentially infectious agents. Indeed, our prior results show that although they initially appear primed to protect against an attack, in the absence of actual pathogens or damage, repopulated microglia revert to a resting/surveillant state within 14 days (Elmore et al., 2015).

With an understanding that our model of microglial repopulation involves proliferation and differentiation of unidentified microglial precursor cells, we looked to examples of similar paradigms with OPCs to guide us in exploring the kinetics of microglial repopulation. Administration of cuprizone leads to demyelination of axons through the selective death of oligodendrocytes. Once demyelinated, OPCs then proliferate and differentiate into new oligodendrocytes, effectively remyelinating the axons (Mason et al., 2000; Sachs et al., 2014). Using a model of chronic cuprizone treatment, it has been shown that the OPCs become progressively depleted resulting in failed remyelination (Mason et al., 2004). Paralleling these observations, I found that with rapid cycles of microglial elimination and withdrawal (7 days' treatment, 7 days' withdrawal), microglia failed to repopulate a second or third time, suggesting that the source of repopulating microglia is exhausted. In both cases, it would appear that the progenitors require time to replenish themselves in order to contribute to prolonged or cyclic functional differentiation and repopulation. Further similarities were also found with oligodendrocyte depletion and subsequent remyelination. Varying the dose and/or time of CSF1R inhibitor treatment affects the extent/speed of microglial depletion. For example, administration of PLX3397 at 290 mg/kg in chow leads to 50% depletion of

microglia within 7 days. Repopulation following 50% microglial depletion is slow, and does not recover microglial numbers to control levels within 7 days following inhibitor withdrawal. On the other hand, inhibitor withdrawal following >95% microglial elimination, either through 21 days' treatment with PLX3397 at the same dose (290/mg/kg in chow; (Elmore et al., 2014), or with 7 days' treatment with PLX3397 at 600mg/kg in chow, is rapid, with microglial densities reaching 150% of control levels within 7 days. Thus, the brain responds differentially to varying extents of microglial depletion, suggesting a sensing mechanism for mounting an appropriate repopulation response, with greater depletion requiring more powerful and rapid repopulation. Similar observations have been made with the remyelination that occurs following cuprizone-mediated demyelination; remyelination only occurs with extensive demyelination, and does not occur with incomplete demyelination (Doan et al., 2013).

Thus, having shown a limited capacity for microglial repopulation presumably due to exhaustion of source cells with 7-day cycles, I wanted to assess if this pool could recover and extend the number of useful cycles. Indeed, when greater time (28d) was allowed for recovery between treatment cycles, I found that microglia were repopulated a second and third time, indicative of a capacity of the precursor pool to replenish itself between cycles of differentiation. Curiously though, cycling treatment with long recovery periods also revealed a population of $Iba1^{+}/P2ry12^{-}$ and $Iba1^{+}/Tmem119^{-}$ cells after the third repopulation event that lacked the extensive ramifications indicative of resident microglia, suggestive of a non-microglial cell type. As P2yr12 and Tmem119 are expressed exclusively by microglia (Butovsky et al., 2014; Bennett et al., 2016), and not peripheral myeloid populations, this suggests that multiple cycles can result in monocyte

infiltration into the brain parenchyma, leading to heterogeneous populations of myeloid cells. Thus, while allowing for extended recovery periods between cycles does prolong the number of useful elimination-repopulation events, it does also appear to have effects on the source and properties of the repopulating cells.

In conclusion, I have shown that the kinetics of microglial repopulation closely mirror those of remyelination by OPCs following oligodendrocyte death. Firstly, the rate of repopulation is proportional to the extent of microglial depletion, with more extensive depletion stimulating more rapid and powerful repopulation. Secondly, I have found that there is a limited capacity for repopulation, suggesting that the source of repopulating cells is exhausted within one depletion/repopulation cycle. However, given sufficient time these pools will recover and further cycles are then possible. These similarities to OPCs provide a biological comparison between properties of two distinct CNS progenitor cell populations. Finally, it appears that multiple repopulation cycles take a toll on the brain, with evidence of peripheral infiltrating cells seen in the 3rd repopulation event.

CHAPTER THREE

IDENTIFICATION OF A NOVEL ROUTE OF MICROGLIAL REPOPULATION ALONG THE ROSTRAL MIGRATORY STREAM AND PROJECTING AXONS

INTRODUCTION

Microglia are the primary immune cell in the brain, and are responsible for coordinating dynamic responses to insults and injury. Microglial development is unique from other myeloid cells, in that microglia derive directly from yolk sac macrophages, and do not go through a monocyte intermediate cell. The brain is the first organ to be colonized with myeloid cells. Interestingly, white matter areas of the brain or areas that lie in close proximity to white matter, such as the SVZ, and the RMS, are among the first regions in the CNS to be colonized by microglia (Ueno et al., 2013; Arno et al., 2014). Of note, colonization of the SVZ has been shown to be essential for normal BP development (Arno et al., 2014). Microglia are long-lived cells with a low turnover rate, and are physically separated from circulating myeloid populations by the BBB. Although under certain conditions studies have shown that peripheral myeloid cells can enter the brain and differentiate into brain parenchymal macrophages, it is generally understood that this is does not occur under normal physiological conditions.

Previously, we have demonstrated that microglial survival is critically dependent upon CSF1R signaling (Elmore et al., 2014; Elmore et al., 2015; Spangenberg et al., 2016; Rice et al., 2017). These studies demonstrated that CSF1R inhibition results in ablation of up to 99% of microglia, and the extent of depletion can be modulated in a dose-

dependent manner (Dagher et al., 2015). Notably, with the doses and duration of treatment utilized previously, ~1-2% of the resident microglial population survive CSF1R inhibition. Although peripheral myeloid populations depend on signaling through the CSF1R for immune functions such as migration and proliferation, they are not depleted with CSF1R inhibition (Elmore et al., 2014). Importantly, upon cessation of treatment with CSF1R inhibitors, microglia rapidly repopulate brain-wide (Elmore et al., 2014; Rice et al., 2017), which is mediated by proliferation of both surviving microglia and CNS-resident microglial precursor cells. Within seven days of inhibitor withdrawal, new microglia have fully repopulated the brain, with numbers surpassing those of control, and by 14 days, exhibit similar numbers and phenotypes to control microglia (Elmore et al., 2014). Similar repopulation kinetics have been reported in an alternative model of microglial depletion utilizing an acute administration of diphtheria toxin, confirming that repopulation occurred from within the CNS, with no peripheral contributions (Bruttger et al., 2015)). These studies show that the adult brain has a remarkable capacity to repopulate the entire microglial tissue, and gives insights into the regulation of microglial homeostasis and inflammatory responses.

Here, I have uncovered a strategy to deplete 100% of brain microglia using CSF1R antagonists, and find that normal CNS-derived repopulation is subsequently inhibited, instead leading to alternative repopulation dynamics. Following complete ablation, the timing and pattern of microglial repopulation is drastically altered; only a fraction of myeloid cells return to the brain by 7 days CSF1R inhibitor withdrawal, and are preferentially found along the RMS and its projecting axons. I propose that this repopulation is driven by a specific population of white matter/RMS microglia, which

then proliferates and populates the rest of the brain parenchyma. This indicates that there are subpopulations with differences in regenerative capacities and potentially in function, and we have uncovered the tool with which to explore these niches.

MATERIALS AND METHODS

Compounds

PLX3397 was provided by Plexxikon, Inc. and formulated in standard chow by Research Diets Inc. at 290- and 600mg/kg.

Animal Treatments

All rodent experiments were performed in accordance with animal protocols approved by the Institutional Animal Care and Use Committee at the University of California, Irvine. 2-9 month-old age-matched male mice were provided with control chow or PLX3397 chow for 7 or 14 days at a time. Following each treatment cycle, PLX3397 was withdrawn and all mice maintained on control chow for 0-28 days. At the conclusion of experiments, mice were sacrificed via CO_2 inhalation and perfused transcardially with 1X phosphate-buffered saline (PBS). Brains were extracted and dissected down the midline, with one half flash-frozen on dry ice for subsequent RNA and protein analyses, and the other half drop-fixed in 4% paraformaldehyde (PFA) in 1X PBS. Fixed brains were cryopreserved in a 30% sucrose solution, frozen, and sectioned at 40 μm on a Leica SM2000 R sliding microtome for subsequent immunohistochemical analyses.

Confocal microscopy

Fluorescent immunolabeling followed a standard indirect technique (primary antibody followed by fluorescent secondary antibody), as previously described (Elmore et al., 2014). Acid pretreatments were used for BrdU detection. Primary antibodies used include Iba1 (1:1000; Wako), Cd11b (1:100; Bio-Rad), anti-Ki67 (1:1000; Abcam), anti-BrdU (1:1000; Abcam), IB4 (1:P2ry12 (1:500; Sigma). Colocalization scores and numbers of myeloid cells and astrocytes were determined using the colocalization and spots modules in Bitplane Imaris 7.5 software. Stained tissue was mounted on slides and coverslipped with Dapi Fluoromount-G (SouthernBiotech).

RNA Extraction and NanoString RNA Analysis

RNA was extracted and purified from frozen half brains using an RNA Plus Universal Mini Kit (Cat. #73404, Qiagen, Hilden, Germany) per the manufacturer's instructions. Total RNA was monitored for quality control using the Agilent Bioanalyzer Nano RNA chip and Nanodrop absorbance ratios for 260/280nm and 260/230nm. Using the PanCancer Immune Profiling Panel, seven hundred and seventy genes for immune cell types, antigens, and immune response were analyzed by NanoString nCounterTM technologies (NanoString) against mouse genes. Counts for target genes were normalized to house-keeping genes (*Eef1g, G6pdx, Hprt, Polr1b, Polr2a, Ppia, Rpl19, Sdha,* and *Tbp*) to account for variability in the RNA content. Background signal was calculated as a mean value of the negative hybridization control probes. Normalized counts were log-transformed for downstream statistical analysis.

Statistics

All analyses apart from RNA-seq were performed using one-way ANOVAs with post-hoc Tukey's Multiple Comparison tests for all multiple comparisons (Graphpad Prism 6). For non-RNA-seq analyses, statistical significance was accepted at $p<0.05$; trends at $p<0.10$.

RESULTS

Repopulation occurs through proliferating microglia and non-microglial cells following robust microglial depletion:

To demonstrate microglial repopulation, I treated 2-month old male mice with PLX3397 (600mg/kg in chow) for 7 days, withdrew the inhibitor and then examined the brains 1, 2, 3, and 7 days later (n=4/group). As expected, very few surviving microglia were found in treated brains (~1%; Figure 3.1A, B), and $IBA1^+$ cells were first observed at 2 days' recovery (Figure 3.1E). While many of these cells were $IB4^+$, some were not. $IBA1^+$ cell numbers increased to ~10% of control levels by 3 days' recovery, and shot to ~150% of control levels by 7 days' recovery (Figure 3.1B), consistent with our prior results showing an overshoot with robust depletion (Elmore et al., 2014). Staining for proliferating cells with Ki67 revealed many non-microglial proliferating cells throughout the brain appearing at 1-day recovery

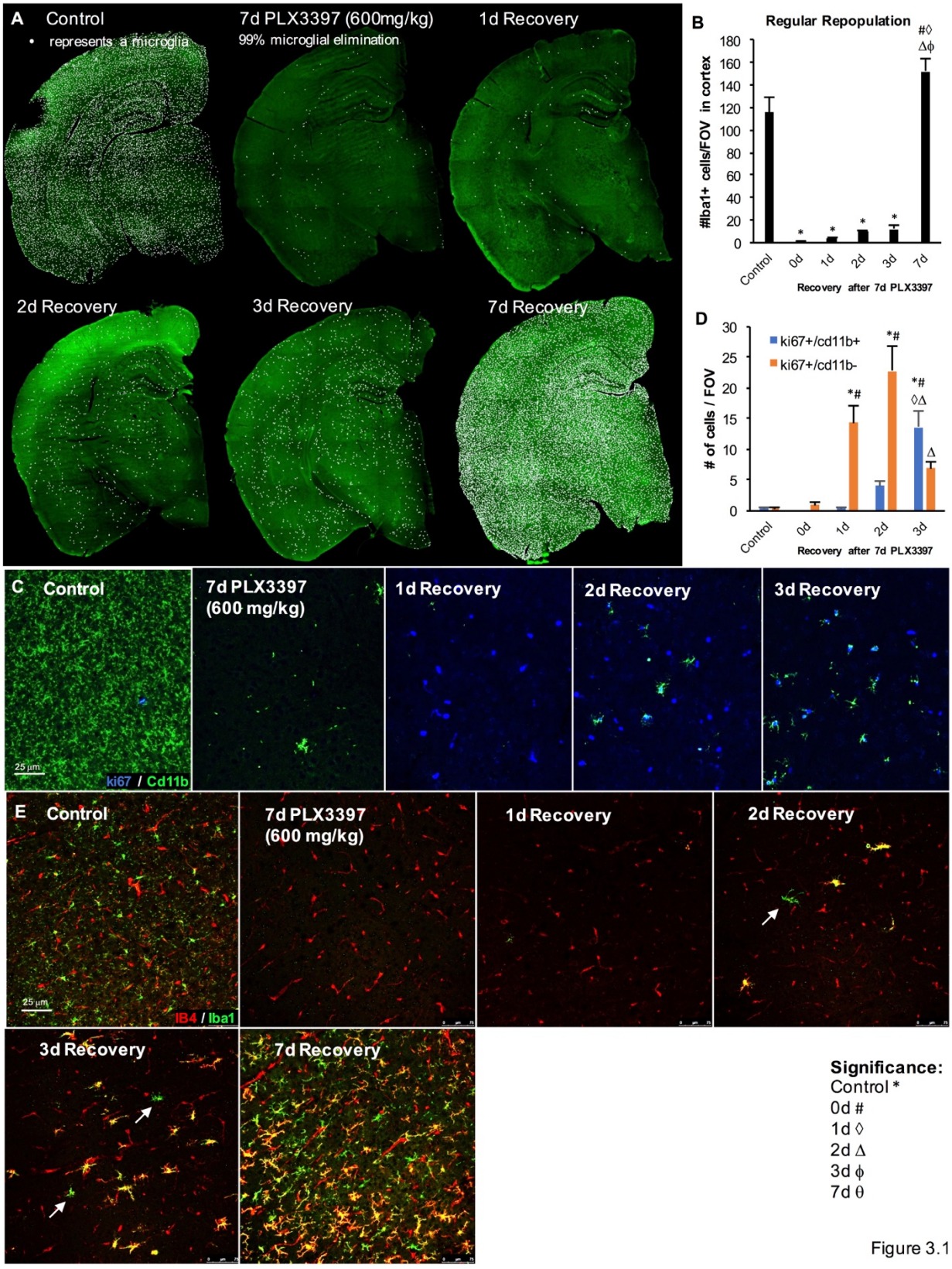
A
Control
• represents a microglia
7d PLX3397 (600mg/kg)
99% microglial elimination
1d Recovery
2d Recovery
3d Recovery
7d Recovery
B
Regular Repopulation
#◊
Δϕ
#Iba1+ cells/FOV in cortex
180
160
140
120
100
80
60
40
20
0
Control
0d
1d
2d
3d
7d
Recovery after 7d PLX3397
D
ki67+/cd11b+
ki67+/cd11b-
# of cells / FOV
30
25
20
15
10
5
0
*#
*#
◊Δ
*#
Δ
Control
0d
1d
2d
3d
Recovery after 7d PLX3397
C
Control
7d PLX3397
(600 mg/kg)
1d Recovery
2d Recovery
3d Recovery
25 μm
ki67 / Cd11b
E
Control
7d PLX3397
(600 mg/kg)
1d Recovery
2d Recovery
25 μm
IB4 / Iba1
3d Recovery
7d Recovery
Significance:
Control *
0d #
1d ◊
2d Δ
3d ϕ
7d θ

Figure 3.1

Figure 3.1 Assessment of early repopulation following 7-day treatment with 600 mg/kg PLX3397. Wild-type mice were treated with PLX3397 (600 mg/kg) for 7 days to deplete microglia, and subsequently recovered for 1, 2, 3, or 7 days after withdrawal of CSF1R inhibitors. ***A-B,*** Representative brain stitches of recovery timepoints with white dots superimposed over $Iba1^+$ cells and quantification of cortical cells. ***C-D,*** 20X representative images of tissue stained for Ki67 and Cd11b and quantification of number of cells colocalized or staining positively for only Ki67. ***E,*** 20X representative images of $IB4^+$ and $Iba1^+$ cells reveal most returning microglia are $IB4^+$, while some are not. Error bars represent SEM, (n=4). p<0,05; significance symbols represent comparison groups: Control *, 0d #, 1d ◊, 2d Δ, 3d ϕ, 7d θ.

(Figure 3.1C, D). By 2 days' recovery, ~20% of proliferating cells were also expressing CD11b, a common myeloid cell marker. By 3 days' recovery, most proliferating cells were also $CD11b^+$ (Figure 3.1C), consistent with our prior findings (Chapter 1, (Elmore et al., 2014), and reflecting cells that appear to initially lack canonical microglial markers, but slowly switch on these classic myeloid markers over the course of a day.

Differential myeloid repopulation with complete microglial elimination:

Administration of CSF1R inhibitors reliably eliminates microglia from the CNS, but a small fraction of cells has always remained (between 1-5% of total microglia), even with extended treatment durations (Chapter 2, (Elmore et al., 2014)). These remaining cells are scattered throughout the CNS, and do not appear restricted to any specific location. Administration of PLX3397 at 600 mg/kg in chow was sufficient to reduce microglia numbers by >98% in just 7 days (Figure 3.1B) – the largest/most rapid effect to date. Thus, I sought to determine whether extended treatments could eliminate the remaining 1-2% of microglia. Two-month old male mice (n=4/group) were treated with PLX3397 (600 mg/kg in chow) for 14 days, and their brains examined for $IBA1^+$ cells. With this treatment duration, microglia depletion was absolute, with no $IBA1^+$ cells found in any brains examined (Figure 3.2A). I determined levels of PLX3397 in brains and compared them to mice treated for 7 days, and found no significant differences (Figure 3.2B) – thus, complete elimination is a factor of sustained CNS exposure of CSF1R inhibition.

One of the remarkable observations that we have made about microglial repopulation is that it does not occur until CSF1R inhibitors are removed from the CNS. Thus, there is a sensing mechanism in place that responds to a lack of CSF1R inhibition and initiates repopulation. As microglia are reported to be the primary cell type in the CNS that expresses the receptor, it suggests that these few percent of surviving microglia may be key to driving repopulation, upon inhibitor withdrawal. Thus, to explore how complete elimination affected microglial repopulation, I treated groups of mice with PLX3397 (600 mg/kg) for 14 days, then withdrew the inhibitor and examined their brains 3, 7, 14, and 28 days later. Normally, repopulation is apparent by 3 days, and the brain has overshot microglial numbers by 7 days (Figure 1.1E, F). Here, I found zero $IBA1^+$ cells with 3 days' recovery, but by 7 days, sparse $IBA1^+$ cells were found almost exclusively in white matter tracts surrounding ventricles and the hippocampus (Figure 3.2A). However, by 14 and 28 days, these cells had spread throughout the CNS. Quantification of these $IBA1^+$ cells showed that absolute numbers of cortical cells were 50% lower than microglia in control cortices (Figure 3.2C), even after 28 days' recovery. Thus, I hypothesized that the complete elimination of all microglia inhibits brain-wide repopulation (as seen in Figure 1.1), and instead stimulates repopulation from a specific source or niche, spreading out from white matter tracts to fill the brain. Our findings indicate that these cells initially appear in the white matter tracts and display altered morphology, including large cell somas (Figure 3.2J-L). Furthermore, returning cells at 7 days' recovery stain positively for IB4, which is commonly used as an activation marker, and 28d Recovery myeloid

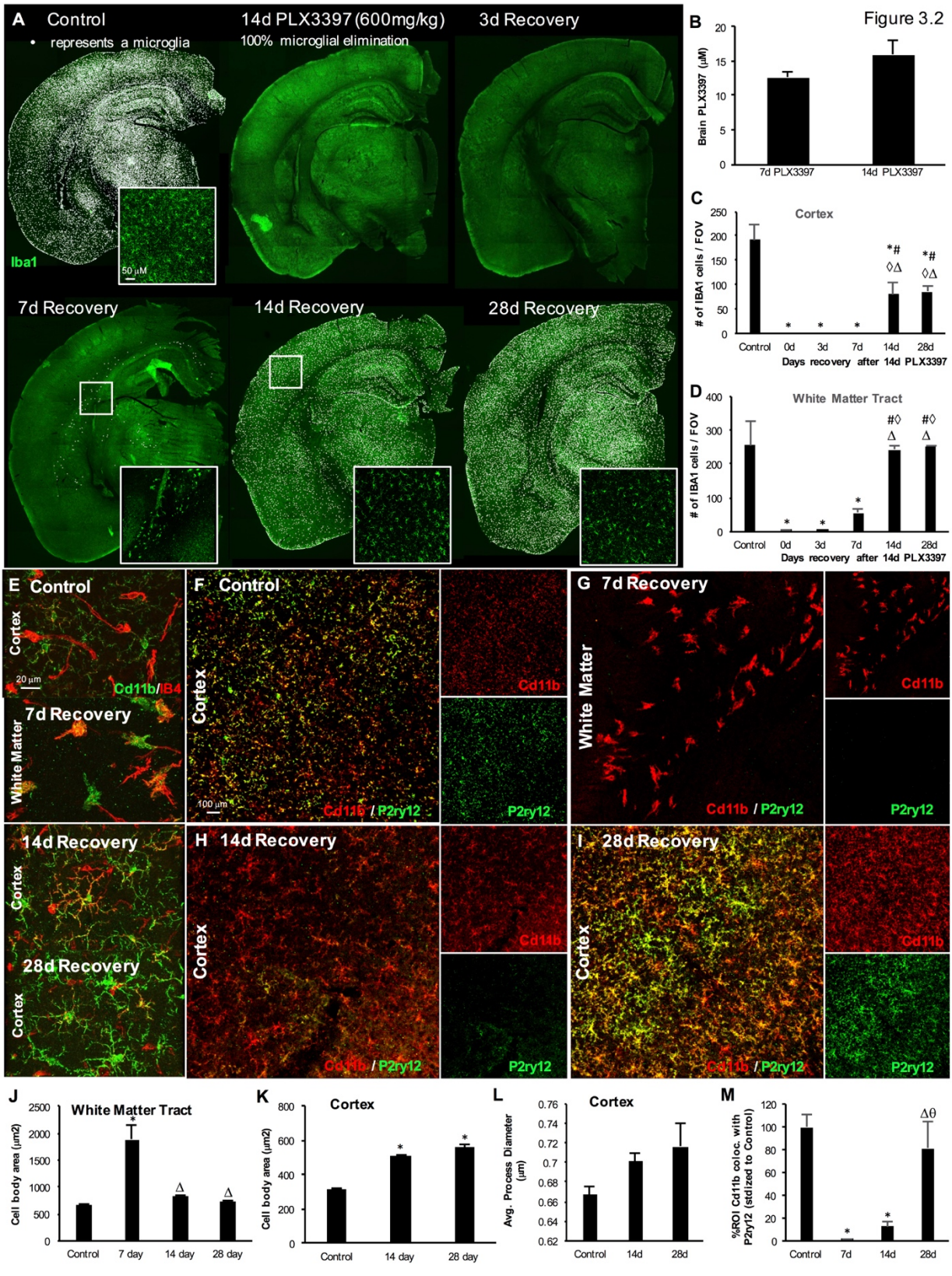
A Control
• represents a microglia
14d PLX3397 (600mg/kg)
100% microglial elimination
3d Recovery
Iba1
50 µM
7d Recovery
14d Recovery
28d Recovery
B
Figure 3.2
Brain PLX3397 (µM)
7d PLX3397
14d PLX3397
C
Cortex
# of IBA1 cells / FOV
Control
0d
3d
7d
14d
28d
Days recovery after 14d PLX3397
D
White Matter Tract
# of IBA1 cells / FOV
Days recovery after 14d PLX3397
E Control
Cortex
20 µm
Cd11b/IB4
7d Recovery
White Matter
F Control
Cortex
100 µm
Cd11b / P2ry12
Cd11b
P2ry12
G 7d Recovery
White Matter
Cd11b / P2ry12
14d Recovery
28d Recovery
H 14d Recovery
I 28d Recovery
J
White Matter Tract
Cell body area (µm2)
Control
7 day
14 day
28 day
K
Cortex
Cell body area (µm2)
L
Cortex
Avg. Process Diameter (µm)
M
%ROI Cd11b coloc. with P2ry12 (stdized to Control)
Control
7d
14d
28d

Figure 3.2 Altered repopulation dynamics following 100% microglial elimination with 14d PLX3397 (600 mg/kg) treatment. Wild-type mice were treated with 600 mg/kg PLX3397 for 14 days to eliminate all microglia, and 3-, 7-, 14-, and 28-day recovery timepoints assessed. ***A, C-D,*** Representative brain stitches of recovery timepoints with white dots superimposed over Iba1$^+$ cells. ***B,*** Brain PK levels of PLX3397 with 7- or 14-day treatment (600 mg/kg). ***E,*** Immunostaining for P2ry12 and CD11b reveals returning cells are not initially P2ry12$^+$, but are by 28d recovery. ***J-M,*** Analyses of cell body area in white matter and cortex, average process diameter, and percent colocalization in cortex, respectively. Error bars represent SEM, (n=4). $p<0,05$; significance symbols represent comparison groups: Control *, 0d #, 3d ◊, 7d Δ, 14d ϕ, 28d θ.

cells are still staining positively for IB4 (Figure 3.2E). To examine the identity of these repopulating microglia, I immunolabeled tissue for P2ry12, a specific marker for resident microglia, and found repopulating microglia to be P2ry12-negative (Figure 3.2G). However, with 28 days' recovery, microglia begin to express P2ry12 (Figure 3.2H, I, and quantified in M). Interestingly, these repopulating cells maintain different morphologies to resident microglia, with enlarged cell sizes and thickened processes out to 28 days' recovery (Figure 3.2K, M).

Gene expression profile of differentially repopulated brains

To characterize the profile of the fully-depleted and differentially-repopulated brain, I isolated RNA and analyzed transcript levels for immune cell-related genes using Nanostring nCounter technology. Here, I show significantly changed genes between each group to help illustrate and identify key differences in expression profiles (Figure 3.3). As expected, given the complete absence of microglia, I identified many genes that were downregulated with 14d treatment of 600 mg/kg PLX3397 compared to Control. Of these downregulated genes, a substantial number were core myeloid genes, such as CSF1R, CX3CR1, TREM2, CD33, etc. (Figure 3.3A). I also identified a number of genes

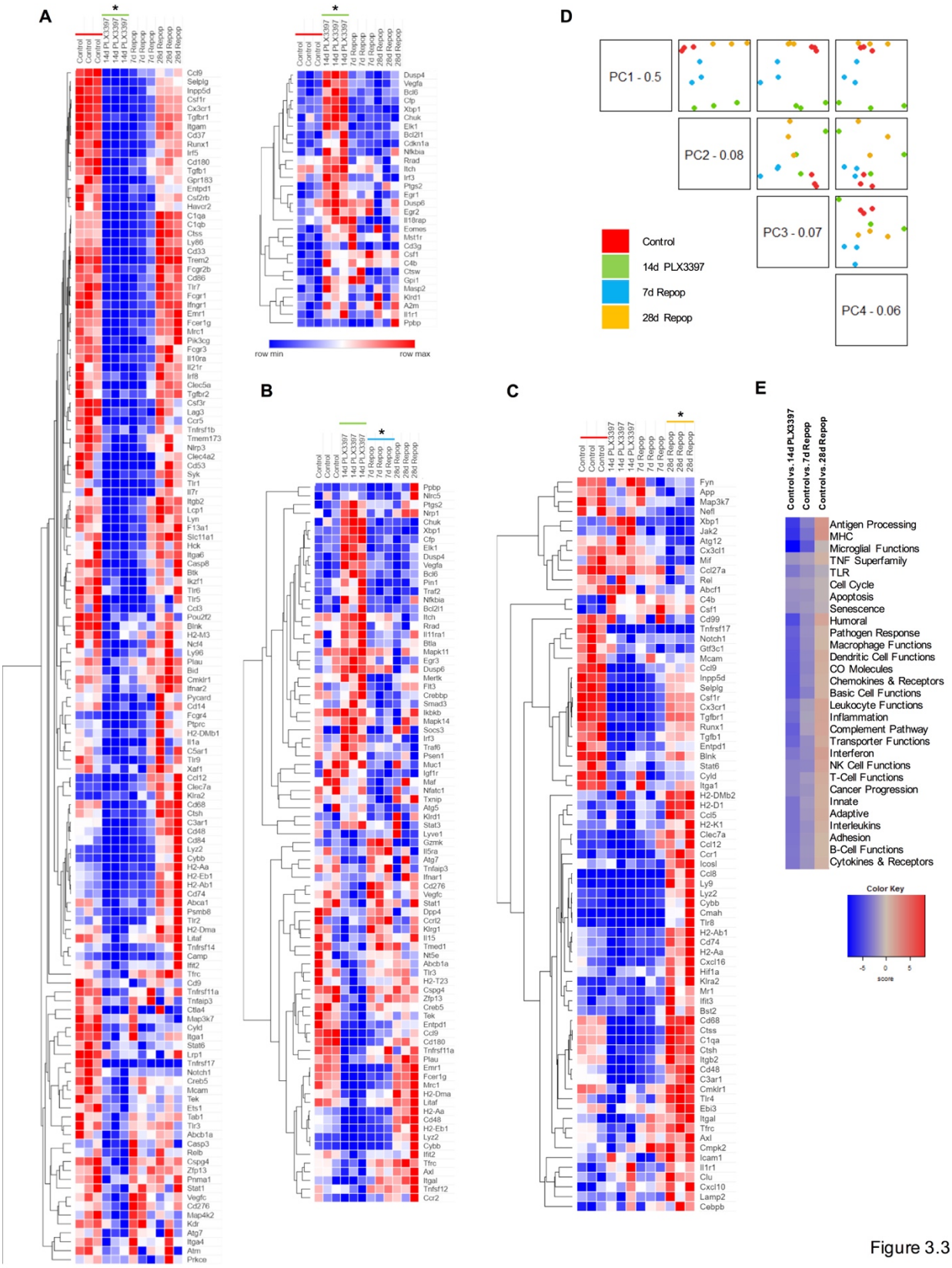
A
B
C
D
E
PC1 - 0.5
PC2 - 0.08
PC3 - 0.07
PC4 - 0.06
Control
14d PLX3397
7d Repop
28d Repop
row min
row max
Color Key
score
Antigen Processing
MHC
Microglial Functions
TNF Superfamily
TLR
Cell Cycle
Apoptosis
Senescence
Humoral
Pathogen Response
Macrophage Functions
Dendritic Cell Functions
CO Molecules
Chemokines & Receptors
Basic Cell Functions
Leukocyte Functions
Inflammation
Complement Pathway
Transporter Functions
Interferon
NK Cell Functions
T-Cell Functions
Cancer Progression
Innate
Adaptive
Interleukins
Adhesion
B-Cell Functions
Cytokines & Receptors

Figure 3.3

Figure 3.3 Immune cell gene expression changes persist at 28d recovery. Transcipt levels for immune cell signaling-related genes were analyzed using NanoString nCounter technology. Morpheus software was employed to generate heatmaps and highlight overarching changes in gene expression between groups. ***A-C,*** Heatmaps shown for comparisons between Control vs. 14d PLX3397, 14d PLX3397 vs. 7d Repop, and Control vs. 28d Repop, respectively, displayed with hierarchical clustering between comparisons and all group expression levels. ***D,*** PCA plot of all groups. ***E,*** Immune cell function heatmap between Control vs. 14d PLX3397, Control vs. 7d Repop, and Control vs. 28d Repop.

that were upregulated with 14d PLX3397, including several involved in cell proliferation, such as DUSP4, DUSP6, EGFR1, EGFR2, and CHUK. Other upregulated genes included VEGFA and XBP1, both associated with angiogenesis, as well as the transcription factors ELK1 and BCL6, and the complement factors C4b and CFP (Figure 3.3A). In addition, we compared gene expression changes between microglia-depleted brains (14d Elim) and those at 7 days' recovery (7d Repop), whereby myeloid cells were observed only within white matter tracts and around ventricles (Figure 3.3B). Many of the genes that had been elevated with 14d Elim vs. Control returned to control levels by 7 days' recovery (Figure 3.3B). Interestingly, within this comparison, core myeloid gene expression was outpaced by increases in other inflammatory genes at 7d Repop, including IL5RA, CD276, VEGFC, STAT1, CCRL2, TFRC, AXL, and TNFSF12, suggesting that the myeloid cells that had initially returned had a different expression profile to resident microglia. For instance, GZMK, normally found in T and B cells and circulating monocytes, was found to be upregulated with repopulation, but not downregulated with microglial elimination. Comparisons between control brains and those at 28 days' recovery, by which time new cells had fully populated the entire CNS for at least 14 days, revealed vast differences. Core myeloid genes remained downregulated, such as INpp5d, CSf1R, CX3CR1, TGFBR1, RunX1, and TGFB1, reflecting the fact that microglial densities in some regions were only 50% of those found in control brains (Figure 3.3C). Despite the reduced numbers of cells, many

genes are upregulated at 28 day repopulation compared to control brain. These genes are implicated in several immune functions including antigen processing and MHC presentation (Figure 3.3E). These findings indicate that even at 28d Repop, cells maintain a unique profile, distinct from control brains. Interestingly, within the list of upregulated genes at 28d Repop is the gene for CCR1, an inflammatory myeloid cell marker not expressed in the brain under normal conditions (Sunnemark et al., 2003) as well as H2-D1, LY9, CYBB, CMAH, LYZ2, and TLR8. As such, this list of upregulated genes may provide us with a specific marker for the microglial niche responsible for differential repopulation. These results suggest that the cells produced by this route of repopulation retain a distinct genetic profile from resident microglia, or from microglia that have repopulated via the normal mechanism defined in Chapters 1 and 2 and as determined by a recent studying showing RNA analysis of 28 day-repopulated microglia to be similar to untreated brains (Elmore et al., 2014; Elmore et al., 2015; Rice et al., 2017).

Myeloid cells first appear along rostral migratory stream:

Given the lack of P2ry12 reactivity, a specific microglial marker over other myeloid populations, the initial appearance of repopulating cells around the ventricles, and the fact that the repopulating cells never reached normal microglial densities or morphologies, we hypothesized that repopulation was occurring from peripheral cell sources. We explored whether returning cells were originating via the choroid plexus, a highly vascularized CSF-producing structure within the ventricles, as several studies report that peripheral cells infiltrate the CNS via the choroid plexus, under disease

conditions (Chinnery et al., 2010; Demeestere et al., 2015). However, examination of myeloid cells revealed that while all choroid macrophages and dendritic cells were fully eliminated with 14 days PLX3397 treatment, they did not repopulate until the 14-day recovery timepoint, despite the appearance of myeloid cells in the adjacent caudate putamen by 7 days' recovery (Figure 3.4A-CB). Ruling out the choroid plexus as a route of infiltration, I took advantage of natural variability in the numbers and location of repopulating cells at the 7-day recovery time point to identify the anatomical locations at

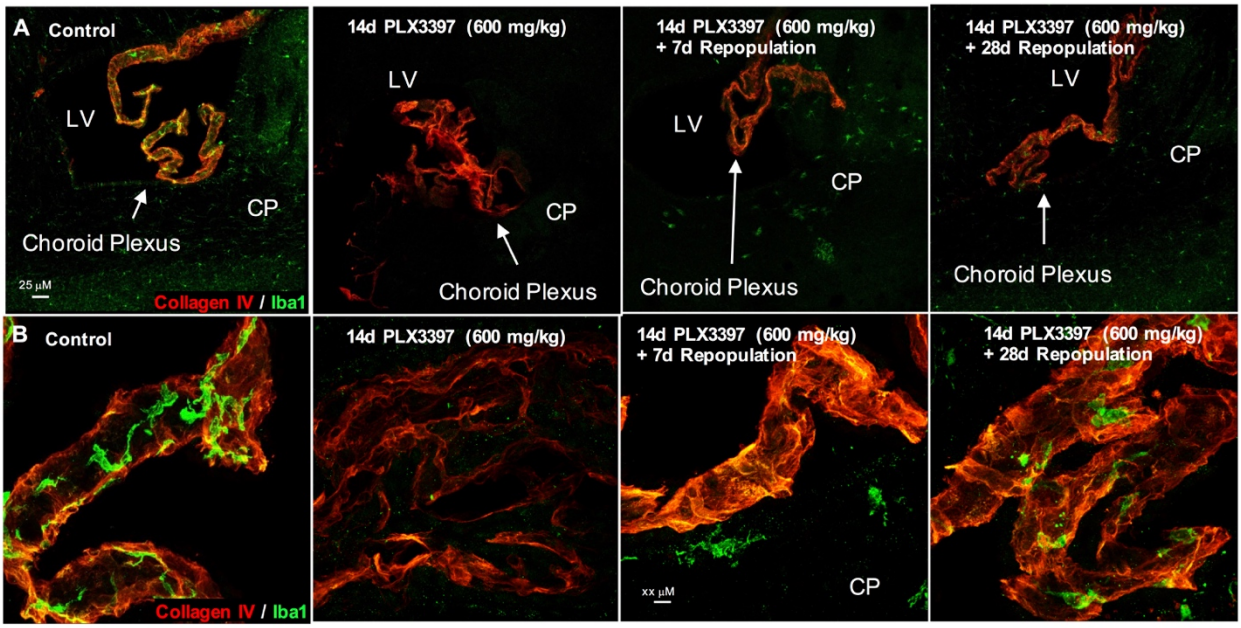

Figure 3.4

Figure 3.4 Repopulating cells do not originate from the choroid plexus. ***A-C,*** Representative 20X, 63X, and 10X images of the choroid plexus immunolabeled with Collagen IV and Iba1 or DAPI and Iba1 from same cohort of mice as in Figure 2, respectively.

which repopulating cells were first appearing. We constructed a spatial heatmap for repopulating cells at three locations within the brain (Figure 3.5A-C). Across all brains surveyed, I found cells around the lateral ventricular areas, particularly in the caudate putamen, cingulate cortex, and subependymal zone (SEZ) and anterior commissure (ACO) of the olfactory bulb. Notably, these regions all correspond to the RMS, a pathway by which neuroblasts migrate from SVZ to the OB.

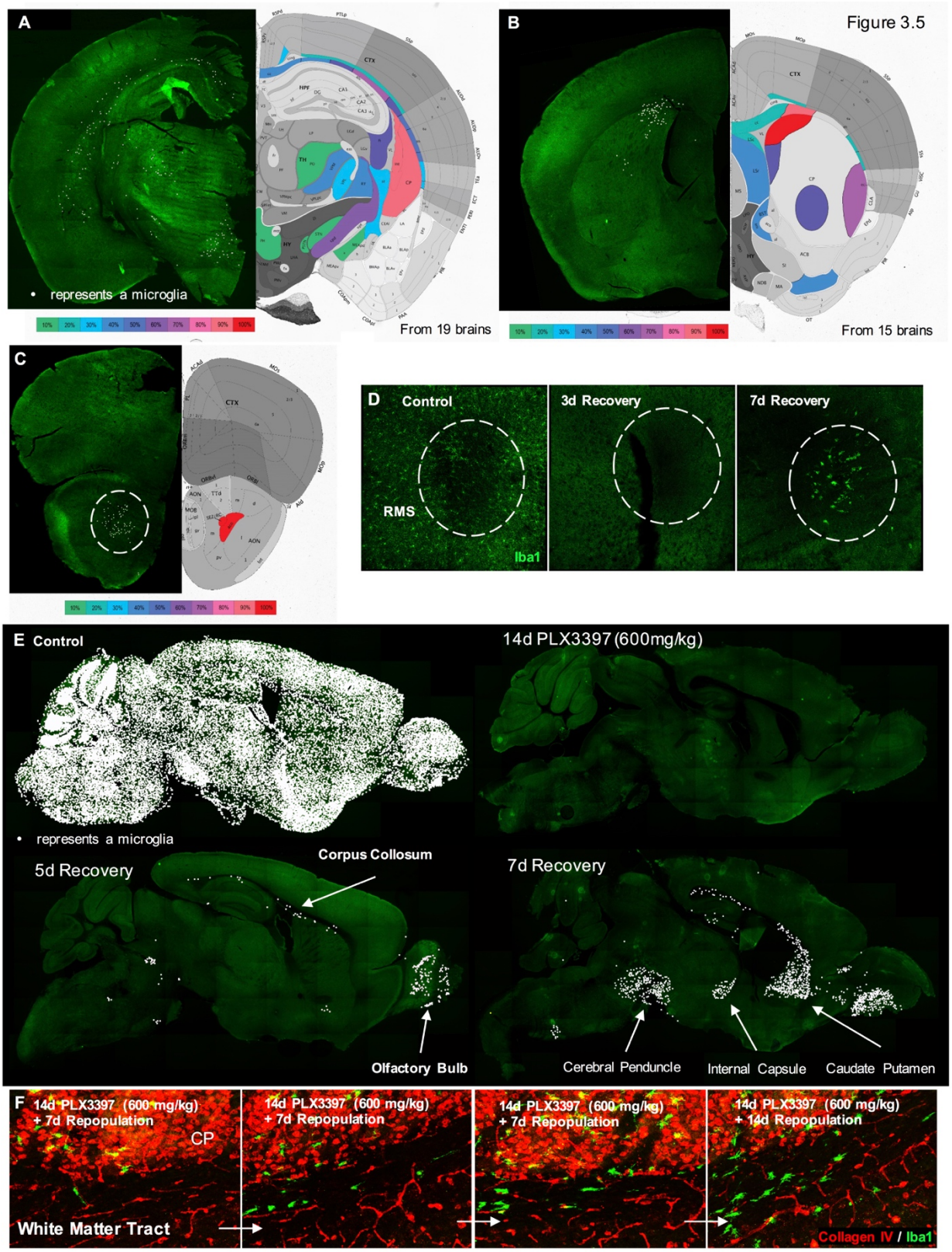
A
• represents a microglia
From 19 brains
B
Figure 3.5
From 15 brains
C
D
Control
3d Recovery
7d Recovery
RMS
Iba1
E Control
14d PLX3397 (600mg/kg)
• represents a microglia
5d Recovery
Corpus Collosum
7d Recovery
Olfactory Bulb
Cerebral Penduncle
Internal Capsule
Caudate Putamen
F
14d PLX3397 (600 mg/kg) + 7d Repopulation
CP
White Matter Tract
14d PLX3397 (600 mg/kg) + 7d Repopulation
14d PLX3397 (600 mg/kg) + 7d Repopulation
14d PLX3397 (600 mg/kg) + 14d Repopulation
Collagen IV / Iba1

Figure 3.5 Differentially repopulated cells first appear along RMS and projecting axons. ***A-C,*** Anatomical brain heat maps were constructed from half-brain stitches of three regions along the RMS at the 7d recovery timepoint (n=15-19). ***D,*** Representative 20X images of Iba1-immunolabeled brains at an anterior section of the RMS, with RMS tracts circled. ***E,*** Whole brain sagittal sections with white dots representing Iba1-immunolabeled cells at 14d PLX3397 treatment and 5- and 7-day recovery timepoints reveals cells closely associating with regions of the RMS and other projecting axons. ***F,*** Representative images of Iba1-immunolabeled cells along white matter tracts at 7d and 14d recovery.

Given this, we then repeated the experiment and allowed for recovery timepoints of 5 and 7 days, sectioning the brains sagittally (Figure 3.5E). The 5-day recovery timepoint revealed cells within the corpus callosum and the olfactory bulb, while by 7 days recovery cells were also found in the caudate putamen, internal capsule, and cerebral peduncles. Thus, repopulation occurs throughout the RMS, but also other projecting axonal tracts such as the cerebral peduncle. Notably, microglia along the RMS and other projecting axonal tracts have been shown to exhibit different properties from parenchymal gray matter microglia, including the lack of purinergic receptor expression (Ribeiro-Xavier et al., 2015). Examination of the white matter tracts lining the caudate putamen close to where repopulating cells were first observed appeared to suggest that cells initially appeared close to the white matter tract before migrating into the tract itself (Figure 3.5F).

Repopulation does not occur from CCR2-expressing cells:

Given the initial appearance of repopulating cells within the projecting axonal tracts, we wanted to differentiate between the infiltration of these cells from peripheral sources, and the *de novo* appearance of these cells. The CCR2/CCL2 signaling axis is known to be necessary for signaling from the CNS to peripheral infiltrates (Mildner et al., 2009; Ajami et al., 2011). To address peripheral contributions, CCR2-RFP$^{+/-}$/CX3CR1-GFP$^{+/-}$ mice were utlized to visualize any infiltrating CCR2^{+} monocytes. Microglia were again depleted in these mice (data not shown), and 7d recovery revealed CX3CR1-GFP^{+} cells

along the RMS and projecting axons (surrounding the LV and caudate putamen), but no CCR2^{+} cells were evident, with the exception of a handful of cells within the choroid plexus (Figure 3.6).

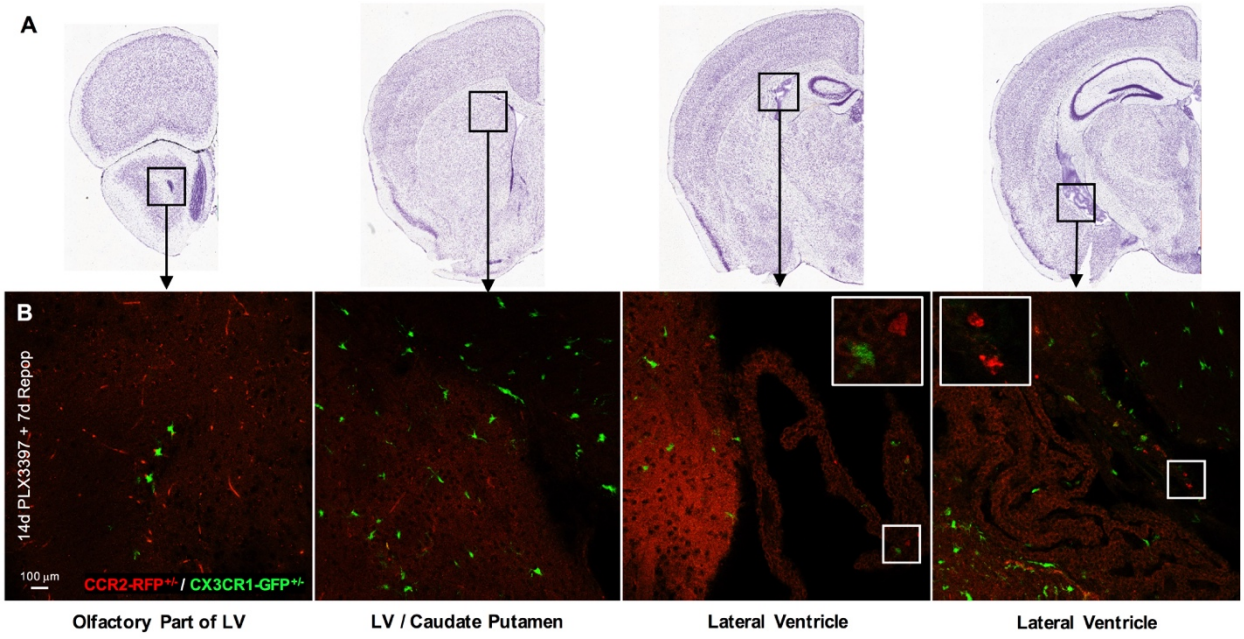

Figure 3.6

Figure 3.6 Absence of CCR2+ cells with differential RMS-associated repopulation. ***A-C,*** CCL2$^{-/-}$ mice were treated for 14d with PLX3397 (600 mg/kg) and allowed to recover for 7 days. Brains were immunolabeled for Iba1 and half brain stitches are shown in ***A***. Representative 20X images are shown in ***B***, with quantification in ***C. D,*** Homozygous knockouts for CCR2 and CX3CR1 were treated with the same paradigm as in ***A***, and representative 10X images shown for anterior LV, caudate putamen, and LV.

To further study the CCR2/CCL2 axes we repeated studies in CCL2$^{-/-}$ mice as well as homozygous CCR2-RFP$^{+/+}$/CX3CR1-GFP$^{+/+}$ mice, which have both of these genes knocked out. CCR2-RFP$^{+/+}$/CX3CR1-GFP$^{+/+}$ mice were treated with the same 14d 600 mg/kg PLX3397 paradigm, and elimination in these mice reached the same levels as controls (Figure 3.7A). Crucially, repopulation in the absence of CCR2 is indistinguishable from WT repopulation (Figure 3.7A), signifying that this is not a CCR2-mediated pathway, and as such, is likely not occurring from peripheral infiltration.

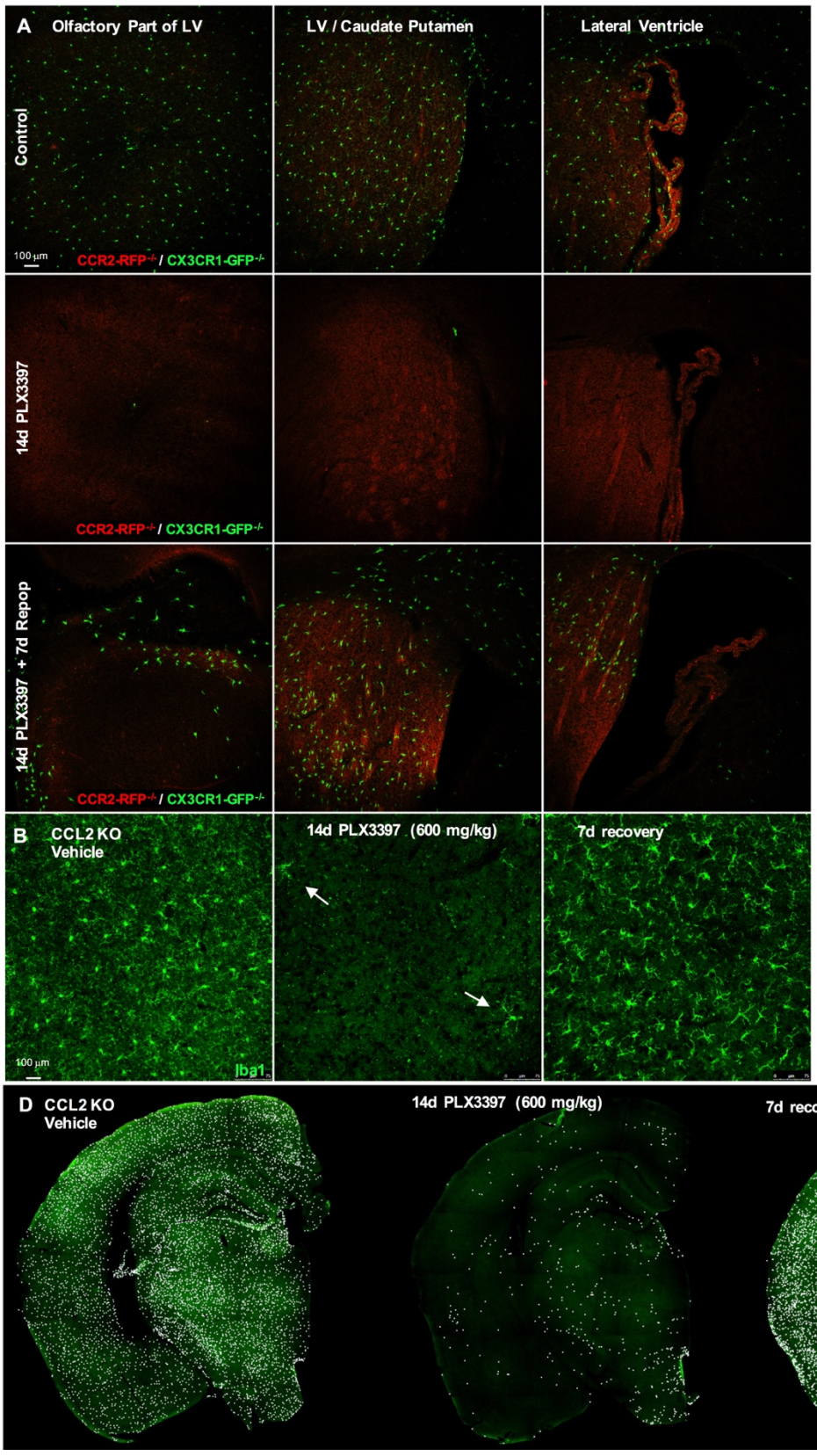
A
Olfactory Part of LV
LV / Caudate Putamen
Lateral Ventricle
Control
100 μm
CCR2-RFP-/- / CX3CR1-GFP-/-
14d PLX3397
CCR2-RFP-/- / CX3CR1-GFP-/-
14d PLX3397 + 7d Repop
CCR2-RFP-/- / CX3CR1-GFP-/-
B
CCL2 KO
Vehicle
14d PLX3397 (600 mg/kg)
7d recovery
100 μm
Iba1
C
Cortex
WM tract
Iba1+ cells / FOV
200
150
100
50
0
Vehicle
14d PLX3397
7d recovery
D
CCL2 KO
Vehicle
14d PLX3397 (600 mg/kg)
7d recovery

Figure 3.7 ***Differential repopulation occurs in the absence of CCR2 signaling.*** CCR2-RFP$^{+/-}$/CX3CR1-GFP$^{+/-}$ mice were treated for 14d with PLX3397 (600 mg/kg) and allowed to recover for 7d. ***A,*** Allen Brain Atlas coronal brain slices used to demonstrate region of interest shown in ***B***. ***B,*** 7d recovery reveals CX3CR1-GFP+ cells in RMS-associated areas, but small numbers of CCR2-RFP+ cells are only present in choroid plexus.

Notably, we found that repopulation in CCL2$^{-/-}$ mice, following 14 days' treatment with PLX3397 at 600 mg/kg in chow and 7 days' recovery, was "normal" (as defined by repopulation following incomplete elimination of all microglia) and robust throughout the entire brain (Figure 3.7B-D). To explain this, examination of brains from mice treated for 14 days without any recovery revealed incomplete microglial elimination, with ~1% of cells still surviving despite 14 days of treatment, suggesting that the CCL2$^{-/-}$ phenotype conveys increased microglial resistance to CSF1R inhibition. Thus, these results confirm that 100% microglial elimination is a requirement for alternative repopulation, rather than a non-microglial-dependent effect associated with extended treatments of high-dose PLX3397, and highlight the crucial role that the surviving microglia play in determining the source of subsequent repopulation.

Microglia are depleted from RMS:

While we have previously shown that microglia are eliminated with CSF1R inhibitor treatment, as opposed to downregulating their microglial signatures (Chapter 1, (Spangenberg et al., 2016)), I had not confirmed this of cells within the RMS, as they have reported differences to other microglia (Doorn et al., 2015), nor with this treatment paradigm (14 days of 600mg/kg PLX3397). To ensure that microglia are depleted within the RMS, I also used progeny of CSF1R-iCRE mice crossed with Rosa26YFP reporter mice (generated from Chapter 1) and treated with the same paradigm. As seen previously, Cd11b-immunolabeled microglia colocalized with YFP-

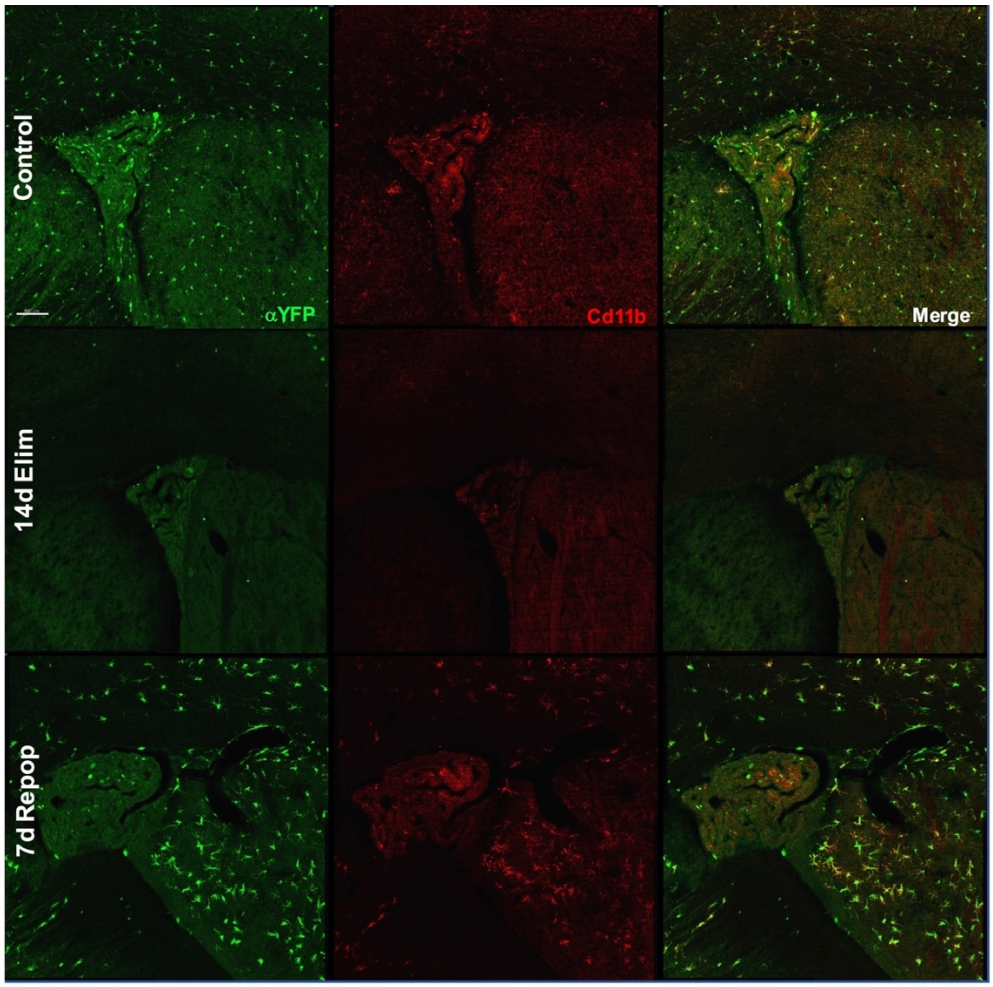

Figure 3.8. RMS microglia labeled by CSF1R lineage tracing are depleted with 14d PLX3397 (600 mg/kg) treatment. CSF1R-iCRE mice were crossed with Rosa-eYFP mice, so that progeny will express YFP in CSF1R expressing/derived cells. Progeny were treated for 14 days with 600 mg/kg PLX3397, and allowed to recover for 7 days. Immunolabeling for anti-GFP and Cd11b was performed, and representative images are shown

Figure 3.8

labeled cells in controls (Figure 3.8). In periventricular areas along the RMS, YFP+ cells were depleted with 14d PLX3397 treatment, demonstrating that there is not a microglial niche along the RMS that survives this treatment paradigm.

Repopulating cells derive from proliferation:

Having demonstrated that the cells in the RMS do not appear to derive from $CCR2^{+}$ monocytes, I next determined if they arose from proliferation. To that end, a cohort of mice received intraperitoneal BrdU injections (1/day for 6 days) during the repopulation period (n=4/group). At the 7-day timepoint, BrdU was found incorporated into

repopulating cells (Figure 3A), showing that they were undergoing, or had recently derived from, proliferation. Further analyses of all timepoints with the cell division marker ki67 confirmed that cells appearing at the 7-day recovery timepoint in white matter tracts were mostly dividing (Figure 3B), but by 14 and 28 days' recovery, cells had ceased proliferation. No proliferating cells were seen at the 14-day PLX3397 treatment timepoint, or at the 3-day recovery time point. Thus, collectively, these results suggest that we can stimulate repopulation from a specific microglial niche.

Repopulating cells are dependent on CSF1R signaling:

I have demonstrated previously that multiple cycles of treatment with CSF1R inhibitors can result in resistance, with an increased number of cells that survive treatment (Chapter 2). With cyclic treatment, the CSF1R inhibitor-resistant cells are also P2ry12-negative, thus I hypothesize that they are peripherally derived. As monocytes are also CSF1R inhibitor-resistant (Elmore et al., 2014), I wanted to identify the CSF1R-dependence of differentially repopulated cells to further elucidate their source, by treating repopulated brains again for 7 or 14 days with 600 mg/kg PLX3397. After both 7- and 14-day treatment, repopulated cells are depleted and shown to be dependent on CSF1R signaling for their survival (Figure 3.1, 3.2). This is in stark contrast to the cells that we believe to be infiltrating monocytes in Chapter 2, as a result of cyclic CSF1R inhibition, offering further evidence that differentially repopulated cells (with the 14d 600 mg/kg PLX3397 paradigm) are not infiltrates.

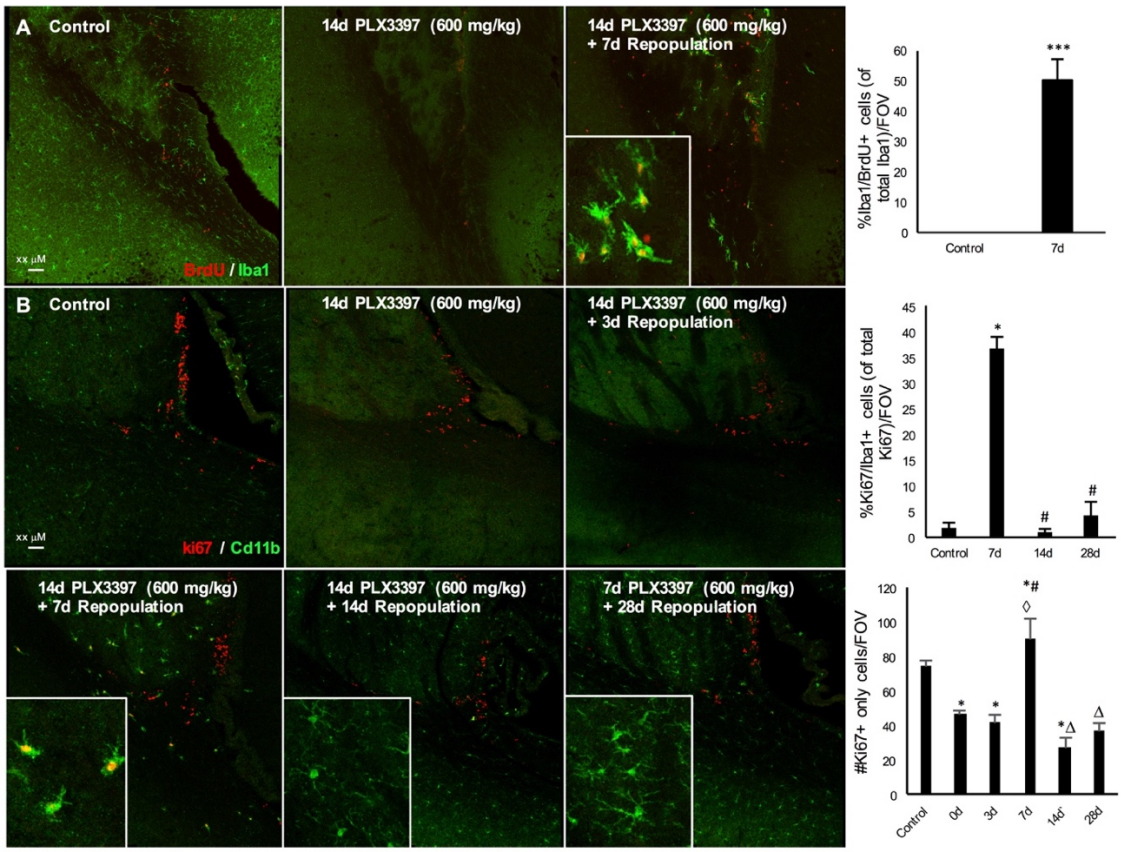

Figure 3.9

Figure 3.9 Returning microglia are initially proliferative. ***A,*** Control, eliminated, and 7d repopulation groups were injected with BrdU once a day for 6 days prior to sacrifice. Represenatitive images shown of BrdU and Iba1^{+} cells; quantification. ***B,*** ki67 immunostaining at all recovery timepoints after 14d treatment with PLX3397 reveals microglia are proliferating only at the 7d recovery timepoint; quantification of percentage of Ki67^{+} cells that are Iba1^{+} and total number of Ki67^{+} cells per FOV.

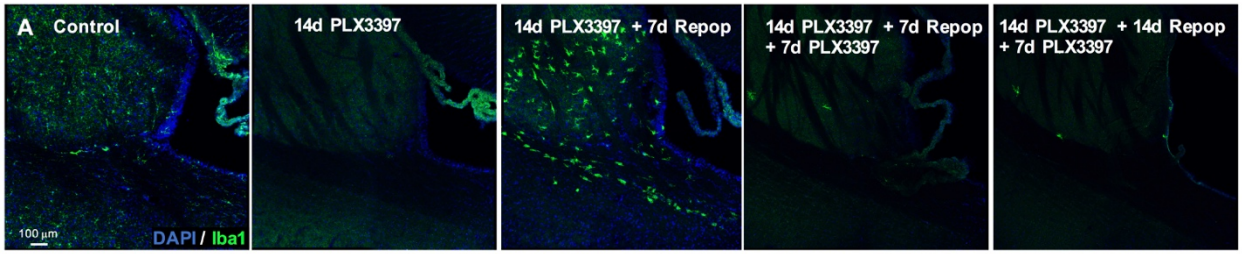

Figure 3.10

Figure 3.10. Repopulating cells are dependent on CSF1R signaling. Wild type mice were treated for 14 days with 600 mg/kg PLX3397, recovered for 7 days, and then treated again for either 7 or 14 days. Representative 10X images are shown of Iba1-immunolabeled cells around the lateral ventricle.

DISCUSSION

I have discovered an experimental paradigm that results in the complete elimination of microglia within 14 days, and explored the ways in which the complete ablation of the microglial compartment affects the brain's capacity to repopulate with new cells. Previously, up to 99% microglial elimination was possible with CSF1R inhibitors, and the withdrawal of inhibitors then stimulated a rapid repopulation that derived from the few surviving microglia as well as unidentified proliferating cells throughout the brain. By 28 days' recovery, the repopulating microglia were virtually indistinguishable from the resident microglia that they had replaced, in densities, spacing, morphologies, gene expression, and response to inflammatory stimuli (Elmore et al., 2015). Here, I have found that these few surviving microglia are key to "normal" brainwide repopulation, and that the elimination of 100% of microglia prevents "normal" repopulation, and instead stimulates an alternative repopulation event. With 7 days of recovery following 100% microglial depletion, rather than a full and brainwide return of microglia, ~85% of microglia remain depleted, and those cells that do appear are primarily aligned with white matter tracts and periventricular areas along the RMS. Initially, these myeloid cells do not express the microglia-specific marker P2ry12, suggesting that they may be peripheral in origin. By 14 days, these cells have spread out and filled the cortex, and begin to switch on P2ry12. By 28 days, most cells now express P2ry12, but cell densities remain at 50% of those normally found in control brains, while cell morphologies also remain altered, with larger cell bodies and thickened processes. Thus, this alternative repopulation event does not appear to resolve in a phenotype

similar to resident microglia, which is further confirmed by the altered immune gene expression profiling of these brains.

In exploring the anatomical locations at which these repopulating cells first appear, we ruled out peripheral infiltration via the choroid plexus. These cells do not appear to derive from peripheral monocytes, at least those expressing CCR2, or dependent on the CCL2/CCR2 signaling axis, but do arise from proliferation sometime between 3 and 7 days' recovery. Whether there is a unique microglial progenitor cell found within these projecting axonal tracts remains to be uncovered, as well as why repopulation occurs within these specific locations, but we have confirmed the complete elimination of microglia/myeloid cells from these tracts and the rest of the brain, and further confirmed that elimination is due to a physical absence of cells rather than a downregulation of myeloid signatures. Instead, cells initially appear throughout the RMS and other axonal projecting tracts, including the caudate putamen and cerebral peduncle. Notably, studies have shown that P2ry12 expression, as well as other purinergic and canonical microglial markers, are suppressed in RMS microglia (Ribeiro-Xavier et al., 2015), which may explain the lack of P2ry12 in the repopulating cells.

Interestingly, resident RMS and other axonal projecting tract microglia have been shown to be phenotypically distinct from other parenchymal microglia, with a unique expression profile and variances in reaction to stimuli. Many of these cells do not express, or express lower levels of, microglial purinergic receptors and as a result are insensitive to ATP, nor do they appreciably phagocytose neuroblasts (Ribeiro-Xavier 2015). Cells along the SVZ/RMS are proposed to have a specific function in promoting neuroblast cell survival, and may assist in the migration of new neurons to the OB. Moreover,

microglia isolated from the SVZ have 20x the proliferative potential in vitro than any other region analyzed in the brain (Marshall et al., 2008). We speculate that resident RMS microglia may support crucial functions in the brain, and the preferential appearance of myeloid cells along this zone at 7d recovery following full depletion of microglia may be coordinated in an attempt to preserve these functions. Once these cells have populated the RMS, proliferation occurs and myeloid cells spread throughout the rest of the parenchyma.

These data implicate a small percentage of surviving microglia as critical for parenchymal repopulation. In the absence of surviving microglia following CSF1R inhibition, differential repopulation occurs from an alternate source, specifically, the RMS and other projecting axonal tracts. Furthermore, differential repopulation from the RMS is not an artifact of extended treatment with high-dose CSF1R inhibitors, as the same dose and duration results in normal repopulation in the $CCL2^{-/-}$ mice. However, these mice undergo incomplete elimination, attributing further importance to the surviving cells for normal repopulation to occur. Notably, other models of incomplete microglial depletion using Cd11b-HSVTK mice have witnessed peripheral cell infiltration along similar rostral-caudal axes as we demonstrate here (Varvel et al., 2012), potentially arguing against the importance of full depletion for differential repopulation. However, this method also requires i.c.v. infusion of ganciclovir, disrupting the BBB and providing a route of entry for peripheral cells, possibly establishing a niche of BM-derived cells and inhibiting normal parenchymal microglial repopulation.

I demonstrate here that the mechanisms by which the brain repopulates itself with new myeloid cells following microglial depletion is variable, confirming studies by other

groups (Bruttger et al., 2015; Varvel et al., 2015). The response to microglial depletion is complex – somewhat intuitively, various methods of depletion achieve different repopulation outcomes (i.e. ganciclovir results in peripheral cell infiltration whereas CSF1R inhibition/diphtheria toxin mediated microglial death results in CNS-driven repopulation), but merely extending the duration of the same CSF1R inhibitor treatment completely switches repopulation source and dynamics. The brain appears to be a delicate sensor of microglial elimination, responding in kind to apparently small shifts in the balance of microglial number and mode of elimination. This highlights the dynamic capabilities of the brain to respond to microglial depletion, and signifying the importance of maintaining microglial homeostasis.

DISSERTATION CONCLUDING REMARKS

As microglia are implicated in many diseases and disorders, my thesis took the approach of microglial ablation as a tool to understand basic microglial functions and homeostasis. Microglial depletion and homeostasis have been explored in a number of different models. Genetic models utilizing ganciclovir require i.c.v. infusions, resulting in focal breaches of the BBB, allowing an access point for peripheral infiltration of BM-derived myeloid cells (Waisman et al., 2015, Varvel et al., 2015). Additionally, genetic models result in cytokine storms and behavioral impairments, possibly as a result of toxin administration, and method of microglial cell death. Here, we report a non-invasive microglial ablation model of CSF1R inhibition using PLX3397, which leaves the BBB intact, retains full cognitive and behavioral capabilities, and does not produce a cytokine storm. Moreover, upon removal of CSF1R inhibitors, microglia fully repopulate the brain through the proliferation of both a small population of surviving microglia and non-microglial cells, which differentiate into microglia within 24 hours.

The projects described within this thesis highlight the powerful control we have over the microglial compartment – both in terms of microglial number and function (Dagher et al., 2015). I have discovered four distinct routes of microglial repopulation via administration and withdrawal of various doses and durations of CSF1R inhibitors: 1) through contributions made by proliferating surviving microglia, 2) the proliferation and differentiation of a previously undescribed brainwide CNS-resident progenitor cell, 3) through infiltration of peripheral cells as seen with multiple cycles of CSF1R

treatment/withdrawal, and 4) through proliferation of a specific regional niche of white matter/RMS microglia.

Short or extended treatment with 290 mg/kg PLX3397 results in the rapid repopulation of the brain via proliferation of both surviving microglia and a CNS-resident progenitor cell. This cell expresses nestin at an early proliferating timepoint, and produces microglia which establish a normal population within 21 days, with no discernible differences when compared to control microglia (Elmore et al., 2015).

Multiple short cycles of treatment/recovery result in stunted repopulation, with only one successful repopulation event. However, multiple cycles with extended recovery periods stimulate at least three successful repopulation events, albeit with the introduction of P2ry12-negative cells by the third cycle which maintain this signature by 28 days' recovery, indicative of infiltrative cells. Nevertheless, the brain is able to repopulate itself with new myeloid cells at least three times, identifying the limits of successful repopulation following CSF1R inhibitor-mediated depletion, and potentially identifying a method by which to introduce peripherally-derived cells into the CNS.

Moreover, extended treatment (14d) with 600 mg/kg PLX3397 ablates 100% of microglia, eradicating the last 2% of microglia that had resisted less aggressive CSF1R inhibition paradigms. This treatment drastically alters the repopulation pattern, with myeloid cells initially aligning with RMS white matter and projecting axons. By 28 days of recovery, these cells have spread out to cortical regions, although the number of cells never reaches control, and morphological differences are sustained. Immunostaining reveals these cells to be P2ry12-negative at 7 days' recovery, but express P2ry12 by 14 and 28 days. Rather than indicative of an infiltrative origin for these cells, this pattern of

P2ry12 expression likely reflects that white matter RMS microglia express lower levels of purinergic receptors, but upon populating gray matter areas, these cells express P2ry12. Indeed, knocking out the CCR2/CCL2 signaling pathway does not inhibit differential RMS- and projecting axon-associated microglial repopulation, suggesting that monocytes are not infiltrating via CCR2 signaling. Therefore, we have identified an alternate source of repopulating microglia, that aligns initially with the RMS and projecting axons.

The ability to eliminate microglia and then repopulate has potential therapeutic implications. For example, after traumatic brain injuries, microglia become chronically activated, and impede functional recovery (Smith et al., 1997; Nagamoto-Combs et al., 2007; Loane et al., 2014). The ability to remove these reactive microglia and then repopulate with fresh microglial cells offers a strategy to resolve the neuroinflammation and promote recovery (Rice et al. 2017). Crucially, our lab has discovered that repopulated microglia are efficient at resolving chronic inflammatory states in the brain in response to a chronic focal lesion. Subsequent to the loss of 80% of hippocampal neurons via genetic lesion, mice with repopulated microglia functionally recover, with improvements in behavior, increases in synaptic puncta, and a resolution of inflammatory responses and cytokine levels.

The identification of four distinct sources of microglial repopulation may have differential effects on behavior, and should be thoroughly assessed as a precaution when considering potential therapies. Repopulation of microglia via CNS-resident brainwide progenitor proliferation has been proven to not only produce no behavioral deficits in wild-type mice (Elmore et al., 2014), but can be beneficial in resolving chronic injury

(Rice et al., 2017). However, it has been shown that knocking out a subtype of Hoxb8-expressing microglia results in a pathological grooming pattern similar to obsessive compulsive disorder (Chen et al., 2010). Interestingly, these Hoxb8-expressing microglia were often found near the SVZ and choroid plexus. This study highlights the relative importance of maintaining the balance of microglial subtypes, which may be altered with differential repopulation routes (with 14d 600 mg/kg PLX3397). Ultimately, CSF1R inhibition is a powerful tool with which to study microglial elimination and various routes of repopulation, but whether introducing peripheral myeloid cells into the CNS in the absence of injury or populating the brain with a distinct microglial subtype will affect normal CNS myeloid functions, remains to be seen.

REFERENCES

Ajami B, Bennett JL, Krieger C, Tetzlaff W, Rossi FM (2007) Local self-renewal can sustain CNS microglia maintenance and function throughout adult life. Nat Neurosci 10:1538-1543.

Ajami B, Bennett JL, Krieger C, McNagny KM, Rossi FM (2011) Infiltrating monocytes trigger EAE progression, but do not contribute to the resident microglia pool. Nat Neurosci 14:1142-1149.

Alliot F, Godin I, Pessac B (1999) Microglia derive from progenitors, originating from the yolk sac, and which proliferate in the brain. Brain Res Dev Brain Res 117:145-152.

Antony JM, Paquin A, Nutt SL, Kaplan DR, Miller FD (2011) Endogenous microglia regulate development of embryonic cortical precursor cells. J Neurosci Res 89:286-298.

Arno B, Grassivaro F, Rossi C, Bergamaschi A, Castiglioni V, Furlan R, Greter M, Favaro R, Comi G, Becher B, Martino G, Muzio L (2014) Neural progenitor cells orchestrate microglia migration and positioning into the developing cortex. Nat Commun 5:5611.

Bennett ML, Bennett FC, Liddelow SA, Ajami B, Zamanian JL, Fernhoff NB, Mulinyawe SB, Bohlen CJ, Adil A, Tucker A, Weissman IL, Chang EF, Li G, Grant GA, Hayden Gephart MG, Barres BA (2016) New tools for studying microglia in the mouse and human CNS. Proc Natl Acad Sci U S A 113:E1738-1746.

Beutner C, Roy K, Linnartz B, Napoli I, Neumann H (2010) Generation of microglial cells from mouse embryonic stem cells. Nat Protoc 5:1481-1494.

Beutner C, Linnartz-Gerlach B, Schmidt SV, Beyer M, Mallmann MR, Staratschek-Jox A, Schultze JL, Neumann H (2013) Unique transcriptome signature of mouse microglia. Glia 61:1429-1442.

Bruttger J, Karram K, Wortge S, Regen T, Marini F, Hoppmann N, Klein M, Blank T, Yona S, Wolf Y, Mack M, Pinteaux E, Muller W, Zipp F, Binder H, Bopp T, Prinz M, Jung S, Waisman A (2015) Genetic Cell Ablation Reveals Clusters of Local Self-Renewing Microglia in the Mammalian Central Nervous System. Immunity 43:92-106.

Butovsky O, Ziv Y, Schwartz A, Landa G, Talpalar AE, Pluchino S, Martino G, Schwartz M (2006) Microglia activated by IL-4 or IFN-gamma differentially induce neurogenesis and oligodendrogenesis from adult stem/progenitor cells. Mol Cell Neurosci 31:149-160.

Butovsky O, Jedrychowski MP, Moore CS, Cialic R, Lanser AJ, Gabriely G, Koeglsperger T, Dake B, Wu PM, Doykan CE, Fanek Z, Liu L, Chen Z, Rothstein JD, Ransohoff RM, Gygi SP, Antel JP, Weiner HL (2014) Identification of a unique TGF-beta-dependent molecular and functional signature in microglia. Nat Neurosci 17:131-143.

Cardona AE, Pioro EP, Sasse ME, Kostenko V, Cardona SM, Dijkstra IM, Huang D, Kidd G, Dombrowski S, Dutta R, Lee JC, Cook DN, Jung S, Lira SA, Littman DR, Ransohoff RM (2006) Control of microglial neurotoxicity by the fractalkine receptor. Nat Neurosci 9:917-924.

Carson MJ, Bilousova TV, Puntambekar SS, Melchior B, Doose JM, Ethell IM (2007) A rose by any other name? The potential consequences of microglial heterogeneity during CNS health and disease. Neurotherapeutics 4:571-579.
Chen KA, Laywell ED, Marshall G, Walton N, Zheng T, Steindler DA (2006) Fusion of neural stem cells in culture. Exp Neurol 198:129-135.
Chen SK, Tvrdik P, Peden E, Cho S, Wu S, Spangrude G, Capecchi MR (2010) Hematopoietic origin of pathological grooming in Hoxb8 mutant mice. Cell 141:775-785.
Chin BY, Petrache I, Choi AM, Choi ME (1999) Transforming growth factor beta1 rescues serum deprivation-induced apoptosis via the mitogen-activated protein kinase (MAPK) pathway in macrophages. J Biol Chem 274:11362-11368.
Chinnery HR, Ruitenberg MJ, McMenamin PG (2010) Novel characterization of monocyte-derived cell populations in the meninges and choroid plexus and their rates of replenishment in bone marrow chimeric mice. J Neuropathol Exp Neurol 69:896-909.
Chiu IM, Morimoto ET, Goodarzi H, Liao JT, O'Keeffe S, Phatnani HP, Muratet M, Carroll MC, Levy S, Tavazoie S, Myers RM, Maniatis T (2013) A neurodegeneration-specific gene-expression signature of acutely isolated microglia from an amyotrophic lateral sclerosis mouse model. Cell Rep 4:385-401.
Cho Y, Son HJ, Kim EM, Choi JH, Kim ST, Ji IJ, Choi DH, Joh TH, Kim YS, Hwang O (2009) Doxycycline is neuroprotective against nigral dopaminergic degeneration by a dual mechanism involving MMP-3. Neurotox Res 16:361-371.
Cornelis S, Bruynooghe Y, Van Loo G, Saelens X, Vandenabeele P, Beyaert R (2005) Apoptosis of hematopoietic cells induced by growth factor withdrawal is associated with caspase-9 mediated cleavage of Raf-1. Oncogene 24:1552-1562.
Dagher NN, Najafi AR, Kayala KM, Elmore MR, White TE, Medeiros R, West BL, Green KN (2015) Colony-stimulating factor 1 receptor inhibition prevents microglial plaque association and improves cognition in 3xTg-AD mice. J Neuroinflammation 12:139.
Damani MR, Zhao L, Fontainhas AM, Amaral J, Fariss RN, Wong WT (2011) Age-related alterations in the dynamic behavior of microglia. Aging Cell 10:263-276.
Davalos D, Grutzendler J, Yang G, Kim JV, Zuo Y, Jung S, Littman DR, Dustin ML, Gan WB (2005) ATP mediates rapid microglial response to local brain injury in vivo. Nat Neurosci 8:752-758.
DeKoter RP, Walsh JC, Singh H (1998) PU.1 regulates both cytokine-dependent proliferation and differentiation of granulocyte/macrophage progenitors. Embo j 17:4456-4468.
Demeestere D, Libert C, Vandenbroucke RE (2015) Clinical implications of leukocyte infiltration at the choroid plexus in (neuro)inflammatory disorders. Drug Discov Today 20:928-941.
Dhawan G, Floden AM, Combs CK (2012) Amyloid-beta oligomers stimulate microglia through a tyrosine kinase dependent mechanism. Neurobiol Aging 33:2247-61.

Doan V, Kleindienst AM, McMahon EJ, Long BR, Matsushima GK, Taylor LC (2013) Abbreviated exposure to cuprizone is sufficient to induce demyelination and oligodendrocyte loss. J Neurosci Res 91:363-373.
Doorn KJ, Breve JJ, Drukarch B, Boddeke HW, Huitinga I, Lucassen PJ, van Dam AM (2015) Brain region-specific gene expression profiles in freshly isolated rat microglia. Front Cell Neurosci 9:84.
El-Nefiawy N, Abdel-Hakim K, Yamashita A, Kanayama N (2002) Embryonic macrophages of early rat yolk sac: Immunohistochemistry and ultrastructure with reference to endodermal cell layer. Immunol Cell Biol 80:441-447.
Elmore MR, Lee RJ, West BL, Green KN (2015) Characterizing newly repopulated microglia in the adult mouse: impacts on animal behavior, cell morphology, and neuroinflammation. PLoS One 10:e0122912.
Elmore MR, Najafi AR, Koike MA, Dagher NN, Spangenberg EE, Rice RA, Kitazawa M, Matusow B, Nguyen H, West BL, Green KN (2014) Colony-stimulating factor 1 receptor signaling is necessary for microglia viability, unmasking a microglia progenitor cell in the adult brain. Neuron 82:380-397.
Erblich B, Zhu L, Etgen AM, Dobrenis K, Pollard JW (2011) Absence of colony stimulation factor-1 receptor results in loss of microglia, disrupted brain development and olfactory deficits. PLoS One 6:e26317.
Fogg DK, Sibon C, Miled C, Jung S, Aucouturier P, Littman DR, Cumano A, Geissmann F (2006) A clonogenic bone marrow progenitor specific for macrophages and dendritic cells. Science 311:83-87.
Frank MG, Barrientos RM, Biedenkapp JC, Rudy JW, Watkins LR, Maier SF (2006) mRNA up-regulation of MHC II and pivotal pro-inflammatory genes in normal brain aging. Neurobiol Aging 27:717-722.
Fraser DA, Pisalyaput K, Tenner AJ (2010) C1q enhances microglial clearance of apoptotic neurons and neuronal blebs, and modulates subsequent inflammatory cytokine production. J Neurochem 112:733-43.
von Furth R, Cohn ZA, Hirsch JG, Humphrey JH, Spector WG, Langevoort HL (1972) The mononuclear phagocyte system: a new classification of macrophages, monocytes, and their precursor cells. Bull World Health Organ 46:845-52.
Garcia-Alcalde F, Garcia-Lopez F, Dopazo J, Conesa A (2011) Paintomics: a web based tool for the joint visualization of transcriptomics and metabolomics data. Bioinformatics 27:137-139.
Gautier EL, Shay T, Miller J, Greter M, Jakubzick C, Ivanov S, Helft J, Chow A, Elpek KG, Gordonov S, Mazloom AR, Ma'ayan A, Chua WJ, Hansen TH, Turley SJ, Merad M, Randolph GJ (2012) Gene-expression profiles and transcriptional regulatory pathways that underlie the identity and diversity of mouse tissue macrophages. Nat Immunol 13:1118-1128.
Gehrmann J, Banati RB, Kreutzberg GW (1993) Microglia in the immune surveillance of the brain: human microglia constitutively express HLA-DR molecules. J Neuroimmunol 48:189-198.
Gehrmann J, Matsumoto Y, Kreutzberg GW (1995) Microglia: intrinsic immuneffector cell of the brain. Brain Res Brain Res Rev 20:269-287.
Gemma C, Bachstetter AD (2013) The role of microglia in adult hippocampal neurogenesis. Front Cell Neurosci 7:229.

Ginhoux F, Lim S, Hoeffel G, Low D, Huber T (2013) Origin and differentiation of microglia. Front Cell Neurosci 7:45.
Ginhoux F, Greter M, Leboeuf M, Nandi S, See P, Gokhan S, Mehler MF, Conway SJ, Ng LG, Stanley ER, Samokhvalov IM, Merad M (2010) Fate mapping analysis reveals that adult microglia derive from primitive macrophages. Science 330:841-845.
Godbout JP, Johnson RW (2004) Interleukin-6 in the aging brain. J Neuroimmunol 147:141-144.
Gomez Perdiguero E, Klapproth K, Schulz C, Busch K, Azzoni E, Crozet L, Garner H, Trouillet C, de Bruijn MF, Geissmann F, Rodwald HR (2015) Tissue-resident macrophages originate from yolk-sac-derived erythro-myeloid progenitors. Nature 518:547-51.
Green KN, Khashwji H, Estrada T, Laferla FM (2011) ST101 induces a novel 17 kDa APP cleavage that precludes Abeta generation in vivo. Ann Neurol 69:831-844.
Greter M, Merad M (2013) Regulation of microglia development and homeostasis. Glia 61:121-127.
Hanisch UK, Johnson TV, Kipnis J (2008) Toll-like receptors: roles in neuroprotection? Trends Neurosci 31:176-82.
Hashimoto D et al. (2013) Tissue-resident macrophages self-maintain locally throughout adult life with minimal contribution from circulating monocytes. Immunity 38:792-804.
Hayes GM, Woodroofe MN, Cuzner ML (1987) Microglia are the major cell type expressing MHC class II in human white matter. J Neurol Sci 80:25-37.
Haynes SE, Hollopeter G, Yang G, Kurpius D, Dailey ME, Gan WB, Julius D (2006) The P2Y12 receptor regulates microglial activation by extracellular nucleotides. Nat Neurosci 9:1512-1519.
Heppner FL, Ransohoff RM, Becher B (2015) Immune attack: the role of inflammation in Alzheimer disease. Nat Rev Neurosci 16:358-372.
Hickey WF, Vass K, Lassmann H (1992) Bone marrow-derived elements in the central nervous system: an immunohistochemical and ultrastructural survey of rat chimeras. J Neuropathol Exp Neurol 51:246-256.
Hickman SE, Kingery ND, Ohsumi TK, Borowsky ML, Wang LC, Means TK, El Khoury J (2013) The microglial sensome revealed by direct RNA sequencing. Nat Neurosci 16:1896-1905.
Hoeffel G, Chen J, Lavin Y, Low D, Almeida FF, See P, Beaudin AE, Lum J, Low I, Forsberg EC, Poidinger M, Zolezzi F, Larbi A, Ng LG, Chan JK, Greter M, Becher B, Samokhvalov IM, Merad M, Ginhoux F (2015) C-Myb(+) erythro-myeloid progenitor-derived fetal monocytes give rise to adult tissue-resident macrophages. Immunity 42:665-678.
Hoek RM, Ruuls SR, Murphy CA, Wright GJ, Goddard R, Zurawski SM, Blom B, Homola ME, Streit WJ, Brown MH, Barclay AN, Sedgwick JD (2000) Down-regulation of the macrophage lineage through interaction with OX2 (CD200). Science 290:1768-1771.
Huang da W, Sherman BT, Lempicki RA (2009a) Bioinformatics enrichment tools: paths toward the comprehensive functional analysis of large gene lists. Nucleic Acids Res 37:1-13.

Huang da W, Sherman BT, Lempicki RA (2009b) Systematic and integrative analysis of large gene lists using DAVID bioinformatics resources. Nat Protoc 4:44-57.
Kierdorf K et al. (2013) Microglia emerge from erythromyeloid precursors via Pu.1- and Irf8-dependent pathways. Nat Neurosci 16:273-280.
Kim WG, Mohney RP, Wilson B, Jeohn GH, Liu B, Hong JS (2000) Regional difference in susceptibility to lipopolysaccharide-induced neurotoxicity in the rat brain: role of microglia. J Neurosci 20:6309-6316.
Kraft AD, Harry GJ (2011) Features of microglia and neuroinflammation relevant to environmental exposure and neurotoxicity. Int J Environ Res Public Health 8:2980-3018.
Langmead B, Trapnell C, Pop M, Salzberg SL (2009) Ultrafast and memory-efficient alignment of short DNA sequences to the human genome. Genome Biol 10:R25.
Lawson LJ, Perry VH, Gordon S (1992) Turnover of resident microglia in the normal adult mouse brain. Neuroscience 48:405-415.
Lawson LJ, Perry VH, Dri P, Gordon S (1990) Heterogeneity in the distribution and morphology of microglia in the normal adult mouse brain. Neuroscience 39:151-170.
Li B, Dewey CN (2011) RSEM: accurate transcript quantification from RNA-Seq data with or without a reference genome. BMC Bioinformatics 12:323.
Li J, Chen K, Zhu L, Pollard JW (2006) Conditional deletion of the colony stimulating factor-1 receptor (c-fms proto-oncogene) in mice. Genesis 44:328-335.
Liddelow SA et al. (2017) Neurotoxic reactive astrocytes are induced by activated microglia. Nature 541:481-487.
Lin H, Lee E, Hestir K, Leo C, Huang M, Bosch E, Halenbeck R, Wu G, Zhou A, Behrens D, Hollenbaugh D, Linnemann T, Qin M, Wong J, Chu K, Doberstein SK, Williams LT (2008) Discovery of a cytokine and its receptor by functional screening of the extracellular proteome. Science 320:807-811.
Loane DJ, Kumar A, Stoica BA, Cabatbat R, Faden AI (2014) Progressive neurodegeneration after experimental brain trauma: association with chronic microglial activation. Journal of neuropathology and experimental neurology 73:14-29.
Luo XG, Ding JQ, Chen SD (2010) Microglia in the aging brain: relevance to neurodegeneration. Mol Neurodegener 5:12.
Marshall GP, 2nd, Demir M, Steindler DA, Laywell ED (2008) Subventricular zone microglia possess a unique capacity for massive in vitro expansion. Glia 56:1799-1808.
Mason JL, Jones JJ, Taniike M, Morell P, Suzuki K, Matsushima GK (2000) Mature oligodendrocyte apoptosis precedes IGF-1 production and oligodendrocyte progenitor accumulation and differentiation during demyelination/remyelination. J Neurosci Res 61:251-262.
Mason JL, Toews A, Hostettler JD, Morell P, Suzuki K, Goldman JE, Matsushima GK (2004) Oligodendrocytes and progenitors become progressively depleted within chronically demyelinated lesions. Am J Pathol 164:1673-1682.
Mildner A, Mack M, Schmidt H, Bruck W, Djukic M, Zabel MD, Hille A, Priller J, Prinz M (2009) CCR2+Ly-6Chi monocytes are crucial for the effector phase of autoimmunity in the central nervous system. Brain 132:2487-2500.

Mildner A, Schmidt H, Nitsche M, Merkler D, Hanisch UK, Mack M, Heikenwalder M, Bruck W, Priller J, Prinz M (2007) Microglia in the adult brain arise from Ly-6ChiCCR2+ monocytes only under defined host conditions. Nat Neurosci 10:1544-1553.
Miron VE, Franklin RJ (2014) Macrophages and CNS remyelination. J Neurochem 130:165-171.
Miron VE, Boyd A, Zhao JW, Yuen TJ, Ruckh JM, Shadrach JL, van Wijngaarden P, Wagers AJ, Williams A, Franklin RJ, ffrench-Constant C (2013) M2 microglia and macrophages drive oligodendrocyte differentiation during CNS remyelination. Nat Neurosci 16:1211-1218.
Mizuno T, Kawanokuchi J, Numata K, Suzumura A (2003) Production and neuroprotective functions of fractalkine in the central nervous system. Brain Res 979:65-70.
Monier A, Adle-Biassette H, Delezoide AL, Evrard P, Gressens P, Verney C (2007) Entry and distribution of microglial cells in human embryonic and fetal cerebral cortex. J Neuropathol Exp Neurol 66:372-382.
Nagamoto-Combs K, McNeal DW, Morecraft RJ, Combs CK (2007) Prolonged microgliosis in the rhesus monkey central nervous system after traumatic brain injury. J Neurotrauma 24:1719-1742.
Nandi S, Gokhan S, Dai XM, Wei S, Enikolopov G, Lin H, Mehler MF, Stanley ER (2012) The CSF-1 receptor ligands IL-34 and CSF-1 exhibit distinct developmental brain expression patterns and regulate neural progenitor cell maintenance and maturation. Dev Biol 367:100-113.
Neely KM, Green KN, LaFerla FM (2011) Presenilin is necessary for efficient proteolysis through the autophagy-lysosome system in a gamma-secretase-independent manner. J Neurosci 31:2781-2791.
Nimmerjahn A, Kirchhoff F, Helmchen F (2005) Resting microglial cells are highly dynamic surveillants of brain parenchyma in vivo. Science 308:1314-1318.
Njie EG, Boelen E, Stassen FR, Steinbusch HW, Borchelt DR, Streit WJ (2012) Ex vivo cultures of microglia from young and aged rodent brain reveal age-related changes in microglial function. Neurobiol Aging 33:195.e191-112.
Pang Y, Cai Z, Rhodes PG (2003) Disturbance of oligodendrocyte development, hypomyelination and white matter injury in the neonatal rat brain after intracerebral injection of lipopolysaccharide. Brain Res Dev Brain Res 140:205-214.
Paolicelli RC, Bolasco G, Pagani F, Maggi L, Scianni M, Panzanelli P, Giustetto M, Ferreira TA, Guiducci E, Dumas L, Ragozzino D, Gross CT (2011) Synaptic pruning by microglia is necessary for normal brain development. Science 333:1456-1458.
Patel S, Player MR (2009) Colony-stimulating factor-1 receptor inhibitors for the treatment of cancer and inflammatory disease. Curr Top Med Chem 9:599-610.
Peferoen L, Kipp M, van der Valk P, van Noort JM, Amor S (2014) Oligodendrocyte-microglia cross-talk in the central nervous system. Immunology 141:302-313.
Perry VH, Matyszak MK, Fearn S (1993) Altered antigen expression of microglia in the aged rodent CNS. Glia 7:60-67.

Ribeiro Xavier AL, Kress BT, Goldman SA, Lacerda de Menezes JR, Nedergaard M (2015) A distinct population of microglia supports adult neurogenesis in the subventricular zone. J Neurosci 35:11848-61.
Rice RA, Pham J, Lee RJ, Najafi AR, West BL, Green KN (2017) Microglial repopulation resolves inflammation and promotes brain recovery after injury. Glia.
Rice RA, Spangenberg EE, Yamate-Morgan H, Lee RJ, Arora RP, Hernandez MX, Tenner AJ, West BL, Green KN (2015) Elimination of Microglia Improves Functional Outcomes Following Extensive Neuronal Loss in the Hippocampus. J Neurosci 35:9977-9989.
Robinson MD, McCarthy DJ, Smyth GK (2010) edgeR: a Bioconductor package for differential expression analysis of digital gene expression data. Bioinformatics 26:139-140.
Sachs HH, Bercury KK, Popescu DC, Narayanan SP, Macklin WB (2014) A new model of cuprizone-mediated demyelination/remyelination. ASN Neuro 6.
Sahin Kaya S, Mahmood A, Li Y, Yavuz E, Chopp M (1999) Expression of nestin after traumatic brain injury in rat brain. Brain Res 840:153-7.
Samokhvalov IM, Samokhvalova NI, Nishikawa S (2007) Cell tracing shows the contribution of the yolk sac to adult haematopoiesis. Nature 446:1056-1061.
Sasaki A, Nakazato Y (1992) The identity of cells expressing MHC class II antigens in normal and pathological human brain. Neuropathol Appl Neurobiol 18:13-26.
Schafer DP, Lehrman EK, Kautzman AG, Koyama R, Mardinly AR, Yamasaki R, Ransohoff RM, Greenberg ME, Barres BA, Stevens B (2012) Microglia sculpt postnatal neural circuits in an activity and complement-dependent manner. Neuron 74:691-705.
Schulz C, Gomez Perdiguero E, Chorro L, Szabo-Rogers H, Cagnard N, Kierdorf K, Prinz M, Wu B, Jacobsen SE, Pollard JW, Frampton J, Liu KJ, Geissmann F (2012) A lineage of myeloid cells independent of Myb and hematopoietic stem cells. Science 336:86-90.
Sierra A, Gottfried-Blackmore AC, McEwen BS, Bulloch K (2007) Microglia derived from aging mice exhibit an altered inflammatory profile. Glia 55:412-424.
Sieweke MH, Allen JE (2013) Beyond stem cells: self-renewal of differentiated macrophages. Science 342:1242974.
Smith DH, Chen XH, Pierce JE, Wolf JA, Trojanowski JQ, Graham DI, McIntosh TK (1997) Progressive atrophy and neuron death for one year following brain trauma in the rat. J Neurotrauma 14:715-727.
Soza-Ried C, Hess I, Netuschil N, Schorpp M, Boehm T (2010) Essential role of c-myb in definitive hematopoiesis is evolutionarily conserved. Proc Natl Acad Sci U S A 107:17304-17308.
Spangenberg EE, Lee RJ, Najafi AR, Rice RA, Elmore MR, Blurton-Jones M, West BL, Green KN (2016) Eliminating microglia in Alzheimer's mice prevents neuronal loss without modulating amyloid-beta pathology. Brain 139:1265-1281.
Styren SD, Civin WH, Rogers J (1990) Molecular, cellular, and pathologic characterization of HLA-DR immunoreactivity in normal elderly and Alzheimer's disease brain. Exp Neurol 110:93-104.
Sunnemark D, Eltayeb S, Wallstrom E, Appelsved L, Malmberg A, Lassmann H, Ericsson-Dahlstrand A, Piehl F, Olsson T (2003) Differential expression of the

chemokine receptors CX3CR1 and CCR1 by microglia and macrophages in myelin-oligodendrocyte-glycoprotein-induced experimental autoimmune encephalomyelitis. Brain Pathol 13:617-629.
Theriault P, ElAli A, Rivest S (2015) The dynamics of monocytes and microglia in Alzheimer's disease. Alzheimers Res Ther 7:41.
Tremblay ME, Lowery RL, Majewska AK (2010) Microglial interactions with synapses are modulated by visual experience. PLoS Biol 8:e1000527.
Ueno M, Fujita Y, Tanaka T, Nakamura Y, Kikuta J, Ishii M, Yamashita T (2013) Layer V cortical neurons require microglial support for survival during postnatal development. Nat Neurosci 16:543-551.
Valdearcos M, Robblee MM, Benjamin DI, Nomura DK, Xu AW, Koliwad SK (2014) Microglia dictate the impact of saturated fat consumption on hypothalamic inflammation and neuronal function. Cell Rep 9:2124-2138.
Varvel NH, Grathwohl SA, Degenhardt K, Resch C, Bosch A, Jucker M, Neher JJ (2015) Replacement of brain-resident myeloid cells does not alter cerebral amyloid-beta deposition in mouse models of Alzheimer's disease. J Exp Med 212:1803-1809.
Varvel NH, Grathwohl SA, Baumann F, Liebig C, Bosch A, Brawek B, Thal DR, Charo IF, Heppner FL, Aguzzi A, Garaschuk O, Ransohoff RM, Jucker M (2012) Microglial repopulation model reveals a robust homeostatic process for replacing CNS myeloid cells. Proc Natl Acad Sci U S A 109:18150-18155.
Waisman A, Ginhoux F, Greter M, Bruttger J (2015) Homeostasis of Microglia in the Adult Brain: Review of Novel Microglia Depletion Systems. trends Immunol 36:625-36.
Wang Y, Szretter KJ, Vermi W, Gilfillan S, Rossini C, Cella M, Barrow AD, Diamond MS, Colonna M (2012) IL-34 is a tissue-restricted ligand of CSF1R required for the development of Langerhans cells and microglia. Nat Immunol 13:753-760.
Wegiel J, Wisniewski HM, Dziewiatkowski J, Tarnawski M, Kozielski R, Trenkner E, Wiktor-Jedrzejczak W (1998) Reduced number and altered morphology of microglial cells in colony stimulating factor-1-deficient osteopetrotic op/op mice. Brain Res 804:135-139.
Wohl SG, Schmeer CW, Friese T, Witte OW, Isenmann S (2011) In situ dividing and phagocytosing retinal microglia express nestin, vimentin, and NG2 in vivo. PLoS One 6:e22408.
Wright GJ, Jones M, Puklavec MJ, Brown MH, Barclay AN (2001) The unusual distribution of the neuronal/lymphoid cell surface CD200 (OX2) glycoprotein is conserved in humans. Immunology 102:173-179.
Yokoyama A, Yang L, Itoh S, Mori K, Tanaka J (2004) Microglia, a potential source of neurons, astrocytes, and oligodendrocytes. Glia 45:96-104.
Yona S, Kim KW, Wolf Y, Mildner A, Varol D, Breker M, Strauss-Ayali D, Viukov S, Guilliams M, Misharin A, Hume DA, Perlman H, Malissen B, Zelzer E, Jung S (2013) Fate mapping reveals origins and dynamics of monocytes and tissue macrophages under homeostasis. Immunity 38:79-91.
Zhang Y, Chen K, Sloan SA, Bennett ML, Scholze AR, O'Keeffe S, Phatnani HP, Guarnieri P, Caneda C, Ruderisch N, Deng S, Liddelow SA, Zhang C, Daneman R, Maniatis T, Barres BA, Wu JQ (2014) An RNA-sequencing transcriptome and

splicing database of glia, neurons, and vascular cells of the cerebral cortex. J Neurosci 34:11929-11947.
Ziv Y, Schwartz M (2008) Orchestrating brain-cell renewal: the role of immune cells in adult neurogenesis in health and disease. Trends Mol Med 14:471-478.
Zujovic V, Benavides J, Vige X, Carter C, Taupin V (2000) Fractalkine modulates TNF-alpha secretion and neurotoxicity induced by microglial activation. Glia 29:305-315.